Technische Universität München
TUM School of Medicine and Health

Investigation of resistance mechanisms in acute myeloid leukaemia towards tyrosine kinase inhibitors with mass spectrometry

Nora Hannane

Vollständiger Abdruck der von der TUM School of Medicine and Health der Technischen Universität München zur Erlangung einer

Doktorin der Medizinischen Wissenschaft (Dr. med. sci.)

genehmigten Dissertation.

Vorsitz: apl. Prof. Dr. Sylvie Lorenzen

Prüfer*innen der Dissertation:

1. Priv.-Doz. Dr. Peer- Hendrik Kuhn, Ph.D.
2. apl. Prof. Dr. Katharina S. Götze

Die Dissertation wurde am 14.07.2023 bei der Technischen Universität München eingereicht und durch die TUM School of Medicine and Health am 08.11.2023 angenommen.

Investigation of resistance mechanisms in acute myeloid leukaemia towards tyrosine kinase inhibitors with mass spectrometry

Nora Hannane

This work was submitted for publication under the title “Proteomic changes in Midostaurin and Sorafenib resistant FLT3 mutated AML cells point to new therapeutic vulnerabilities such as Bcl-XL inhibition” to the Journal for Medical and clinical proteomics.

Table of Content

Abbreviations

AML	Acute myeloid leukaemia
ALL	Acute lymphocytic leukaemia
CML	Chronic myeloid leukaemia
CLL	Chronic lymphocytic leukaemia
FDA	U.S. Food and drug administration
FLT3	Fms-like tyrosine kinase receptor 3
ITD	Internal tandem duplication
TKD	Tyrosine kinase domain
TKI	Tyrosine kinase inhibitor
MS	Mass spectrometry
P- MS	Phosphorylation detecting mass spectrometry
WB	Western Blot
STAT	Signal transducer and activator of transcription
P- STAT5	Phosphorylated Signal transducer and activator of transcription
BCL	B- cell lymphoma
JAK	Janus kinase
ICAM3	Intercellular adhesion molecule 3
SLAM Family	Signalling lymphocyte activation molecule
CD84	SLAM Family Member 5
SAMHD1	Sterile alpha motif and histidine-aspartic domain-containing protein 1
CHEK1	Checkpoint kinase 1
MAPK/ ERK	Mitogen-activated protein kinase/ Extracellular- signal-regulated kinase
PI3K/ AKT	Phosphatidylinositol- 3 kinase/ protein kinase B
PTPN6	Tyrosine-protein phosphatase non-receptor type 6
CRLF3	Cytokine receptor-like factor receptor 3
IGF1R	Insulin-like growth factor 1 receptor
MNAR	Missing not at random
KEGG	Kyoto Encyclopaedia of Genes and Genomes
TMT	Tandem mass tag
FC	Fold- change
LFQ	Label-free quantification
PCA	Principal component analysis
IC_{50}	Half maximal inhibitory concentration

Table Index

1. Introduction

1.1. Leukaemia, an overview

1.1.1. History and Definitions

Leukaemia is a group of heterogenic cancerous haematopoietic system diseases, first described as “milky serum” by Peter Cullen in 1810 (Kampen, 2012). A further definition and the name “Leukämie”, from the Greek “leukos” white and “haima” blood, was developed by Robert Virchow in the 1850th (Virchow, 1856). The disease is caused by the proliferation and release of malignant haematopoietic precursor cells into the organism. In the first place, based on the proliferation rate of the malignant cells, leukaemia is classified as chronic or acute. High white blood cell counts are the manifestation point of the first symptoms. Chronic forms are often diagnosed in a late disease stage or by accident due to a slow and unspecific clinical appearance. In contrast, acute forms of leukaemia quickly induce the first symptoms by vast numbers of cancer cells, so-called blasts, in the organism. The second classification scheme considers the haematopoietic precursor cell from which cancer derives. The leukaemia subtypes are grouped as lymphocytic or myeloid leukaemia, depending on whether they derive from the common lymphoid or myeloid progenitor cell. (The American Cancer Society medical and editorial content team, 9,2014).

1.1.2. Basic principles of Haematopoiesis and Leukaemia

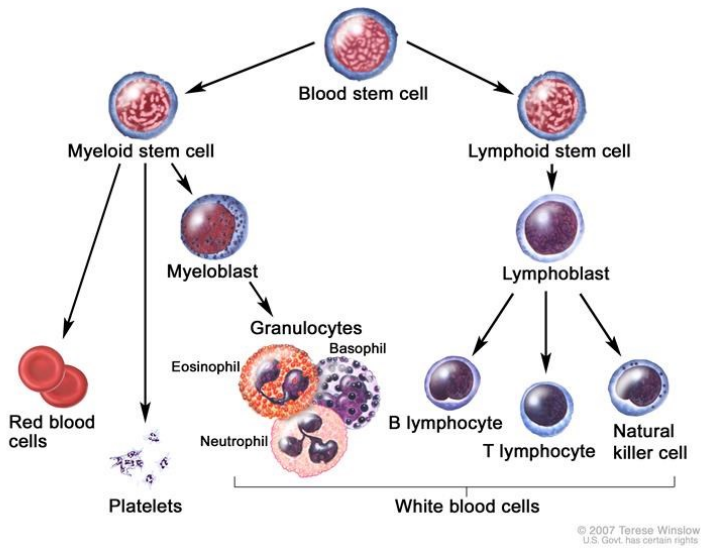

Figure 1: Blood cell development. A blood stem cell goes through several stages to become a red blood cell, platelet, or white blood cell (Terese Winslow, 2007, National Cancer Institute).

The production of functional blood cells occurs in the red bone marrow and underlies a wide range of regulatory mechanisms. Two major parts of haematopoiesis are the proliferation of stem and progenitor cells and the further differentiation and maturation into specific cellular subtypes such as erythrocytes, thrombocytes, and various classes of leukocytes. As mentioned above, the first level of

differentiation of haematopoietic stem cells in haematopoiesis leads to the formation of the common myeloid and common lymphoid stem cells, giving rise to two large cell groups with different cell types. The common lymphoid progenitor produces the different lymphocytes: B-, T-, and natural killer cells. The myeloid group is formed by Erythrocytes, Thrombocytes, and Granulocytes of different granules (eosinophil, basophil, neutrophil). Accumulation of genetic mutations introduced by radiation, viruses, chemical contact, or often unknown sources can lead to an oncogenic transformation of the progenitor cells in different ways. In myelodysplastic syndromes, transformed cells cannot maturate correctly and die early, leading to a deficit of functional blood cells, so-called cytopenia. On the contrary, transformations inhibiting cell death result in the accumulation of non-functional progenitor cells leading to chronic leukaemia over time. When transformed leukemic cells accumulate mutations that inhibit cell death and promote their proliferation, acute leukaemia arises. Additional mutations can shift the pathological mechanism and, thus, the resulting disease type, such as the progression of myelodysplastic syndromes and chronic leukaemia toward acute myeloid leukaemia (Fiegl, 2016, 2016).

1.1.3. Statistics

Leukaemia is the most common type of cancer in children and the 10th most common in adults, with estimated 59 610 new cases and 23 710 deaths in the U.S. in 2023. Approximately 1.6% of the U.S. population will be diagnosed with leukaemia during their lifetime (National Cancer Institute's Surveillance, Epidemiology and End Results Program).

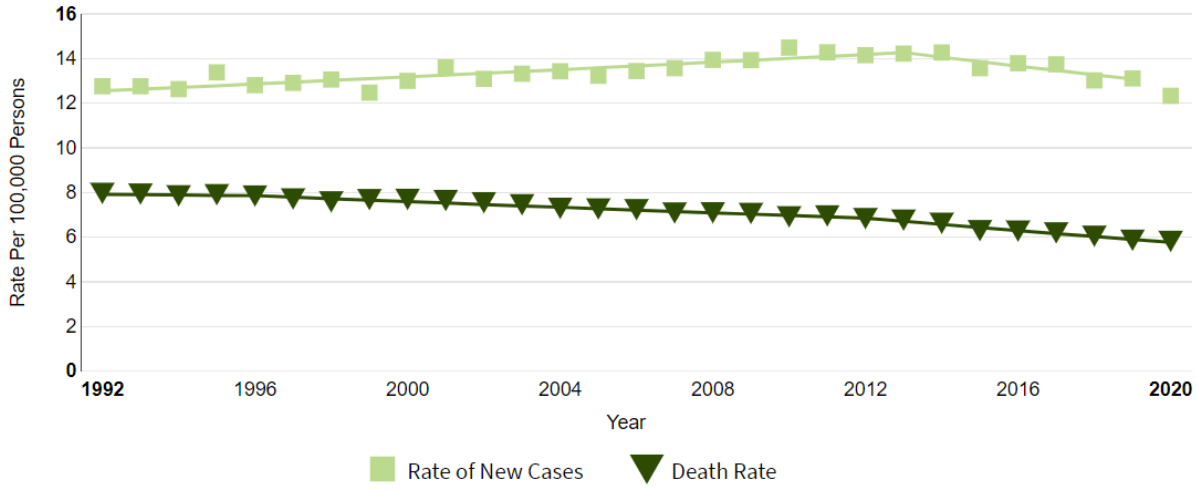

Figure 2: Number of new cases and death of leukaemia per 100.000 persons in the U.S. National cancer institute Surveillance, Epidemiology, and End results program.
https://seer.cancer.gov/statfacts/html/leuks.html

Whereas complete healing of the chronic forms isn't possible in most cases, requiring long-term therapies, the five-year survival rates improved a lot in the last decades to 84,3% of patients with chronic lymphocytic leukaemia (CLL) and 66,5% of patients with chronic myeloid leukaemia (CML). Those improvements are often due to therapies allowing long time maintenance of a steady disease state. 5-year survival rates of acute forms are 68,2% for patients with acute lymphocytic leukaemia (ALL) and 31,7 % for patients with acute myeloid leukaemia. The general five years survival rate of leukaemia is 66,7%, which doubled in the last decades, compared to 33.1% back in 1975 (National Cancer Institute's Surveillance, Epidemiology and End Results Program).

1.1.4. Disease manifestation and Symptoms

The symptomatic manifestation of leukaemia is primarily due to the overwhelming production of cancer cells in the bone marrow. This leads to a lack of normal blood cell synthesis and a reduced number of functional blood cells in the organism. Thrombocytopenia and the resulting lack of blood clotting ability increase the patient's risk of developing bruises, bleedings, and wound healing disorders. Missing erythrocytes provoke general anaemia symptoms such as fatigue, pallor, and dyspnoea. A deficit of immunological cells such as leukocytes and lymphocytes often causes infectious and sometimes autoimmune complications, worsening the patients' physical condition. The accumulation of cancer cells in peripheral organs such as lymph nodes, liver, and spleen can result in additional symptoms characterized by swellings and pain, as well as nausea and weight loss. In acute forms, an accumulation of blasts in the brain can cause headaches and migraine-like symptoms (Cancer Treatment Centers of America, 2015).

1.2. Acute myeloid Leukaemia

1.2.1. Statistics of acute myeloid leukaemia

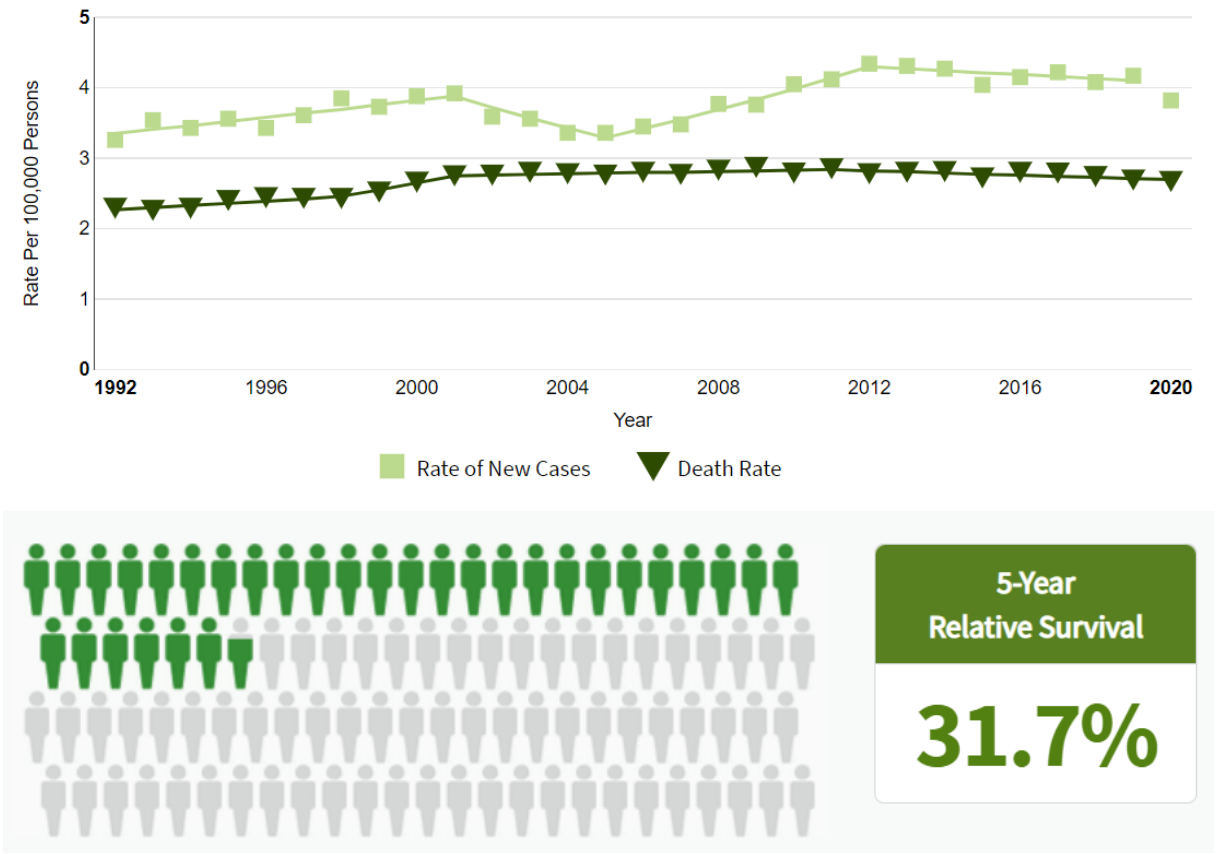

Figure 3: Number of new cases and death of acute myeloid leukaemia per 100.000 persons in the U.S., the five-year survival rate from 2013-2019 (grey figures represent deaths, green figures represent those who survived 5 years or longer) https://seer.cancer.gov/statfacts/html/leuks.html

Acute myeloid leukaemia (AML) is the second most common type of leukaemia in adults and children, with an estimated 20.380 new cases and over 11.310 deaths in the US in 2023 (Miller et al., 2020). Thanks to intense scientific and clinical research over the last decades, it was possible to raise the 5-year survival rate from 6.4% in 1975 to 31.7% in 2019. (National Cancer Institute's Surveillance, Epidemiology and End Results Program). Nevertheless, more than 60% of patients still succumb to AML within the first year upon diagnosis, remaining the most deadly type of blood cancer (Abelson et al., 2018).

1.2.2. Diagnosis

Diagnosing acute myeloid leukaemia combines different steps beginning with the anamnesis and examination of the patient. Once leukaemia is suspected, blood and bone marrow samples are analysed in various manners. The foundation of bone marrow and blood analysis is the morphological and quantitative analysis of cells of all haematopoietic lineages, including blast quantification in the bone marrow and peripheral blood. Acute leukaemia is diagnosed if the leukemic blast count in the bone marrow or blood exceeds 20% of the total count. In purpose to determine the lineage of leukemic blasts, either cytochemistry (Myeloperoxidase, Sudan- Black B and non-specific esterase) or immunophenotyping of blasts in the peripheral blood via multi-parameter flow cytometry and of blasts in the bone marrow via immune histochemistry (IHC) are performed (higher sensitivity for minimal differentiation). Another crucial step, due to the high incidence of chromosomal alterations in AML Patients, is the cytogenetic analysis and the molecular genetic analysis (Döhner et al., 2010; Döhner et al., 2017). These methods attempt to comprehensively classify and analyse myeloid cancer cells to provide the best possible treatment options and specific prognosis. Studies showed that stable and especially older patients would benefit from detailed chromosomal, cytogenetic and phenotyping diagnostics, even if a slight delay in the beginning of treatment would be caused (Röllig et al., 2020).

1.2.3. Classification

As described previously, further discrimination according to the specific differentiation of the malignant blood cell and genetic phenotypes is crucial for therapeutic planning. The French American British cancer association classified leukaemia in 1976 into nine subtypes corresponding to the differentiation steps of haematopoiesis (Bennett et al., 1976).

FAB Type	Description	Comments
M0	Undifferentiated acute myeloblastic leukaemia	Myeloperoxidase (-), myeloid markers (+)
M1	Acute myeloblastic leukaemia with minimal maturation	Some evidence of granulocytic differentiation
M2	Acute myeloblastic leukaemia with maturation	At or beyond promyelocytic stage, divided into t(8;21) AML1- ETO fusion (+)/(-)
M3	Acute promyelocytic leukaemia (APL)	Most common with t(15;17) PML- RARα or other RARα involving translocation
M4	Acute myelomonocytic leukaemia	
M4Eo	Acute myelomonocytic leukaemia with bone-marrow eosinophilia	Inversion of chromosome 16 involving CBFβ which usually forms a heterodimer with AML1

M5	Acute monocytic leukaemia	
M6	Acute erythroid leukaemia	
M7	Acute megakaryoblast leukaemia	GATA1 mutations in those associated with Down's syndrome

Table 1: FAB Classification of AML

A further detailed classification of AML subtypes carrying genetic mutations with their prognostic impacts was published by the World Health Organization in 2007 (Swerdlow). Due to the strong correlation of variant genetic aberrations to treatment response and prognosis, it is nowadays part of the standard diagnostic procedure of acute myeloid leukaemia ("Genomic Classification in Acute Myeloid Leukemia," 2016; Arber et al., 2016; Papaemmanuil et al., 2016; Swerdlow).

AML with recurrent genetic abnormalities
AML with t(8;21)(q22;q22); RUNX1-RUNX1T1 (AML1 CBFα/ETO)
AML with abnormal bone marrow eosinophils: inv(16)(p13,1q22) or t(16;16)(p13.1;q22); CBFβ-MYH11
Acute promyelocytic leukaemia, AML with t(15;17)(q22;q12); PML- RARα
AML with t(9;11)(p22;q23); MLLT3- MLL
AML with t(6;9)(p23;q34); DEK- NUP214
AML with inv(3)(q21q26.2) or t(3;3)(q21;q26.2); RPN1- EVI1
Acute megakaryoblast leukaemia with t(1;22)(p13;q13); RBM15-MKL1

AML with multi-lineage dysplasia
Following myelodysplastic syndrome or myeloproliferative disorder
Without prior myelodysplastic syndrome

Therapy-related AML and myelodysplastic syndrome
Alkylating agent related
Topoisomerase type II inhibitor-related
Other types

AML, not otherwise specified
Undifferentiated acute myeloblastic leukaemia (FAB M0)
Acute myeloblastic leukaemia with minimal maturation (FAB M1)
Acute myeloblastic leukaemia with maturation (FAB M2)
Acute promyelocytic leukaemia (APL) (FAB M3)
Acute myelomonocytic leukaemia (FAB M4)
Acute myelomonocytic leukaemia with bone-marrow eosinophilia (FAB $M4_{Eo}$)
Acute monocytic leukaemia (FAB M5)
Acute erythroid leukaemia (FAB M6)
Acute megakaryoblastic leukaemia (FAB M7)
Acute basophilic leukaemia
Acute panmyelosis with myelofibrosis
Myeloid Sarcoma

Table 2: WHO classification of tumours of haematopoietic and lymphoid tissues, 2008 World Health Organization, Version 2 (4. ed.)

1.2.4. Treatment options in acute myeloid leukaemia

The standard therapy for all AML types is based on two phases: the remission induction followed by the post-remission therapy, also called consolidation. The induction phase attempts to rapidly decrease the blast cell count in the organism to ensure the patient's survival and allow further treatment. For this goal, high-dose chemotherapy in the so-called "7+3 Regimen" is given, combining seven days of Cytarabine (Ara-C, an antimetabolite) and three days of anthracyclines (mainly Daunorubicin). Consolidation therapy is started once the treatment results in a complete remission of cancer, defined as a blast count lower than 5% of the white blood cells. Therefore, high dose Cytarabine is given for five days every month for 3 or 4 cycles. Other essential consolidation treatments are allogenic and autologous stem cell transplantations (Pratz & Levis, 2017). This intense and aggressive standard therapy is mainly tolerated by patients younger than 60 with good health conditions, including good cardiac function. Older and weaker patients only tolerate less toxic therapy regimens with lower drug doses, leading to even worse survival chances (Kouchkovsky & Abdul-Hay, 2016).

1.2.5. FLT3 and tyrosine kinase inhibitor treatment

Nearly 30% of all AML Patients carry mutations in the gene of the FLT3 receptor tyrosine kinase, leading to constitutive activation of its biochemical functions (Bagrintseva et al., 2004; El Fakih, Rasheed, Hawsawi, Alsermani, & Hassanein, 2018; Gilliland & Griffin, 2002; Kiyoi et al., 1998). Those include activating several downstream pathways such as PI3K/AKT, JAK/STAT, and Raf/MAPK signalling (Gilliland & Griffin, 2002; Rosnet et al., 1996; Tse, Mukherjee, & Small, 2000). The most common type of mutations, with nearly 23% of all cases, are internal tandem duplications (ITD) of base pairs coding for the juxta-membrane area (Kiyoi et al., 1998). Those ITD mutations are correlated to higher relapse risks and lower cure rates in patients (Levis & Small, 2003). The second most common type is the FLT3-tyrosine kinase domain mutation (TKD), with nearly 7% of all modifications, which has a less negative prognostic impact than the internal tandem duplication (Yamamoto et al., 2001). Due to the survival advantage of the cancer cells, the frequency, and the negative prognostic impacts of such a mutation, FLT3 became a promising treatment target (Jones et al., 2020; Kindler, Lipka, & Fischer, 2010)

Various small molecular inhibitors for receptor tyrosine kinases of the FLT3 family have been tested and further developed with variant clinical results. Most drugs convince by little side effects and dose-limiting toxicities, allowing them to be used on top of classical treatments and in older patients (Ossenkoppele & Löwenberg, 2015). In double-blinded randomized placebo-controlled trials, the treatment arms often showed benefits in complete remission rates, event-free and relapse-free survival (Grunwald & Levis, 2013; Megías-Vericat, Ballesta-López, Barragán, Martínez-Cuadrón, & Montesinos, 2020). Nevertheless, most of those trials could not prove a stable improvement in overall survival and risk of death rates. The two main substances used to target FLT3 mutations are Sorafenib and Midostaurin. Sorafenib significantly improved relapse-free survival in combination with chemotherapy in induction and maintenance therapy in FLT3 mutated AML patients (Uy et al., 2017; Xuan et al., 2020). These effects could additionally be observed in high-risk AML patients undergoing allogenic stem cell transplantation, where additional maintenance therapy with Sorafenib significantly reduced the risk of relapse (Brunner et al., 2016; Burchert et al., 2020; Chappell et al., 2019). After showing strong cytotoxic effects on FLT3- ITD mutation carrying leukemic cells *in vitro* and *in vivo* experiments with mice (Stone, Manley, Larson, & Capdeville, 2018; Weisberg et al., 2002), Midostaurin was tested in the international RATIFY trial demonstrating significant improvements of complete remission rates, relapse-free and overall survival in FLT3 mutated patients compared to the control

arm (Schlenk et al., 2019; Stone, Mandrekar et al., 2017), which finally led to its approval as combination therapy agent by the U.S. Food and Drug Administration and the European Medicine Agency in April 2017 (Weisberg, Sattler, Manley, & Griffin, 2018). Since then, multiple studies using Midostaurin in different disease stages and with different co-therapeutics showed promising effects for FLT3-mutated AML patients (Schlenk et al., 2019).

Nevertheless, the relatively modest improvement in overall survival is the main weakness of small molecular FLT3 inhibitors. The main reason is the development of cellular resistance of AML cells against these inhibitors, which frequently occurs after a few months of treatment (Piloto et al., 2007; Stölzel et al., 2010). Therefore, most developed FLT3 inhibitors did not meet the criteria for approval as a general therapeutic agent (Stone, 2017). Comprehensive cellular analyses have been made to identify the main resistance mechanisms of AML cells against these inhibitors. Various genetic alterations and potential resistance mechanisms were analysed, but strong evidence leading to a specific alteration is still rare (Brinda, Khan, Parkin, & Konig, 2018). Mechanisms such as the evolution of resistant clones, cellular adaptations, or protective changes of the leukemic environment have been described (Lam & Leung, 2020). The most important adaptations found in TKI resistant FLT3 mutated AML cells are listed in the table below.

Resistance mechanism	Publication
FLT3- TKD mutations	(Daver et al., 2015; Heidel et al., 2006; Smith, Lin, Stecula, Sali, & Shah, 2015)
Upregulation of FLT3 ligand	(Chen, Ishikawa, Akashi, Naoe, & Kiyoi, 2016; Sato et al., 2011)
Upregulation of AXL Tyrosine kinase	(Park et al., 2015)
Upregulation of PI3K/AKT/mTOR and MAPK/ERK Pathway	(Lindblad et al., 2016; Piloto et al., 2007)
Microenvironment protection	(Baryawno et al., 2019; Javidi-Sharifi et al., 2019; Kojima et al., 2011; Traer et al., 2016; Zeng et al., 2009)

Table 3: Overview of important potential resistance mechanisms in AML against tyrosine kinase inhibitors and their publications

1.2.6. Targeted therapies in AML

Since 2017, several new drugs have been approved for treating AML (Kantarjian, Kadia, DiNardo, Welch, & Ravandi, 2021). Most are targeted therapies in second-line treatments for relapsed patients or those not suited for first-line therapies due to age and comorbidities (Burnett & Stone, 2020). Besides the multi-tyrosine kinase Inhibitors Midostaurin and Gilteritinib, a selective oral FLT3 Inhibitor was approved as a treatment in refractory or relapsed AML after showing significant improvements in overall survival, event-free survival, and complete remission rates as a single agent in comparison to chemotherapy in those cases (Perl et al., 2019).

The monoclonal antibody conjugate Gemtuzumab Ozogamicin targeting CD33 and mediating cytotoxicity through a conjugated bacterial toxin has been approved as a combination therapy for CD33+ AML in 2018. Meta-analysis of clinical trials prior showing incongruent results, proved significant benefits when used as a combination agent (Burnett et al., 2011; Hills et al., 2014).

The hedgehog inhibitor Glasdegib, in combination with low-dose Cytarabine, can be used as a treatment option in patients who are not suited for first-line therapy, e.g. older than 75 years (Hoy, 2019; Thomas & Heiblig, 2020).

The Bcl-2 inhibitor Venetoclax has been approved as therapy in combination with Azacytidine/ Decitabine and even became the therapeutic regimen of choice in combination with low-dose Cytarabine in patients older than 75 years due to low toxicity effects and significantly improved survival rates (DiNardo et al., 2020; Wei et al., 2020).

For relapsed or refractory patients carrying isocitrate-dehydrogenase (IDH) mutations, corresponding inhibitors Ivosidenib (IDH-1 inhibitor) and Enasidenib (IDH-2 inhibitor) have been approved for monotherapy (DiNardo et al., 2018; Kim, 2017). As a non-specific agent, a new liposomal formulation of Daunorubicin/ Cytarabine has been developed for secondary AML, showing a more targeted effect in the leukemic blasts while sparing the normal bone marrow cells (Lancet et al., 2018). Most of those new drugs are limited in their application to a small range of conditions due to missing data and large-scale analyses which are currently running. Nevertheless, they are all essential contributions to the treatment and survival of patients, especially for those who are not suited for first-line therapy or relapsed from it.

1.3. Proteomics

1.3.1. Definition and methods

Proteomics arose in the late 1980th with the development of mass spectrometry and computational analysis methods. It became a crucial part of scientific and clinical research, leading to its designation as the Method of the Year 2012 by Nature magazine ("Method of the Year 2012," 2013). The discipline analyses structures and organisms by detecting their proteomic composition (Adhikari et al., 2020). Proteins represent the functional agents in a cell, fulfilling roles as membrane receptors, channels and markers, intracellular receptors, and mediators in signalling cascades, inducing, or inhibiting processes (Aebersold & Mann, 2016). On the other hand, genetic alterations can be observed on the protein level, due to the expression of altered or newly created proteins or by quantitative changes of specific proteins (Doll, Gnad, & Mann, 2019). Therefore mass spectrometry has reached a crucial position in clinical science and even started being included in patient care systems (Hernandez-Valladares, Bruserud, & Selheim, 2020). The significant progress in the understanding of genetics during the last decades showed the complexity of the processes occurring from the transcription of DNA to the synthesis and degradation of the resulting protein product. The first step encompasses the DNA transcription in the nucleus by an RNA polymerase leading to the primary messenger ribonucleic acid. The pre-mRNA is then spliced to remove intronic non-coding regions, reassembled, and reconnected in a highly controlled and specific manner to generate different isoforms. During this process, "Editing" of the mRNA is performed by exchanging single base pairs or building new links between coding areas. In the second step, protein synthesis is performed by RNA dependent Ribosomes that polymerize amino acids in a predefined order specified by the order of RNA base triplets (so-called codons) and respectively bound transfer ribonucleic acids (tRNAs) with the respectively bound amino acid. Posttranslational modifications are attached after protein synthesis in the endoplasmic reticulum, Golgi, and cytosol, depending on the subcellular localization of the protein to enable and control its function. Protein folding into a three-dimensional structure and conjugation of further molecules such as phosphorylation, acetylation, methylation, and glycosylation occur. All those modifications on the

transcriptional and posttranslational levels enable cells to obtain a broader diversity of proteins. Therefore, proteomics as a method of detecting and analysing the final gene products generates much more comprehensive and detailed information about the functional organism than the analysis of its genome (Nagaraj et al., 2011).

Two significant forms of proteomic methods can be distinguished: bottom-up analysis of whole proteomes and top-down- analysis of specific proteins. Whereas a top-down analysis is performed on entire proteins revealing their structure and configuration, the more common bottom-up analysis is performed on digested peptides lacking this information. On the other hand, detecting whole proteins via mass spectrometry is highly complicated and prone to error, especially in larger sized proteins, and is only suited for single-protein studies (Gregorich & Ge, 2014). The bottom-up analysis by data-dependent acquisition in mass spectrometry became the standard method for whole proteome analysis without a prior target definition. Digested peptides are identified using mass spectrometry, and the reconstruction of the initial protein is performed by computational evaluation of the peptides about standard databases (Dupree et al., 2020).

1.3.2. History and development of mass spectrometry

The beginnings of mass spectrometry reach back into the 19th century when crucial findings about the mass alterations of different atoms (later defined as atomic weight), their isotopes, and principles of the influence of magnetic fields on light and gas spectres were made (Audi, 2006). In 1918, the first modern mass spectrometer was built by Arthur Jeffrey Dempster, who combined an ion source in an electromagnetic field with a magnetic Sector-Analyzer, later enabling him to identify the Uranium isotope 235. In the coming decades, the method and devices were further developed, and numerous important findings of atomic isotopes were made (Rchardt, 1936). In 1953, the first quadrupole mass spectrometer was developed by Wolfgang Paul. It detected the mass-to-charge relation of flying ions and the first Ion-trap, fixing ions in a small space, enabling a more focused manipulation. A few years later, in 1959, mass spectrometry was used to identify proteins for the first time using the quadrupole method (Biemann, Gapp, & Seibl, 1959; Gohlke, 1959). The step from the initial detection of atoms to whole molecules presented new challenges, especially concerning the fragmentation and ionization process. On the one hand, only small volatile ionized particles can be detected by the mass spectrometer, on the other hand, harsh ionization processes, bursting molecules into small fragments are not suited for the reconstruction of the molecule later. Therefore, chemical ionization and tandem mass-spectrometry connecting two spectrometers through a collision-chamber and thermo-spray ionizations were developed, providing a gentler fragmentation and ionization of the molecules at a still high detection sensitivity. In proteomics, mainly electrospray ionization (ESI) and matrix-assisted laser desorption/ ionization (MALDI) are used nowadays (Yamashita & Fenn, 1984).

1.3.3. Modern proteomics

Many modern mass spectrometers specialized for different research purposes are used today. In biochemistry and medical proteomics, quadrupole-tandem mass spectrometers in combination with an Orbitrap became the most common technique (Michalski et al., 2011).

In 1999 Alexander Makarov developed the first Orbitrap mass-spectrometer, which consisted of a central spindle-shaped electrode inducing an orbit-like oscillation movement of the ions around it (Makarov, 2000). The underlying principle came from Ion-Cyclotron-resonance systems, which induce

molecular oscillations around a high-intensity magnet (up to 15 Tesla), allowing a new level of sensitivity and resolution in the measurement (Comisarow & Marshall, 1974; Muller, 1977). Nevertheless, this technique requires enormous technical resources to obtain such intense magnetic fields and adequate cooling systems. Therefore, Makarov designed the spindle-shaped electrode, inducing a similar flight trajectory of the molecules and allowing a comparable measurement result with fewer technical challenges. The ionized molecules are accelerated, decentrally injected, and an ion-trap is used for focused and non-continuous manipulations. The detectors register currents of moving ion packages induced by the moving molecules, increasing the sensitivity because the detection does not consume the molecule, which can be measured multiple times. The mass-to-charge ratio of the molecules can then be calculated using the frequency of their oscillation around the electrode by Fourier transformation.

Tandem mass spectrometry was initially performed by connecting two mass spectrometers with a collision filter to one another. The first analyser would detect the flight trajectory of the molecules and isolate single ones. Those would then be used for collision-induced dissociation with gas in the second analyser, forming smaller fragments for detection. Nowadays, the tandem mass spectrometry function is available in most single-device spectrometers, so that the connection of two devices isn't necessary anymore (Han, Aslanian, & Yates, 2008).

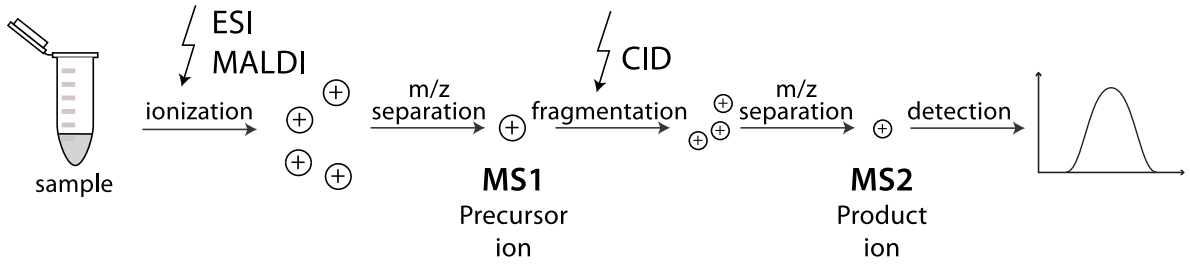

Figure 4: Mass spectrometric procedure, figure by Hannes Röst and M. Steiner, CC BY-SA 3.0

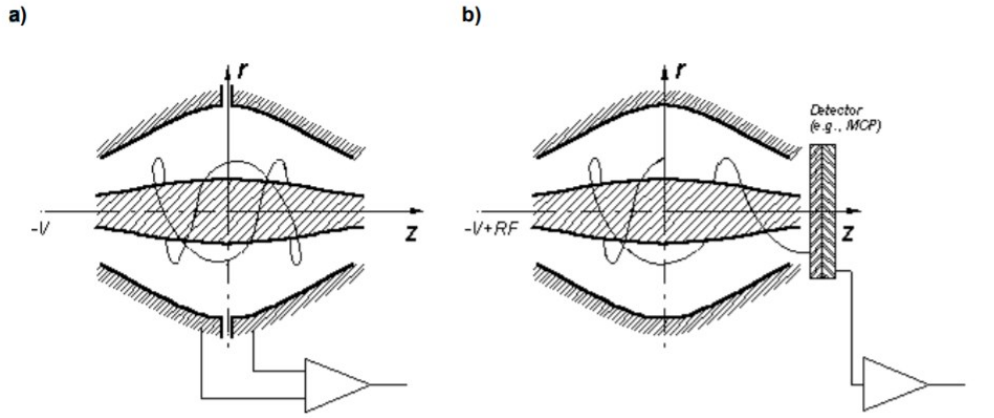

Fig.1. Mass analysis modes available in the Orbitrap: a) image current detection with FFT, b) mass-selective instability via parametric resonance

Figure 5: "The Orbitrap: a novel high-performance electrostatic trap" by Alexander Makarov, 2000

To enable the analysis of samples containing complex mixtures of molecules or peptides in proteomics, the mass spectrometer is connected to a high-performance liquid chromatography (HPLC) or gas-chromatography system, separating the different subgroups before being ionized and entering the mass spectrometer (Blakley, McAdams, & Vestal, 1978).

1.3.4. Advantages and difficulties

The method enables an insight into the whole proteome of a cell or organism, thus showing complete pathways and networks. Other current methods on the protein level, such as Western blot, only permit the detection of single, predefined proteins at once so that a broad range of interactions remain unseen. Cellular regulation mechanisms and the trajectory of whole pathways can be monitored and analysed. On the other hand, specific functional single proteins, which are highly altered, can be identified and investigated concerning their functional role in the cell (Ivanov et al., 2013). This also enables to detect changes and adaptations of organisms to specific circumstances or in comparison to their original tissue.

Nevertheless, the broad information range generated by each mass spectrometric measurement also presents challenges and pitfalls. Especially identifying crucial pathways and proteins is complex due to the widths of detected elements. Not every highly altered protein significantly affects the functional level (Dupree et al., 2020). On the other hand, the mere quantitative analysis of the proteome only captures some dimensions of cellular regulation mechanisms and functions. Countless posttranslational modifications such as methylations, phosphorylation, and other biochemical interactions are more complex to analyse via mass spectrometry. Nevertheless, new assays addressing these limits were developed over the last years, and we were able to perform a phosphorylation analysis in cooperation with the Bavarian mass spectrometry consortium. This allows us to depict a detailed picture of the activation state of crucial proteins, which is commonly mediated through phosphorylation (Ferries et al., 2017).

1.4. Research goal

This work focused on Acute myeloid leukaemia as one of the deadliest common cancer types, with an incidence of 4.1 cases per 100.000 persons in the U.S. (National Cancer Institute's Surveillance, Epidemiology and End Results Program). AML cells carrying a mutation in the receptor tyrosine kinase FLT3 correlate with even worse survival chances and aggressive disease progression. Various targeted therapies enabled improvements in the survival chances of these patients, albeit being limited by the development of resistance towards these therapies over time. Even though broad genetic analysis on AML nowadays is a central part of the diagnostic and clinical procedure, essential information concerning the development of resistance is still lacking — knowledge that remains crucial for the continuous improvement of treatment and survival of these patients. Therefore, we aimed to enlighten those poorly understood processes through a new approach. By performing a proteomic analysis through mass spectrometry, we further understood the whole biochemical system of leukemic cells. We evolved an *in vitro* model to generate resistant leukemic cells towards tyrosine kinase inhibitors to focus on this exact problem (see Chapter 2.1.). At the same time, our goal was to identify general processes which occurred in different cell lines with varying patterns of FLT3-mutation and under different tyrosine kinase inhibitor treatments. Those significant similar adaptations of the cells formed the base to identify potential treatment targets for tyrosine kinase inhibitor-resistant leukaemia.

2. Material and methods

2.1. Cell culture

2.1.1. General cell culture method

Equipment

Sterile Hood	Hera Safe, Heraeus
Incubator	Cytoperm 2, Heraeus
Water bath	Aqualine, Lauda
Centrifuge	4K15, Sigma
Light Microscope	TS100, Nikon Eclipse
Vacuum Pump	Hirschmann™ Pipetus™
Suspension culture flask 250 ml	658195, Greiner bio- one
6 well plates	657160, Cellstar
96 well plates	260860, Thermo Fisher Scientific

Media and Supplements

RPMI-1640- L-Glutamine medium	21875-034, GIBCO
Foetal Bovine Serum	10270-106, GIBCO
Penicillin-Streptomycin	15140-122, GIBCO

Cell lines

KG1α	Human, acute myeloblastic leukaemia without maturation	M1	DSMZ No: ACC421
Kasumi- 1	Human, acute myeloblastic leukaemia with maturation	M2	DSMZ No: ACC220
NB-4	Human, acute promyelocytic leukaemia	M3	DSMZ No: ACC207
OCI- AML5	Human, acute myelomonocytic leukaemia	M4	DSMZ No: ACC247
MV4-11	Human, acute monocytic leukaemia	M5	DSMZ No: ACC102
CMK	Human, acute megakaryocytic leukaemia	M7	DSMZ No: ACC392
Molm 13	Human, acute myeloid leukaemia	M5a	DSMZ No: ACC554

Table 4: Cell culture material

All manipulations are done under sterile conditions beneath the air flow hood. Culture is performed in the Cytoperm incubator at 37°C and 5% CO2. MV4-11 and Molm-13 cells are suspended in RPMI-1640- L-Glutamine medium, supplemented with 1% Penicillin-Streptomycin mix and 10% Foetal Bovine Serum. KG1α, Kasumi- 1, OCI- AML5, and CMK cells are suspended in RPMI-1640- L-Glutamine medium, supplemented with 1% (v/v) Penicillin-Streptomycin mix and 20% (v/v) Foetal Bovine Serum. The cells are cultured in 6 wells with 2ml or T75 Suspension culture flasks filled with 20ml completed medium. Medium and cells are refreshed and split every three days. Therefore, cells and medium are transferred into 50ml falcon tubes and centrifuged for 5 minutes at 600 g, room temperature. Fresh medium is preliminarily warmed up to 37°C in the water bath. The old medium is removed using a vacuum pump and sterile glass Pasteur pipette tips. With a small amount of fresh completed Medium, the cell pellet

is resuspended, split according to the cell count, and retransferred into the T75 flasks or 6 wells. Those are then filled up with the missing amount of completed medium.

For long-term storage, the cells are suspended in 90% (v/v) RPMI Medium + 10% (v/v) DMSO into 2ml volume and frozen at -80°C. Cells are defrosted under sight to start the culture and directly transferred into 20ml fresh warmed RPMI Medium. The tubes are then centrifuged at 600 g for 5 minutes at room temperature, and the further steps to discard the medium and suspend the cells into T75 flasks are performed as described before.

2.1.2. Treatment

	Drugs
Sorafenib	8705, Cell Signalling
Midostaurin hydrate	M 1323, Sigma Aldrich
Dimethyl sulfoxide	A994.2, Carl Roth
Bcl-2 inhibitor Venetoclax	ABT- 199, ADV465750285, Sigma Aldrich
Bcl- XL inhibitor WEHI539	21478, Cayman Chemical
JAK inhibitor I	420099, Sigma Aldrich

Table 5: Drugs for *in vitro* treatment

Treatment experiments are performed on MV4-11 and Molm-13 cells. $2*10^6$ cells are suspended in one T75 suspension culture flask filled with 20 ml RPMI-1640- L-Glutamine medium with 1% (v/v) Penicillin-Streptomycin mix and 10% (v/v) Foetal Bovine Serum. The needed volume of Medium is heated to 37°C, mixed with the corresponding amount of each drug inside 50ml falcon tubes, and then added to the cells. DMSO is used as a treatment control. The drug-supplied Medium is renewed every three days by exchanging the completed RPMI-1640- L-Glutamine medium and freshly adding the drug. After at least four weeks of treatment, and after the T75 culture flasks reach the needed cell counts again, the material is used for SPECS protocol, lysis, and further experiments.

2.1.3. Deep blue survival assay in 96-well format

	Material
Bcl-2 inhibitor Venetoclax	ABT- 199, ADV465750285, Sigma Aldrich
JAK inhibitor I	420099, Sigma Aldrich
Bcl- XL inhibitor WEHI539	21478, Cayman Chemical
Midostaurin 0,01mM	M 1323, Sigma Aldrich
Sorafenib 0,01 mM	8705, Cell Signalling
Dimethyl sulfoxide	A994.2, Carl Roth
Deep Blue Cell Viability™ Kit	424702, Biolegend
Elisa Reader	Infinite F200 Pro, Tecan

Table 6: Material for deep blue survival assay

Medium with the highest utilized concentration in the experiment is prepared. To obtain kill curves of the cell lines MV4-11 and Molm-13 for the different drugs (e.g., Sorafenib, Midostaurin, Venetoclax,

WEHI-539), geometrical 50% dilution steps are performed by mixing 2,5ml of the medium above containing the highest drug concentration with 2,5ml pure medium. This procedure is repeated until the lowest concentration needed is reached. For each concentration step, 100µl drug-containing medium and 15.000 cells are transferred to 96-wells in doublets. As a reference, standard curves with 7.500, 15.000, 30.000, 60.000, and 120.000 cells, and 15.000 cells in 100µl drug-free medium are transferred to the 96-well plates in doublets. The plates are then incubated for 48h at 37°C, 5% CO2. After these two days, 10µl of Deep blue resazurin dye is added to each well. The cells are incubated with the stain for four more hours at 37°C, 5% CO2. The extent of resazurin reduction and resofurin production, indicating the amount of metabolic active cells in each well, is then measured in an ELISA reader with a 590nm filter. The extinctions are then used to calculate the number of viable cells in each well, referring to the standard curve. Those cell counts are then compared to the untreated controls.

2.1.4. Cell lysis

Material

Phosphate buffered Saline	136mM NaCl, 12mM Na_2HPO_4, 1mM KH_2PO_4, 2mM KCl
STET lysis buffer	50 Mm Tris pH 7,5, 150mM NaCl, 2mM EDTA, 1% Triton X
Tris Lysis buffer	50mM Tris pH 7,4, 150mM NaCl, 1% Triton X
Magnetic stirrer	RCT Basic, Ika Labor Technik
Tabletop centrifuge	5430R, Eppendorf
NaCl	S7653, Sigma Aldrich
Na_2HPO_4	255793, Sigma Aldrich
KH_2PO_4	1551139, Sigma Aldrich
KCl	P9333, Sigma Aldrich
Tris	93362, Sigma Aldrich
Triton X	108603, Merck
Sodium Orthovanadate	S6508, Sigma Aldrich

Table 7: Material for cell lysis

Cells and medium are transferred into a 50ml falcon and centrifuged for 5 minutes at 600 g and room temperature. The old medium is removed using a vacuum pump and sterile glass Pasteur pipette tips, and the cell pellet is resuspended in a smaller volume of the fresh, completed medium. 10 µl of the cells are pipetted on a Neubauer cell counting chamber and counted under the light microscope. According to the cell concentration, 3 - $5*10^6$ cells are transferred into 2ml Eppendorf tubes, then centrifuged for 5 minutes at 600 g and 4°C. All cell lysis steps are performed on ice, with buffers and centrifuge tempered at 4°C. The Medium is discarded, and the cells are resuspended in 500µl cold phosphate-buffered Saline, then centrifuged again as described above. After this washing step, the PBS is discarded, the cells are resuspended in 500µl STET lysis buffer and incubated for 10 minutes on ice. The cells are then centrifuged at 18 000 g, and the supernatant, corresponding to our lysate, is transferred into fresh 1,5ml Eppendorf tubes, and stored at -20°C. The same protocol is applied for phosphatase-inhibited lysis using Tris EDTA free lysis buffer, substituted with 2mM Sodium orthovanadate.

2.2. Protein detection experiments

2.2.1. ELISA protein concentration measurement

Material

96-well Plates	144895, Thermo Scientific
BSA Standard	141305, G Bioscience
Red 660 Protein Assay	015R, G Bioscience, 660nm
Elisa Reader	Infinite F200 Pro, Tecan
Magellan™ Software	Tecan

Table 8: Material for ELISA protein concentration measurement

A reference standard with protein concentrations of 0 µg/µl; 0,125 µg/µl; 0,25 µg/µl; 0,5 µg/µl; 1 µg/µl and 2 µg/µl is created by making a geometrical serial dilution of BSA 2 µg/µl in water. 10µl of each concentration is transferred in doublets into a 96-well plate to generate a standard curve. 10µl of each sample is transferred in doublets to the 96-well plate. 200 µl of Red 660 Protein Assay are pipetted into each filled well and two blank wells to define the background absorbance. The ELISA Reader assay is performed after defining the measurement parameters in the Magellan Software. Standard parameters used: orbital shaking 5 seconds, wavelength 660nm, Standard curve wells definition with corresponding concentrations, µg/µl as a unit, blank definition, sample definition incl. replicates, blank reduction, Standard curve generated as linear regression. The measured absorbance data is processed in Excel. Each sample's protein amount is calculated using the gradient coefficient of the standard linear curve (f = a*x + b) and forming the average of the duplicates.

2.2.2. SDS Gel page preparation for electrophoresis

SDS gel page material

Acrylamide 40%	T802.1, 40%, ROTH
Lower Tris Buffer	1,5 M Tris pH 8,8, 0,4% SDS
Upper Tris Buffer	0,5 M Tris pH 6,8, 0.4% SDS
TEMED	2367.3, ROTH
APS	Ammonium persulfate, A3678, Sigma Aldrich

Table 9: Material for SDS gel page preparation

Gel types	6% Gel	8% Gel	10% Gel	12% Gel	15% Gel
Separation Gel					
ddH_2O	19,2 ml	17,6 ml	16 ml	15 ml	12 ml
Acrylamide 40%	4,8 ml	6,4 ml	8ml	9 ml	12 ml
4×Lower TRIS	8 ml	8 ml	8 ml	8 ml	8 ml
TEMED	60 µl	60 µl	60 µl	60 µl	60 µl
APS (10%)	60 µl	60 µl	60 µl	60 µl	60 µl

Stacking Gel					
ddH_2O	13 ml	13 ml	13 ml	13 ml	13 ml
Acrylamide 40%	2,6 ml	2,6 ml	2,6 ml	2,6 ml	2,6 ml
4×Upper TRIS	5 ml	5 ml	5 ml	5 ml	5 ml
TEMED	60 µl	60 µl	60 µl	60 µl	60 µl
APS (10%)	60 µl	60 µl	60 µl	60 µl	60 µl

Table 10: Mixture of SDS gel page preparation

The gel is prepared using the clear Bio-Rad scaffolds completed with Bio-Rad rubber cushions on the ground in the pre-formed shape to prevent the leaking of the fluids before the polymerization of the gel occurs. Two corresponding glass plates are matched and placed into the green Bio-Rad holder. The Glass-holder-construction is fixed into the clear scaffold by clamping it between the clear holding arm and the plastic cushion. Separation gel is prepared according to the concentration table above, and 7,5ml of the mixture is filled into each glass construction. 200µl of Isopropanol is added on top of the separation gel to remove air bubbles and seal it. After 15 minutes, the polymerization of the separation gel is completed, and the Isopropanol can be removed using a paper towel. The stacking gel is mixed as described in the table above and pipetted into the glass construction until it is filled. Bio-Rad well combs are fixed inside the stacking gel, which can be removed after another 15 minutes once the gel gets solid and the wells are correctly formed.

2.2.3. Gel electrophoresis

Electrophoresis material	
Electrophoresis System	Mini-Protean System, Bio-Rad
Power supply	Powerpac 300 HC, Bio-Rad
Vortex	VF2, Ika Labortechnik
Heater	Thermomixer C, Eppendorf
Reducing Laemmli protein sample buffer	8% SDS, 40% Glycerol, 10% DTT, 125mM Tris pH 6.8, 0.025% Bromophenol Blue
Non-reducing protein sample buffer	8% SDS, 40% Glycerol, 125mM Tris pH 6.8, 0.025% Bromophenol Blue
SDS Running Buffer	25mM Tris, 192mM Glycine, 0,1% SDS
MW marker	See blue plus 2, LC5925 Invitrogen

Table 11: Material for SDS gel- electrophoresis

The same protein amount of each sample is transferred into Eppendorf tubes, and the reducing or non-reducing Sample buffer is added in a 1:3 proportion (15µl sample + 5 µl sample buffer). Each tube is vortexed for a few seconds and cooked 5 minutes at 95°C. The SDS Gel Page is mounted in the Mini Protean Gel running system and filled with an SDS running buffer. The molecular weight marker and the samples are loaded in the wells and connected to the power supply at 80V. After overcoming the wells and the stacking gel, the tension is upregulated to 120V until the samples run through the whole gel.

2.2.4. Western Blot

Western Blot Material

Blotting system	Mini-Protean system, Bio-Rad
Power supply	Powerpac 300 HC, Bio-Rad
Sponges and Transfer Cassettes	Bio-Rad
Filter Papers	A. Hartenstein
Nitrocellulose membranes 0.45µm	1228243, GVS North America
Transfer Buffer 1x	25mM Tris, 240 mM Glycine
Tween20	P1379, Sigma Aldrich
PBS-Tween	136mM NaCl, 12mM Na_2PO_4, 1 mM KH_2PO_4, 2mM KCl, pH 7,4 + 1% Tween20
Blocking Buffer	5% Skim milk powder (70166, Sigma Aldrich) dissolved in PBS-Tween
I-Block™ Protein-Based Blocking Reagent	T2015, Thermo fisher, 0,2% in PBS Tween

Table 12: Western Blot Material Part 1

The Mini-Protean blotting system is filled with transfer Buffer, and a Bio-Rad cool pack is placed inside the case. The transfer cassettes are placed in the transfer buffer and mounted, beginning from the black side. Every layer of the blotting unit is soaked in transfer buffer and adapted using a plastic roll to avoid air bubbles between the layers. A sponge and two pieces of filter paper are placed above each other on the black side of the cassette. The SDS gel page from the previous electrophoresis is separated from the stacking gel part, placed on the filter paper, and covered with a Nitrocellulose membrane. Another two filter papers and a sponge are added, and the transfer cassette is closed. Every cassette is placed inside the Mini-Protean blotting system and connected to the Powerpac, with an intensity of 0,4 A per system for at least 1 hour and 5 minutes.

2.2.5. Antibody mediated protein detection

Material

50ml tube roller	RS- TR05, Phoenix instruments
Horizontal shaker	Edmund Buehler GmBH
PBS-Tween	136mM NaCl, 12mM Na_2PO_4, 1 mM KH_2PO_4, 2mM KCl, pH7.4 + 1% Tween20
Western Blot Developer	Amersham Imager 680, GE Lifesciences
Development films	Super RX- N, 47410 19289, Fujifilm
ECL Protein detection reagent	RPN2106V2, GE Healthcare
Primary antibody suspensions	10 ml of PBS + 1% Tween with 0,5% BSA (A2153 Sigma Aldrich) and 50 µl Sodium acid Or 10 ml of 10% Semi-skimmed milk powder in PBS + 1% Tween with 50 µl Sodium acid
Secondary antibody suspension	10 ml 10% Semi-skimmed milk powder in PBS+ 1% Tween
ImageJ™ quantification software	National Institute of Health (USA)

Table 13: Western Blot Material Part 2

Primary Antibodies	Species	Dilution	Product
FLT3	mouse	1 : 500	SC19635, Santa Cruz
FLT3	rabbit	1 : 1 000	3462, Cell Signalling
P-FLT3 Kit	rabbit	1 : 1 000	12596, Cell Signalling
CD84	goat	1 : 1 000	AF1855, RnD Systems
ß-Actin	mouse	1 : 5 000	A5441, Sigma Aldrich
ICAM3	sheep	1 : 10 000	AF715, RnD Systems
Plexin A1	goat	1 : 1 000	AF4309, RnD Systems
APLP2	goat	1 : 1 000	AF4945, RnD Systems
STAT5a	mouse	1 : 1 000	MAB2174, RnD Systems
STAT5b	mouse	1 : 1 000	MAB1584, RnD Systems
P-STAT5 Y694/Y699	rabbit	1 : 1 000	MAB41901, RnD Systems
Bcl- 2	mouse	1 : 1 000	15071, Cell Signalling
Bcl- XL	rabbit	1 : 1 000	2764, Cell Signalling

Secondary Antibodies	Dilution	Product
Anti-mouse HRP	1 : 4 000	W402B, Promega
Anti-rabbit HRP	1 : 4 000	W401B, Promega
Anti-goat HRP	1 : 4 000	SC 2020, Santa Cruz
Anti-sheep HRP	1 : 4 000	HAF 016, RnD Systems

Table 14: Primary and secondary antibodies for Western Blot

When the blotting transfer is completed, the membrane is blocked for 1 hour in the blocking buffer. The blocking buffer is discarded, and the membrane is washed with PBS + 1% Tween three times for 5 minutes at 250 movements per minute on the horizontal shaker. The membrane is then added to the primary antibody and incubated overnight at 4°C with gentle shaking on the roller.

The membrane is removed from the primary Antibody solution and washed three times for 5 minutes at 250 movements per minute on the horizontal shaker with PBS + 1% Tween. The corresponding secondary Antibody is added to the membrane and incubated for one hour at room temperature with gentle horizontal shaking (100 movements per minute). The secondary antibody is discarded, and the membrane is washed three times for each 5 minutes at 250 movements per minute on the horizontal shaker with PBS + 1% Tween. 2ml of ECL Protein detection reagent is added to the membrane, distributed over the whole surface, and incubated for 5 Minutes. The membrane reactions are developed on a Fujifilm and analysed using ImageJ Western blot quantification software.

2.3. Mass spectrometry

2.3.1. SPECS Glycoprotein detection protocol

Material	
N-azidoacetylmannosamine tetraacylated sugar (ManNaz)	provided by Stefan Brase

DBCO-Sulfo-Biotin	(50 mM stock solution) CLKA116-10, Jena Bioscience
High-capacity streptavidin agarose beads	20361, ThermoFisher
Polyprep Columns	731-1550, Bio-Rad
PBS + 2% SDS	136mM NaCl, 12mM Na_2PO_4, 1 mM KH_2PO_4, 2mM KCl, pH 7,4
Lysis Buffer	50 mM Tris, 150 mM NaCl, 1% Triton Lysis Buffer, pH 7,4
PVDF Filters 0.45 µm	SLHV033RS, Millex

Table 15: SPECS protocol material

Metabolic labelling:
40 million cells are transferred into one T75 flask and suspended in 20ml RPMI Medium + 10% (v/v) FBS and 1% (v/v) penicillin/streptomycin, supplied with 100µM of ManNaz sugar for each flask. The standard drug and dose are also applied to the medium when the cells are part of a treatment experiment. ManNaz sugar and cells are incubated for two days to allow the metabolism of the sugar. After the incubation, cells and medium are transferred into 50 ml falcon tubes and centrifuged for 5 minutes at 600 g and room temperature. The supernatant is discarded from the cell pellet and filtrated through a 0,45µm PVDF Filter to remove cell debris and impurities for future use as a Secretome analysis sample. The filtered Medium is stored in the freezer at -20°C.

Biotin-mediated Click- chemistry reaction:
The cell pellet is resuspended in 1ml cold PBS, transferred into 1,5ml Eppendorf tubes, and placed on ice for the next steps. The cells are centrifuged for 5 minutes at 600 g and 4°C and the PBS is discarded. 2µl of the 50mM DBCO-Sulfo-Biotin stock solution is added into 1ml of cold PBS for each Eppendorf tube, and the cell pellets are resuspended with the solution. Cells and Biotin are incubated for 2 hours on ice to mediate the Click-chemistry reaction of ManNaz sugar and Biotin. After incubation, the cells are centrifuged for 5 minutes at 900 g and 4°C, and the PBS- Biotin solution is discarded.

Washing steps and Lysis:
To outwash non-linked click reagents, the cell pellet is resuspended in 1 ml cold PBS and centrifuged for 5 minutes at 900 g and 4°C. The PBS is removed, and the cells are resuspended in 5ml lysis buffer. The cells are incubated for 15 minutes on ice with the buffer to ensure complete lysis. The falcon tubes are then centrifuged for 5 minutes at 18 000 g and 4°C, and the lysate is separated from the remaining cell debris. To ensure the purity of the lysates, each one is filtered through a 0,45µm PVDF Filter into new falcon tubes using a 5 ml syringe. The protein concentration of the lysates is measured with the ELISA Reader and a Red 660 BCA assay, as described in Chapter 2.2.1.

Streptavidin pull-down:
Polyprep- columns are placed inside the corresponding Bio-Rad wrack, and the plastic ends are removed and replaced by the yellow Bio-Rad caps. 300µl of high-capacity binding Streptavidin beads are filled into each column after meticulous vortexing and shaking the bead bottle and using a cut pipette tip. 5 ml of PBS + 2% (v/v) SDS are added on top of the beads and run through by removing the yellow caps. Hereby, all beads are placed on the ground of the column filter and washed. 15ml falcon tubes are placed underneath the columns to collect the next flow-through, then the lysates are filled into the columns according to their protein concentration (same protein amount in each column). When the flow-through is completed, the procedure is repeated with the collected lysate inside the 15 ml falcon tubes to maximize the protein binding of the beads. The part of the lysate which did not bind to the Streptavidin beads corresponds to the non-glycosylated fraction of the proteome and can be used for whole proteome analysis assays (storable at -20°C). To eliminate non-specifically bound

proteins from the Streptavidin beads, 10 ml of PBS + 2% (v/v) SDS are filled into the Polyprep-columns and run through. This washing step is repeated two more times. By using the yellow Bio-Rad caps, the Polyprep-columns are sealed, and the beads are transferred into 1,5 ml Eppendorf tubes, suspended in 900µl PBS + 2% (v/v) SDS. The transfer is performed in 3 steps with 300µl of PBS + 2% (v/v) SDS each, using the same cut pipette tip and rinsing the column walls to avoid any loss of beads. To dry out the beads from the PBS + 2% SDS, the Eppendorf tubes are centrifuged for 5 minutes at 18 000 g at room temperature. A major part of the supernatant is discarded using a pipette, and the rest of the liquid in between the beads is removed by placing the tip of a Hamilton syringe at the bottom of the tubes and soaking out the PBS + 2% SDS remains. The beads can be stored at -20°C until further processing.

2.3.2. SP3 Protocol

Material

Magnetic rack	Dynamag 2 Invitrogen, Thermo Fischer
Sera- Mag speed Beads A and B	A: 9601011, B: 9666073; GE Healthcare
DTT	R0862, Thermo Fisher
Ammonium bicarbonate	BCBP1703V, Sigma Aldrich
Iodoacetamide	SLBJ8175V, Sigma Aldrich
100% Acetonitrile	SZBF290BV, 34967, Sigma Aldrich
Ethanol 70%, ultra-pure	1.00983., Merck
Chromasolv Water	Gradient grade, VWR chemicals
Trypsin 0,1µg/µl	V511A, Promega
LysC 0,1µg/µl	V1671, Promega
AmBic 50mM Solution	0,2g AmBic in 50ml chromasolv water
IAA 400mM Solution	0,147g IAA in 2ml 50mM AmBic solution

Table 16: SP3 protocol material

Bead preparation:
20µl of Sera-Mag A and 20µl of Sera-Mag B beads are transferred into a 1,5ml Eppendorf with cut pipette tips. 160µl of distilled water are added to the beads, then placed into the magnetic rack and left for 2 minutes until all beads are attached to the wall. The supernatant is discarded, and the beads are taken off the magnetic rack. 200µl chromasolv water is used to wash the beads by pipetting a few times. The beads are then placed back into the magnetic rack, and the supernatant is discarded. The washing step is repeated two more times. 100µl of chromasolv water is used to resuspend the beads at the end and to store them in the fridge at 4°C.

Establishing the binding conditions:
This method refers to 50µl samples containing 20µg of protein. If the protein concentration differs, the amounts of reagents until the binding of the beads must be adapted. 0,5µl of 1M DTT is added to the sample, vortexed, and incubated for 10 minutes at 50°C. 5µl of IAA Solution is added to the sample, vortexed, and incubated for 30 minutes at room temperature in the dark (IAA is light sensitive). To quench the sample afterwards, 1µl of DTT is added.

Binding:
120µl of 100% ACN are added to the samples to reach a final 66% v/v ACN concentration, as well as 4µl of the prepared Sera Mag A and B beads. To ensure a complete binding, the samples are vortexed for a few seconds and incubated for 30 minutes on the horizontal shaker at 100 movements per minute

and room temperature. Once the binding is performed, the tubes are placed into the magnetic rack, and the supernatant corresponding to the post-binding fraction is transferred into new tubes.

Bead washing:
To eliminate all non-specific protein bindings at the beads, 400µl of 70% Ethanol is pipetted over the bead pellet attached to the magnetic rack and discarded after 30 seconds. The Ethanol washing is repeated one more time. Then 400µl of 100% ACN is added over the bead pellet and discarded after 15 seconds. The ACN washing step is repeated twice, and all the ACN rests are discarded.

On Bead digestion:
A digestion buffer containing 4µl Trypsin (0,1µg/µl), 4µl LysC (0,1µg/µl), 5µl AmBic 400mM Solution, and 37µl chromasolv water for each sample is prepared, according to the number of tubes needed. The tubes are removed from the magnetic rack, and the beads are extensively suspended and mixed with the digestion buffer. The solution is then incubated overnight on the Thermoheater at 37°C.

Elution:
The samples taken from the Thermoheater are centrifuged for 10 seconds on the table-top centrifuge to collect all fluid at the bottom of the tube and are then placed inside the magnetic rack. The supernatant corresponding to the digested peptides and the final sample are transferred into new tubes. The peptide concentration of each sample is detected by NanoDrop technology.

2.3.3. Analysis of phosphorylated proteome

To gain a deeper insight into the functional protein-mediated processes of the cells, we performed a phosphorylated protein detection mass spectrometry in cooperation with Prof. Bernhard Küster and the laboratory of Proteomics and Bioanalytic at the Technical University of Munich. Cells were cultivated, treated, and lysed, as described in Chapter 2.1. The lysates were then sheared of DNA and cell debris via sonication in 30 cycles, alternating 30 seconds of sonication and 30 seconds of pauses with a Bioruptor Pico (Diagenode). Protein digestion of cell lysates and TMT labelling were further manipulated and analysed according to the protocol workgroup Protocol (Kuster, 2019).

2.3.4. Mass spectrometric measurement

Material	
Q- Exactive™ Hybrid-Quadrupole-Orbitrap mass spectrometer	Thermo Fisher Scientific
Easy nLC 1000 nano ultrahigh performance liquid chromatography system	UHPLC, Proxeon
Nanospray Flex™ ion source	Thermo Fisher Scientific
Column Oven	PRSO-V1, Sonation
C18 Resin, ReproSil-Pur 120	C18-AQ, 1.9µm, Dr. Maisch
30 cm Columns	FS360-75-8-N-S-C30, New objective

Table 17: Mass spectrometry equipment

Samples were analysed with a Q-Exactive Hybrid-Quadrupole-Orbitrap mass spectrometer coupled to a Nanospray Flex ion source with a heat-regulating column oven and an Easy nLC 1000 nano ultrahigh performance liquid chromatography system. 1µg of peptides per sample was separated on custom

packed C18 columns (30 cm x 75 µm, Dr. Maisch) using a binary reverse phase gradient of water (A) and acetonitrile (B) supplemented with 0.1% formic acid inside the column oven adjusted at 50°C. Full mass spectrometer scans were acquired at a resolution of 70.000 and an m/z range of 300-1400 (AGC target: 1E+5). Subsequently, the top 10 most intense peptide ions were chosen for higher-energy collision-trapped Dissociation (HCD). These spectres were detected with a resolution of 17.500, an isolation width of 2 m/z (AGC target: 1E+5, NCE: 25%). A dynamic exclusion of 120s was applied to the detected fragments.

2.3.5. Data analysis

Software

Thermo XCalibur 3.1.66.10	Thermo Fisher Scientific Inc.
MaxQuant 1.6.6.0	Computational Systems Biochemistry
missForest 4.6-14	Computational Systems Biochemistry
ClusterProfiler 3.14.3	Computational Systems Biochemistry
R Version 3.6.3	R Core Team
Cytoscape 3.8.0	National Resource for Network Biology

Table 18: Software for Data processing

General Mass spectrometry

Analysis of raw data files, including protein identification and label-free quantification, was performed with MaxQuant (Version 1.6.6.0) using a reviewed Uniprot Fasta database (13.12.2019) as a reference and the following search settings in MaxQuant: Mass tolerance first Search 20ppm, mass tolerance main search 5ppm, static modifications = Carbamidomethylation, Variable Modifications = acetylation of protein N-terminus, Methionine oxidation. The false discovery rate for peptide/protein identification was set to 0,1% on the peptide and protein level. All experimental conditions were repeated with at least four biological replicates except for MV4-11 control cells (7 replicates). Statistical analysis was performed using R (Version 3.6.3). Missing values of mass spectrometry data were defined as missing not at random (MNAR) when all four biological replicates of one condition (for example, Control) were missing but not detected or detected in only one replicate of the other condition (For example, Midostaurin treatment) or vice versa for every experimental set up (MV4-11 Sorafenib resistant vs. Control, MV4-11 Midostaurin resistant vs. Control, Molm 13 Midostaurin resistant vs. control, Molm-13 Sorafenib resistant vs. Control). Missing values of all other protein groups were defined as missing at random, which were imputed with the package missForest (Version 4.6-14). The MNAR values were subsequently imputed with the package GSimp (Wei et al., 2018). The package ClusterProfiler (Version 3.14.3) was used to perform and visualize an enrichment analysis on the significantly changed protein groups using the KEGG pathway database for cluster and protein-protein network analysis. The mass spectrometry proteomics data have been deposited to the ProteomeXchange Consortium via the PRIDE partner repository with the dataset identifier PXD022188 [**Reviewer Login Credentials**: Username: reviewer_pxd022188@ebi.ac.uk, Password: ZvAZ0Dqh]

Phospho-proteomics analysis

Peptide identification and quantification were performed using MaxQuant (version 1.6.6.0) with its built-in search engine against the human reference proteome (Uniprot Fasta database,13.12.2019). Carbamidomethylated cysteine was set as a fixed modification, and methionine oxidation and N-terminal protein acetylation as variable modifications. Trypsin/P was specified as the proteolytic

enzyme. The precursor tolerance was set to ± 4,5ppm, and fragment ion tolerance to ±20ppm. A false discovery rate of 1% was used on a peptide spectrum match. Three replicates were conducted for each experimental condition. Statistical analysis was performed using R (Version 3.6.3), and the missing value was imputed as described above. To derive the actual quantification of functional genes in metabolic and function pathways, impacts of identified genes on protein level were subtracted from raw data of phosphorylated peptides. In detail, normalization of the intensity of phosphorylated peptides after imputation was conducted as following steps: (1) Ratio of FC_{TMT} (fold change of phosphorylated peptides data) = raw TMT labelling data of each replicate for individual condition / mean value of control groups, (2) Mean $FC_{protein}$ (mean fold change of proteins expression) = mean protein expression value of each condition group / mean protein value of correspondent control group, (3) Normalized FC_{TMT} = Ratio of FC_{TMT} / Mean $FC_{protein}$. (4) Occupation = Log_2 transformation of normalized FC_{TMT}. Normalized FC_{TMT} was used for further P-value calculation and downstream statistical analysis, such as activated kinases prediction and enriched pathways, which was conducted and visualized with PhosR (1.4.0) package with slight modification on the pipelines.

3. Results

3.1. Mass spectrometric analysis

3.1.1. Procedure and treatment validation

We performed broad mass spectrometric measurements and analysis to enlighten the proteomic changes of leukemic cell lines developing resistance towards a tyrosine kinase inhibitor treatment. As further described in the Method chapter (2.1.), FLT3 mutated AML cell lines MV4-11 and Molm-13 were chronically treated with the multityrosine-kinase inhibitors Sorafenib or Midostaurin. As a treatment control, the same cell lines were treated with DMSO as solvent control under the same conditions and time. After a few weeks, resistance manifested in a rise of cell count in prior strongly decimated cell lines due to the treatment and increased metabolic activity seen in the turnover of the culture medium. Interestingly, Molm-13 cells did not respond to the therapy with Sorafenib like with Midostaurin. Cells did not undergo a strong apoptosis process and were not decimated under the regular treatment dose. Therefore, no resistance development occurred due to the lack of survival mechanism selection. Treated cells and their corresponding treatment controls were processed with the single pot, solid-phase enhanced sample preparation method to generate tryptic peptides for mass spectrometry. The resulting peptides, corresponding to the total cell proteome, were measured label-free in an Orbitrap mass spectrometer.

To identify crucial and general proteome alterations, we started with a broad overview analysis to identify similarities and differences between our experimental groups. We then focused on significant similar changes in all TKI-treated samples and placed them in relation to intracellular pathways and metabolic functions. Hereby, we were able to identify the regulation of whole pathways that might contribute to Midostaurin\Sorafenib resistance.

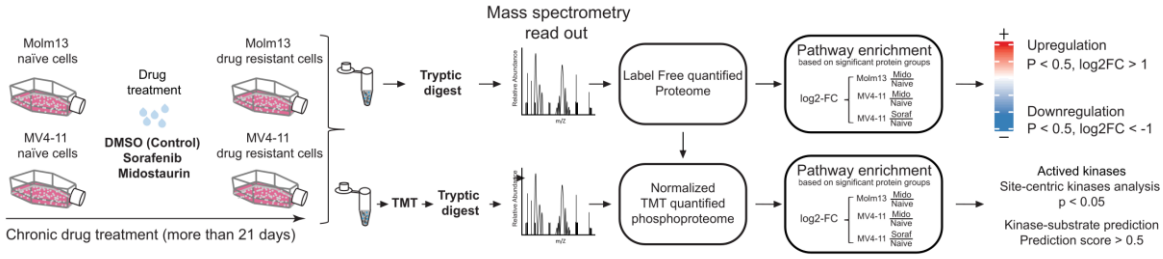

Figure 6: Generation and characterization of TKI resistant Molm-13 and MV4-11 cell pools and general proteome and phosphoproteome analysis workflow.

The spectres of intact peptides (MS1) and fragmented peptides after collision (MS2) were measured with a tandem Quadrupol-Orbitrap mass spectrometer. These raw data sets (MS1 and 2) were then processed in a label-free quantification algorithm to normalize and identify the corresponding peptide. The peptides were quantified by integrating the m/z ratio and the number of detected peptides during this specific peak. In a second step, a phosphoproteome analysis was performed by the Bavarian mass spectrometry consortium, using TMT- labelling for quantification.

To validate the tyrosine-kinase-inhibitor (TKI) resistance upon chronic TKI treatment of leukemic cell lines, we performed a 96-well, Alamar Blue based survival assay. The concentration range tested on the different cell types went from 0 nM to 120nM for Molm-13 and 480nM for MV4-11 cells.

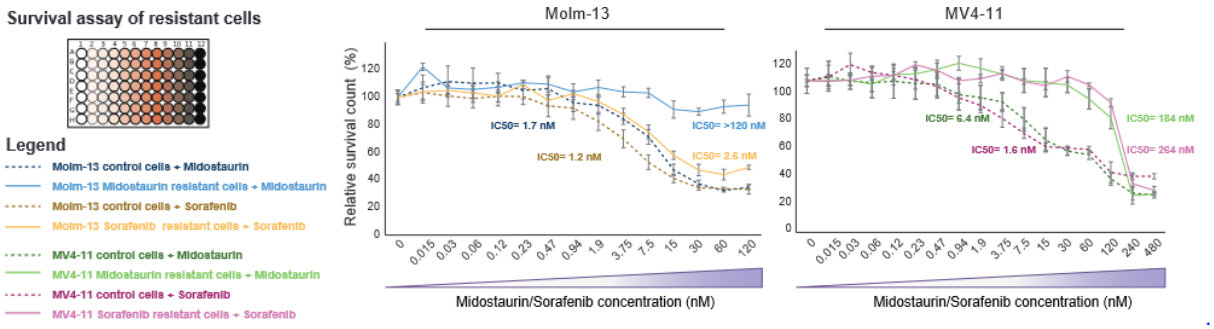

Figure 7: Survival assay of Midostaurin- or Sorafenib-resistant Molm-13 and/or MV4-11 cells applied with increasing concentrations of Midostaurin and Sorafenib. The cell viability was quantified by an AlamarBlue assay, and the $IC_{50,}$ defined as drug concentration lowering cell survival by 50%, was calculated. The dark blue line represents Molm-13 control cells (drug naïve) treated with Midostaurin and the lighter blue line Midostaurin resistant Molm-13 cells treated with Midostaurin. The dark and light orange lines represent Molm-13 control and Sorafenib-resistant Molm-13 cells respectively, treated with Sorafenib. The dark and light green lines represent MV4-11 control and Midostaurin-resistant MV4-11 cells respectively, treated with Midostaurin. Dark and light purple lines represent MV4-11 control and Sorafenib-resistant MV4-11 cells respectively, treated with Sorafenib. In MV4- 11 drug-resistant cell lines an increase of the needed IC_{50} dose to 183nM Sorafenib and 264nM Midostaurin was seen. In the Molm-13 cell line, as described before, only a substantial rise in the IC_{50} up to 120 nM in Midostaurin resistant cells was seen.

As seen in the curves above, we observed a significant difference in the effectiveness of Sorafenib and Midostaurin on cell survival between treatment naïve and chronically TKI-treated MV4-11 and Molm-13 cells. Whereas Molm-13 Midostaurin-resistant cells did not show a relevant impairment in cell survival until a Midostaurin concentration of 120nM, their treatment naïve counterparts were inhibited by concentrations starting at 1,9nM. As described above, drug resistance could not be acquired in Molm-13 cells using Sorafenib, explaining their similar reaction towards the inhibitors as the non-resistant Molm-13 cells. For the MV4-11 cell line, cell survival of chronically TKI-treated cells was significantly higher towards higher Midostaurin\Sorafenib concentrations than in treatment naïve MV4-11 cells. Here the IC_{50}s were elevated from 6.4 to 183 nM Midostaurin and from 1.6 to 264nM Sorafenib in the respective resistant cells. These survival assays enabled us to validate our treatment experiment and the gained tyrosine kinase inhibitor resistance we aimed to analyse.

3.1.2. Heatmaps of all detected proteins

We generated an overview of the proteomic changes in the different cell lines and treatment groups, visualized in a colour-coded heat map (Figure 8). Hierarchical clustering was applied to the expression values of all detected proteins, which resulted in a clear separation of all our experimental groups (Molm-13 naïve, Molm-13 Sorafenib resistant, Molm-13 Midostaurin resistant, MV4-11 naïve, MV4-11 Sorafenib resistant, MV4-11 Midostaurin resistant. This overview showed substantial differences in the proteomic profiles between TKI-treatment naïve and resistant cells. Only Molm-13 cells treated

with Sorafenib showed similar patterns to their untreated controls. However, this observation was in good accordance with the behaviour of Molm-13 cells, lacking a reduction of cell viability under treatment. This reaction was opposite to the samples which received a Midostaurin treatment. Midostaurin induced high death rates despite a lower drug concentration, presenting a strong hurdle to developing resistance. Those blasts which successfully acquired resistance after some time showed substantial alterations in their proteomic profile, often similar to the resistant MV4-11 cells. This divergent reaction of Molm-13 cells towards the two applied tyrosine kinase inhibitors may originate from the mutational FLT3 profile of this cell line, which is heterozygote for the ITD mutation. These relations will be further discussed (Chapter 4.). Due to the weak reaction of the Molm-13 Sorafenib-treated cohort, we excluded it from further comparative analyses and only considered the Midostaurin-treated Molm-13 cells as part of the TKI-resistant group.

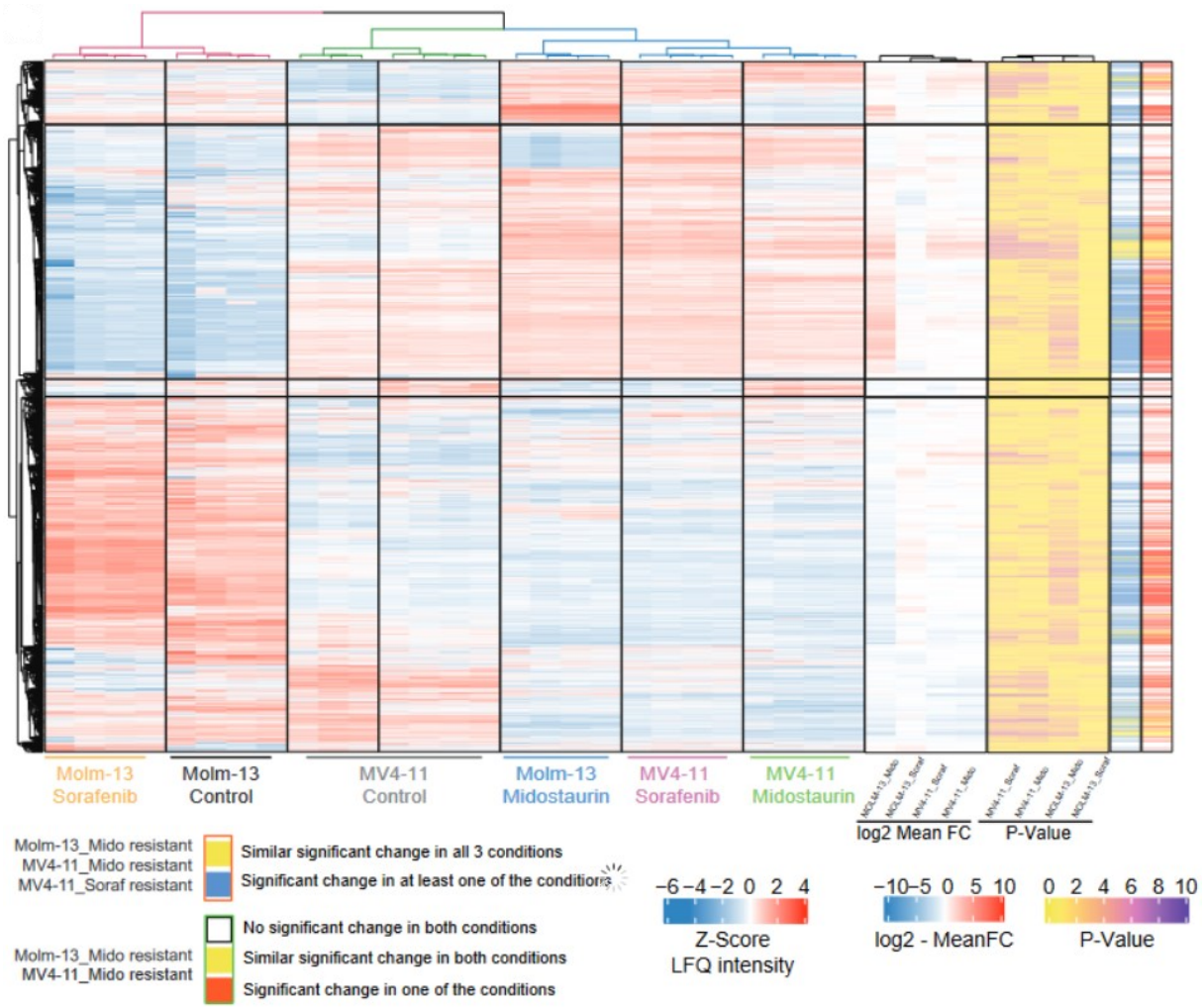

Figure 8: Heat map of protein expression for all experimental conditions. Heatmap of all quantified proteins in Midostaurin-\Sorafenib-resistant or treatment naïve Molm-13 and MV4-11 cell pools receiving either Midostaurin, Sorafenib, or a treatment control (4 biological replicates of each group). Z-scores are displayed in a heatmap with blue indicating a downregulation and red indicating an upregulation in protein expression. The relative mean log2-fold protein expression change in resistant cell pools is shown on the right side compared to their control cell pools. Next, the -log10 transformed calculated p-values are visualized with purple indicating a highly significant change and yellow an insignificant one.

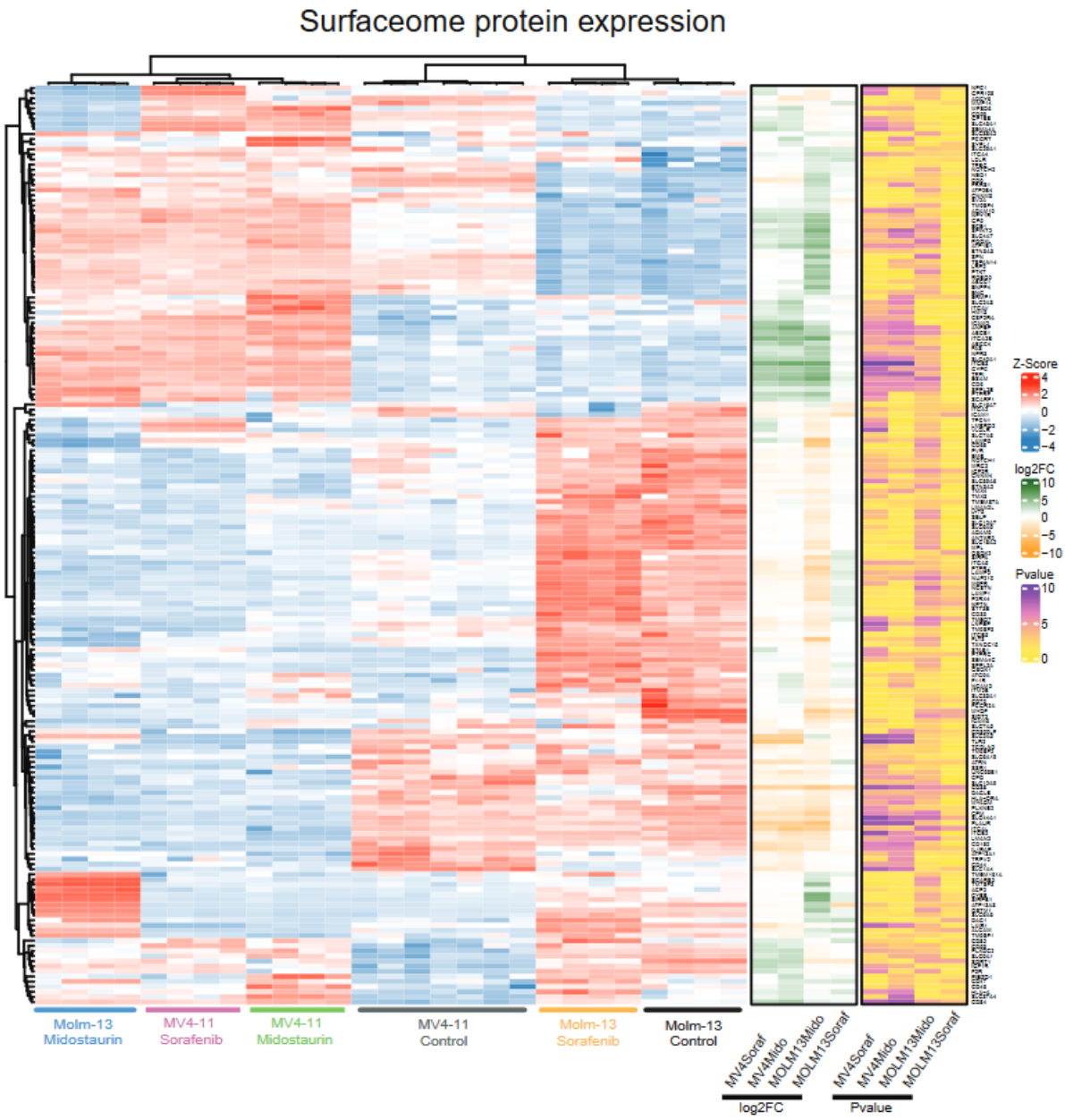

Figure 9: Heatmap of hierarchically clustered expression profiles of surface-localized proteins detected under all experimental conditions lead to a perfect separation of all experimental conditions with all biological replicates clustering in their respective conditions. Every row represents detected proteins, and expression levels of the respective protein are visualized via a colour scale from blue (low expression) to red (high expression). The intensity of the colour indicates the strength of the change. The 7th column shows the relative mean fold change of protein expression in the treated cell lines compared to the control condition. The next column visualizes the statistical significance by colour coding the -log10 transformed calculated p-value for the detected fold changes between control and resistance conditions from yellow, indicating a value close to 0 = not significant and purple values around 10 = highly significant. The 2nd column from the right indicates significant in one (blue) and significant similar changes (yellow) of all three treatment groups (MV4- 11 Sorafenib and Midostaurin and Molm-13 Midostaurin). The last column visualizes the significant changes (red) and similarities (yellow) in Molm-13 and MV4-11 Midostaurin resistant cells.

Comparing the whole and surface proteomes of Midostaurin and Sorafenib-resistant MV4-11 and Midostaurin resistant Molm-13 cells to their respective treatment naïve counterparts using a p-value

cut-off of ≤ 0.05 and a log-fold change of ≥ 1, we identified 2216, 1038 and 1051 significantly changed proteins out of 5877 identified proteins in total in Molm-13_Mido, MV4-11_Soraf, and MV4-11_Mido respectively. Of these 765, 360 and 403 remained significant in Molm-13_Mido, MV4-11_Soraf, and MV4-11_Mido cells after filtering for an FDR of ≤ 0.05. Next, we looked for consistent alterations in the expression profiles of all three experimental settings (MV4-11 Sorafenib, MV4-11 Midostaurin, and Molm-13 Midostaurin) and the Midostaurin experimental conditions (MV4-11 Midostaurin and Molm-13 Midostaurin) by filtering with a p-value threshold of 0.05 and net mean fold-change of ± 0.5. In doing so, we could identify 889 significantly changed protein groups out of 5587 identified protein groups that were significantly altered in all three experimental conditions. When we considered only Midostaurin resistant MV4-11 and Molm-13 cells, we could locate 1145 significantly changed proteins that were consistently changed in Midostaurin resistant MV4-11 and Molm-13 cells. FLT3 was downregulated in all resistant cell lines but to a different extent. Some of the most significantly upregulated proteins found in all three experimental conditions were ESAM, erythroid transcription factor GATA1, and TFPI. In contrast, some of the most strongly downregulated proteins were SAMHD1, Bcl-2, or PLAUR receptor.

3.1.3. Volcano plots

We visualized our data with volcano plots to present a more distinctive overview of the protein expression levels in our different experimental groups compared to their untreated controls. These show the fold change as a ratio of the protein expression in treated and untreated cells on the x-axis. The fold changes between groups were transformed into 2-logarithms, represented on the x-axis for a more precise representation of large-scale effects. The y-axis represents the – 10 logarithms of the p-value, showing the significance of the detected expression changes. The higher the value, the more significant the detected change.

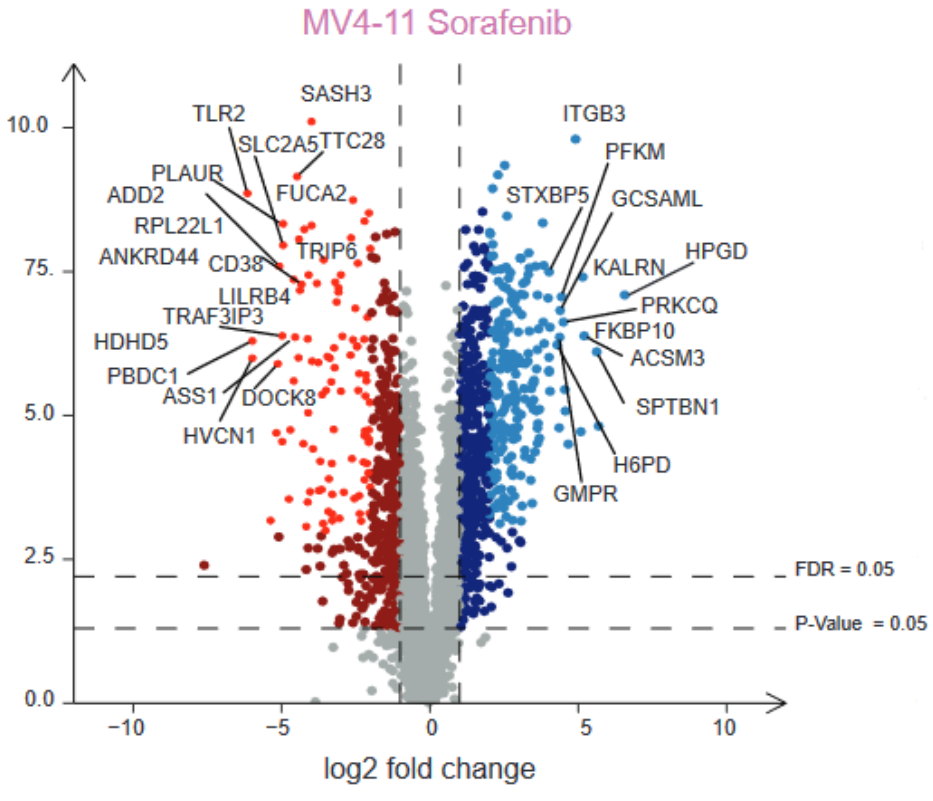

A

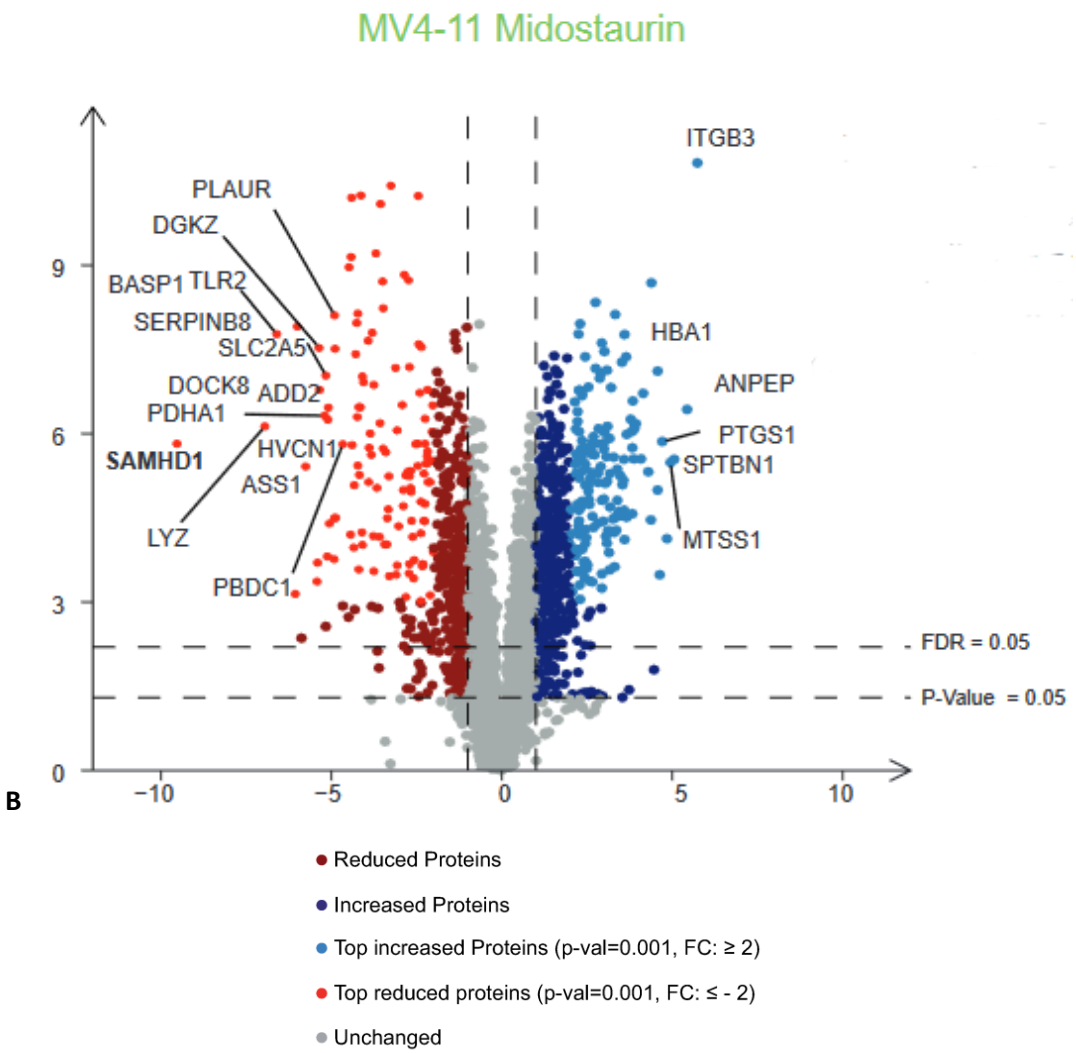

Figure 10 A and B: Volcano Plot of MV4- 11 cells. The proteome of chronically Sorafenib (A) and Midostaurin (B) treated MV4-11 cells compared to their DMSO control are graphically represented. Four biological replicates in each group are analysed. The horizontal axis represents the logarithmic fold change in protein expression between resistant cells and their respective controls. Positive values represent increased protein amounts in the TKI-resistant cells (blue), and negative values show a decrease towards the control (red). The vertical axis displays the significance of the results plotting the negative decadic logarithm of the p-value of every protein. The minimal significance level is placed at 1,3 (p-value = 0.05). The proteins above are considered significantly regulated.

We performed the same protocols and statistical analysis on the proteome of the Molm-13 cell line, due to the insufficient treatment response in the Sorafenib group, only the Midostaurin resistant cells were analysed.

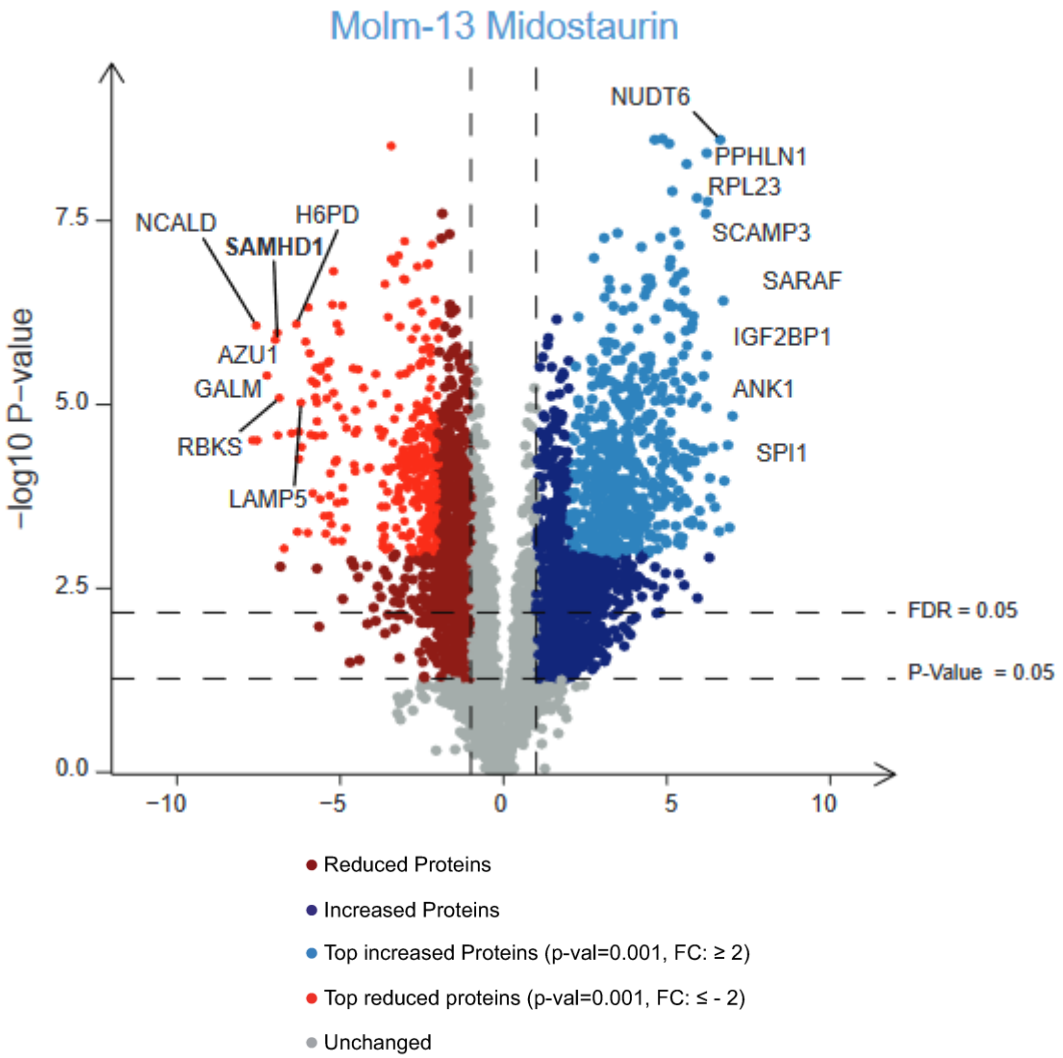

Figure 11: Volcano Plot of Molm-13 cells. Intracellular Proteome of chronically Midostaurin-treated Molm-13 cells compared to their DMSO control are graphically represented. Four biological replicates in each group are analysed. The horizontal axis represents the logarithmic fold change in protein expression between resistant cells and their respective controls. Positive values represent increased protein amount in the TKI-resistant cells (blue), and negative values show a decrease towards the control (red). The vertical axis displays the significance of the results plotting the negative decadic logarithm of the p-value of every protein. The minimal significance level is placed at 1,3 (p-value = 0.05). The proteins above are considered significantly regulated.

The top significantly decreased proteins were FLT3, SAMHD1, Bcl-2, CD68, and NME3. The top increased were ESAM, CHEK1, EDC3, and SCAMP3.

3.1.4. Overlapping changes in all resistant cell lines

To determine general changes that might have contributed to the resistance of the leukemic cells upon chronic FLT3 inhibition, we focused on changes in both cell lines and under both FLT3 inhibitors. Due to the missing toxicity of the therapeutical dose of 10nM Sorafenib on Molm-13 cells, we again excluded this cell line from the overlapping analysis. We observed numerous parallel effects in the protein regulation occurring in the Midostaurin-treated Molm-13 cell pools and the treated MV4-11

cell pools. This analysis enabled us to determine more general, cell line independent adaptation mechanisms, thus increasing the validity of our findings.

To annotate associated biological processes to these significantly changed protein groups, we enriched for functional pathways of the Kyoto Encyclopaedia of Genes and Genome (KEGG) via the Cluster Profiler package in R. We observed that in Sorafenib and Midostaurin resistant Molm-13 and MV4-11 cells, several metabolic pathways (amino sugar and nucleotide sugar metabolism, fructose and mannose metabolism, carbon metabolism, Glycolysis, and Gluconeogenesis) were enriched. Additionally, we identified a perturbed NOD-like pathway that can trigger a pro-inflammatory response under physiological conditions and thus induce Pyroptosis. Further, we enriched for pathways that play a role in cell survival such as Apoptosis, Necroptosis or Platinum drug resistance.

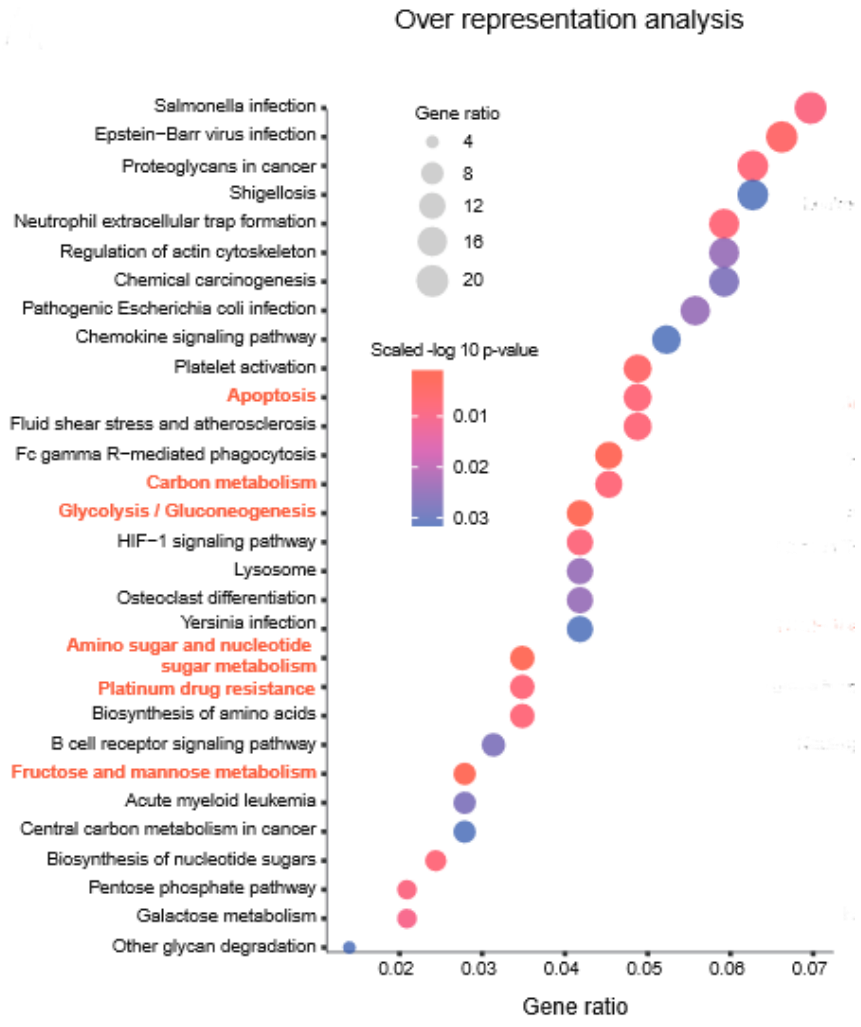

Figure 12: Gene Set and overrepresentation analysis using KEGG pathways under all experimental conditions. Comparison of significant similar changes in all resistant cell pools with proteomic patterns observed under different conditions and in various metabolic pathways. Dot size represents the proteins assigned to an enriched term, while dot colour codes for the p-value with increasing significance from blue to red.

The over representation analysis showed various pathways underlying strong alterations (>12 gene ratios). Patterns detected for infectious disease manifestations such as salmonella, EBV and Shigellosis were among the most modified. However, canonical cancer pathways such as proteoglycan

expression, chemokines and apoptosis were also detected as shown in Figure 12. Also, the metabolism of amino sugars, nucleotides and glucose was strongly alternated. Another interesting finding was the adaptation of platinum drug resistance. The pathways highlighted in red were further analysed through a network-based algorithm due to their biochemical importance for the observed resistance mechanisms and strong alterations.

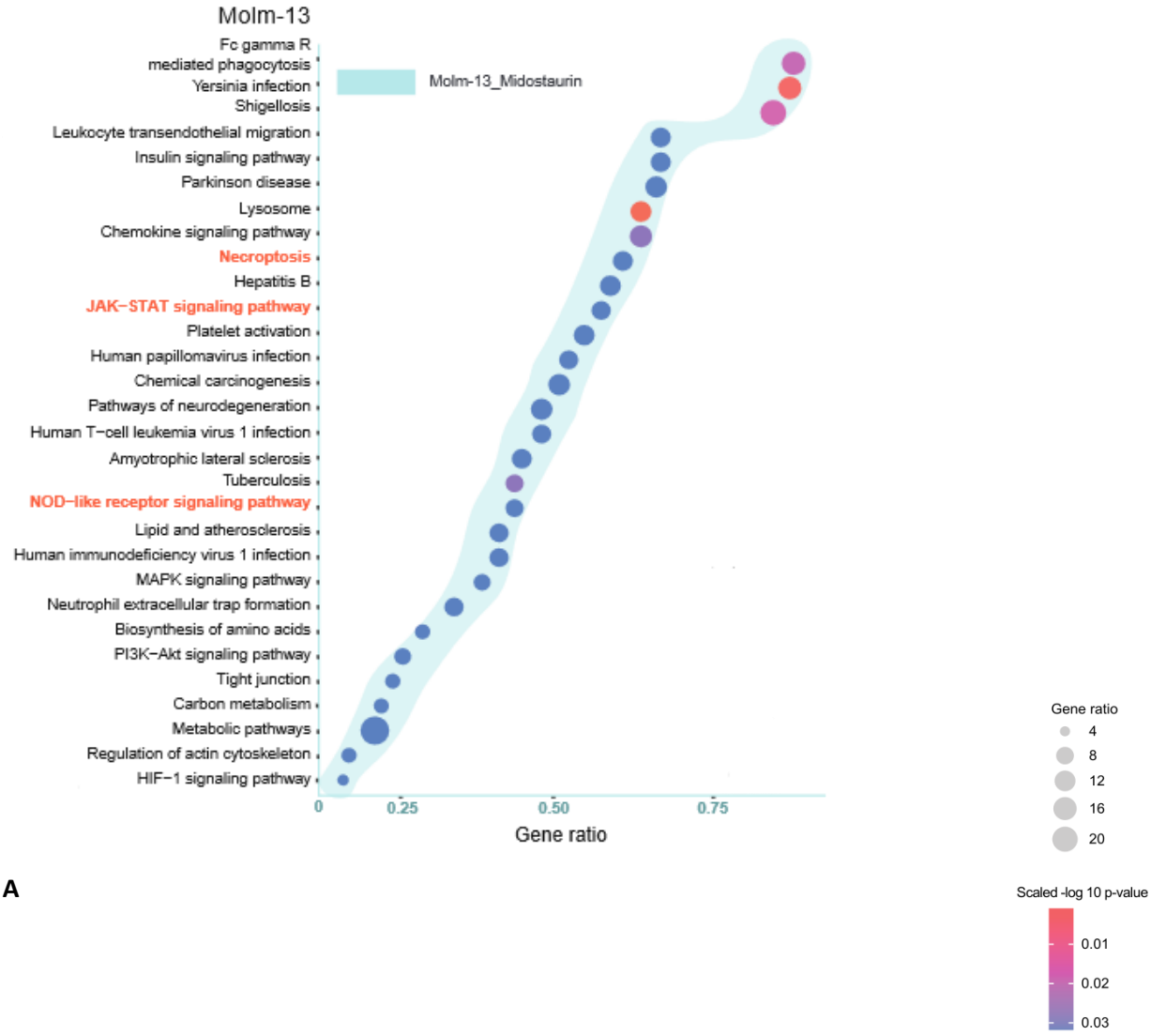

A

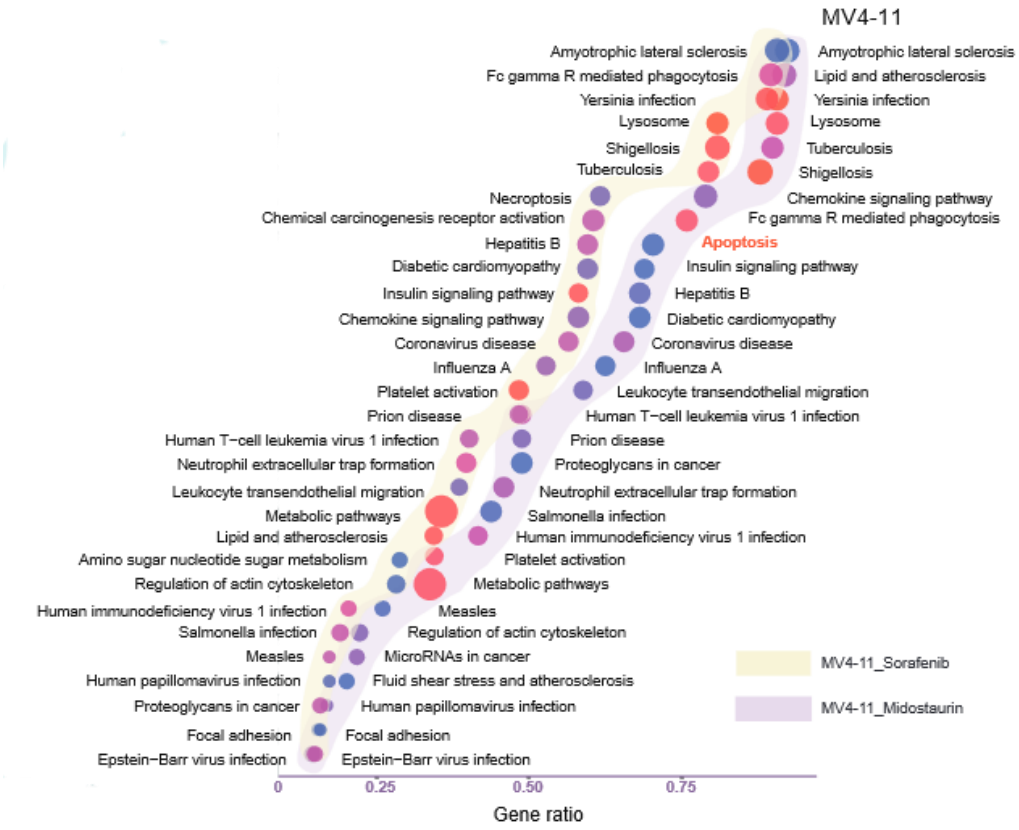

B

Figure 13 A and B: Gene set overrepresentation analysis using KEGG pathways of Molm-13 Midostaurin resistant (A) and MV4-11 Sorafenib and Midostaurin resistant cells (B). Comparison of significant similar changes in all resistant cell pools with proteomic patterns observed under different conditions and in various metabolic pathways. The size of the circles indicates the number of proteins assigned to an enriched term. The colour represents the logarithmic p-value with increasing significance from blue to red.

After the general gene set enrichment analysis, we performed a further detailed enrichment of each experimental condition. Midostaurin resistant Molm-13 cells showed alternations as observed under infectious diseases and changes in the necroptosis and JAK/ STAT- signalling pathway. Sorafenib and Midostaurin resistant MV4-11 cells showed similar patterns and apoptosis alterations (Figure 13).

We wanted to get a more detailed impression of those strongly regulated pathways playing a role in cell survival such as Apoptosis, Necroptosis or Platinum drug resistance. We created an interaction network based on the enrichment analysis and superimposed the expression changes on the significantly altered proteins depicted in the network. This enabled us to show which proteins contributed to the top enriched terms and their role inside the cell.

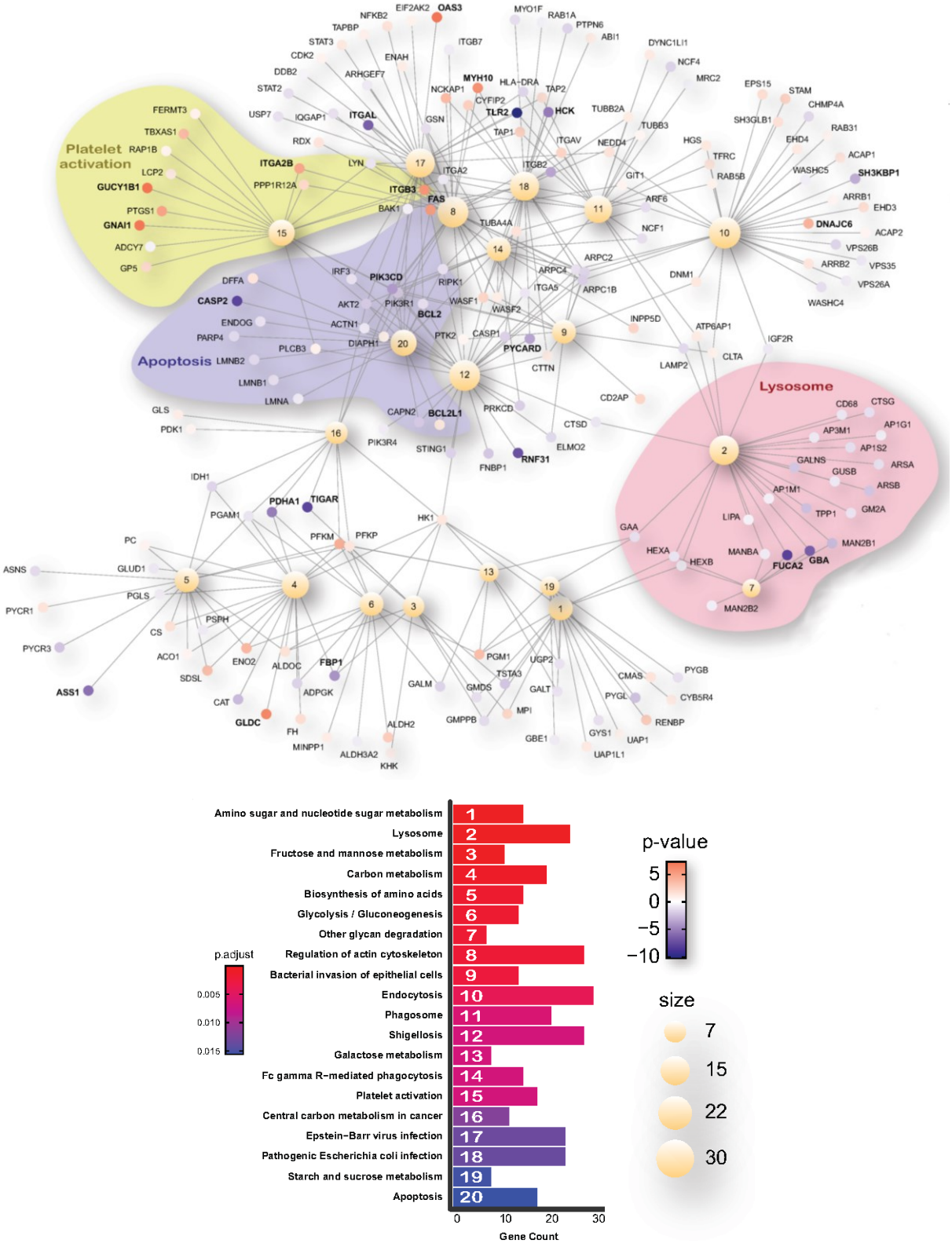

Figure 14: Network representation of crucial cell functions, showing high alterations in TKI resistant cells. The main alterations are observed in metabolic pathways and lysosomal and apoptotic processes. Numbered nodes in light orange are the pathway nodes with proteins contributing to the enrichment of these pathways centred around the pathway nodes. Gray lines between protein nodes describe a protein interaction. The size of the junctions in the network indicates the number of detected and alternated proteins in its group. The colour scale from blue to red indicates the logarithmic fold change in expression of the single detected protein, from highly upregulated in red to low in blue.

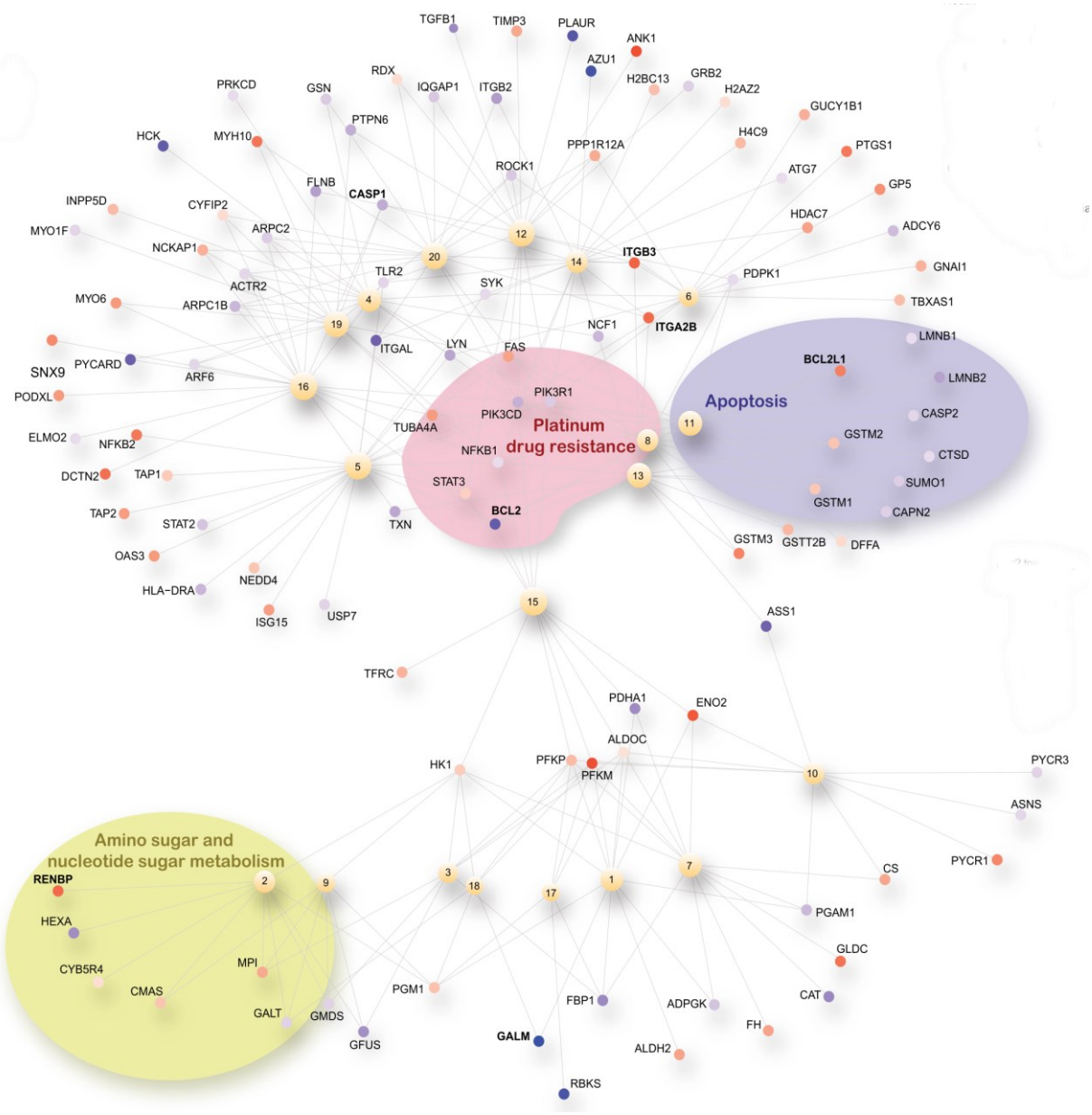
Amino sugar and nucleotide sugar metabolism
Platinum drug resistance
Apoptosis
TGFB1
TIMP3
PLAUR
ANK1
AZU1
RDX
H2BC13
GRB2
H2AZ2
PRKCD
GSN
IQGAP1
ITGB2
GUCY1B1
PTPN6
H4C9
HCK
MYH10
PPP1R12A
PTGS1
ROCK1
ATG7
FLNB
CASP1
GP5
INPP5D
CYFIP2
HDAC7
MYO1F
ARPC2
ADCY6
NCKAP1
ITGB3
TLR2
PDPK1
GNAI1
ACTR2
SYK
MYO6
ARPC1B
TBXAS1
NCF1
ITGA2B
ITGAL
LYN
FAS
LMNB1
SNX9
PYCARD
ARF6
BCL2L1
LMNB2
PODXL
PIK3R1
PIK3CD
CASP2
TUBA4A
ELMO2
NFKB2
NFKB1
GSTM2
CTSD
DCTN2
TAP1
STAT3
SUMO1
GSTM1
TAP2
BCL2
CAPN2
STAT2
TXN
GSTM3
GSTT2B
DFFA
OAS3
HLA-DRA
NEDD4
ISG15
USP7
ASS1
TFRC
PDHA1
ENO2
ALDOC
HK1
PFKP
PFKM
PYCR3
ASNS
RENBP
HEXA
CYB5R4
MPI
CMAS
GALT
GMDS
GFUS
PGM1
FBP1
ADPGK
GALM
ALDH2
FH
CAT
RBKS
CS
PGAM1
GLDC
PYCR1
Log2 fold change
LFQ intensity
6
3
0
−3
−6
size
5
10
15
20
Glycolysis/Gluconeogenesis
Amino/nucleotide sugar metabolism
Fructose and mannose metabolism
Fc gamma R-mediated phagocytosis
Epstein−Barr virus infection
Platelet activation
Carbon metabolism
Platinum drug resistance
Biosynthesis of nucleotide sugars
Biosynthesis of amino acids
Apoptosis
Proteoglycans in cancer
Fluid shear stress/atherosclerosis
Neutrophil extracellular trap formation
HIF−1 signaling pathway
Salmonella infection
Pentose phosphate pathway
Galactose metabolism
Pathogenic Escherichia coli infection
Regulation of actin cytoskeleton
Lysosome
Osteoclast differentiation
Chemical carcinogenesis
B cell receptor signaling pathway
Acute myeloid leukemia
Shigellosis
Central carbon metabolism in cancer
Other glycan degradation
Chemokine signaling pathway
Yersinia infection
0
5
10
15
20
Gene count

Figure 15: Network representation of crucial cell functions, showing high alterations in TKI resistant cells. The main alterations are observed in metabolic pathways, such as amino sugar and nucleotide metabolism, platinum drug resistance, and apoptosis. The specific pathways are summarized in 20 junctions represented in light orange nodes, entitled in the legend below. Proteins involved in these pathways are centred around the node. The size of the junctions in the network indicates the number of detected and alternated proteins in its group. The colour scale from blue to red indicates the logarithmic fold change in expression of the single detected protein, from highly upregulated in red to low in blue. Gray lines between protein nodes describe a protein interaction.

We could show single alternated proteins and their interactions within different pathways. Intense alternations were observed in proteins such as Bcl-2 and Bcl-2L1, modifying apoptosis and platinum drug resistance. Metabolic enzymes were also modified, especially in the amino sugar and nucleotide production. Some well-known platelet activation factors and some lysosomal metabolism promoting proteins were upregulated. Due to the network presentation and pathway analysis, a better understanding of the function of those single alternated proteins and their interaction was possible. Based on this generic overview of the number of alternated proteins in those different functions, we wanted to gain an even more detailed understanding of alterations' interaction and potential effects.

We focused on specific pathways inside the functional clusters to better understand the effects of the modified protein expression. Looking at receptors that can trigger an activation of the JAK/STAT signalling pathway, we observed that FLT3 was significantly downregulated in all resistance conditions, albeit to a different extent, most likely due to a necessary imputation in the resistance condition. Intriguingly, we observed that Cytokine receptor-like factor receptor 3 (CRLF3) and Plasminogen receptor were strongly upregulated in all resistant cell pools, while IGF1R was upregulated in both Midostaurin-resistant cell lines. Upregulation of these three receptors might constitute a compensatory mechanism of missing JAK/STAT activation upon FLT3 loss. Next, investigating the JAK/STAT signalling pathway critical for cell proliferation and growth, we observed a consistent overexpression of proteins of the STAT family, including STAT5A, STAT5B, and STAT3. At the same time, STAT2 and STAT6 were consistently downregulated in all investigated conditions (Figure 19). Furthermore, we observed a significant upregulation of JAK1 and JAK2 in the case of Midostaurin resistant Molm-13 cells, while JAK3 was upregulated in Midostaurin and Sorafenib resistant MV4-11 cells. Additionally, we observed that PTPN6, an JAK/STAT signalling inhibitor, was concomitantly downregulated in all experimental conditions.

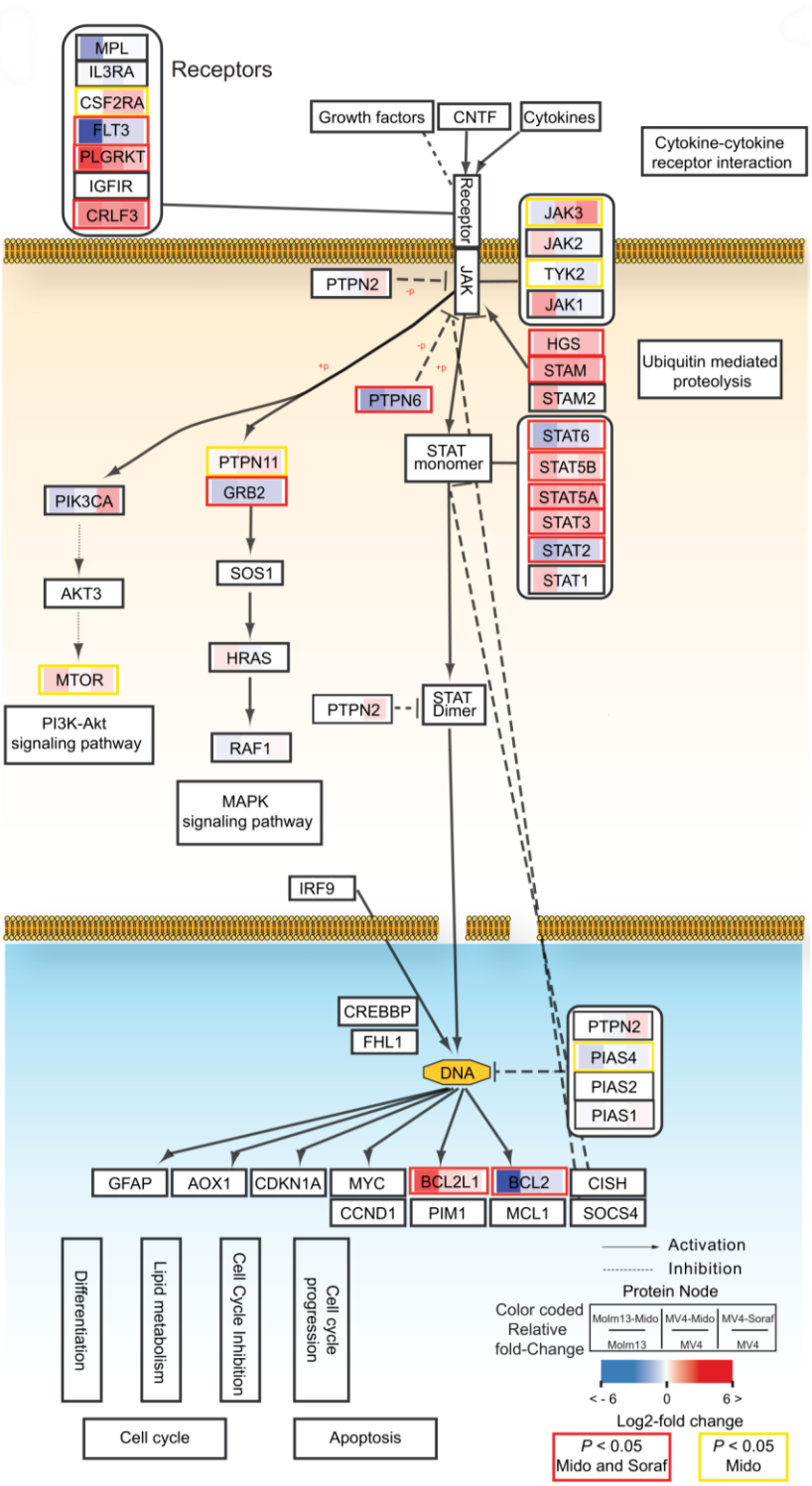

Figure 16: Expression changes of significantly changed proteins of the JAK/STAT signalling pathway in Midostaurin-resistant Molm-13 and Midostaurin- or Sorafenib-resistant MV4-11 cells, were chosen for visualization in the pathway of JAK/STAT activation, which in summary showed a strong activation. Colour coded columns in every protein node visualize the log2 fold-change in protein expression between drug-resistant AML cells (From left to right: Molm-13_Mido, MV4-11_Mido, MV4-11_Soraf) versus their respective treatment naïve control cells. The frame colour of every protein node visualizes whether changes in the respective protein expression were significant in only one condition (black), both Midostaurin-resistant cell lines (yellow), or all three conditions (red). It is divided into three areas

on each protein, indicating the change in Molm-13 or MV4-11 cells and the resistant drug described in the legend in the right corner.

FLT3 mutations and their resulting constitutive FLT3 activation led to strong activation of JAK-STAT, PI3K- Akt, and RAF- MAPK pathways, which mediates proliferation and anti-apoptotic effects. TK-inhibitors show potent inhibition of these effects. Nevertheless, TKI resistant cells present again strong upregulations of those signalling pathways.

Next, we looked at pathways that can induce cell death (Figure 20). Analysing the apoptosis pathway, we observed that the antiapoptotic Bcl- family protein Bcl-2 was strongly downregulated. In contrast, antiapoptotic Bcl-2 family protein Bcl-XL (BCL-2L1) showed a substantial increase in expression in all investigated resistance scenarios (Molm-13 Midostaurin resistant, MV4-11 Sorafenib and Midostaurin resistant). Furthermore, we found that mitochondrial outer membrane permeation (MOMP) inducing protein BAK was consistently downregulated in all investigated treatment conditions. CASP2, an initiator of mitochondrial dependent cell death, was downregulated in all conditions, with the strongest downregulation observed in Midostaurin-resistant MV4-11 cells. DFFA, the Caspase activated nuclease DFFB inhibitor, was strongly overexpressed in all investigated conditions.

Moreover, the inflammasome and necrosome induced cell death pathways showed several altered proteins crucial for this type of cell death (Figure 20B). PYCARD (ASC) and CASP1, central components of inflammasomes, showed a strong downregulation in all treatment scenarios. Furthermore, RIPK1, a major player of the necrosome, was downregulated in all investigated conditions.

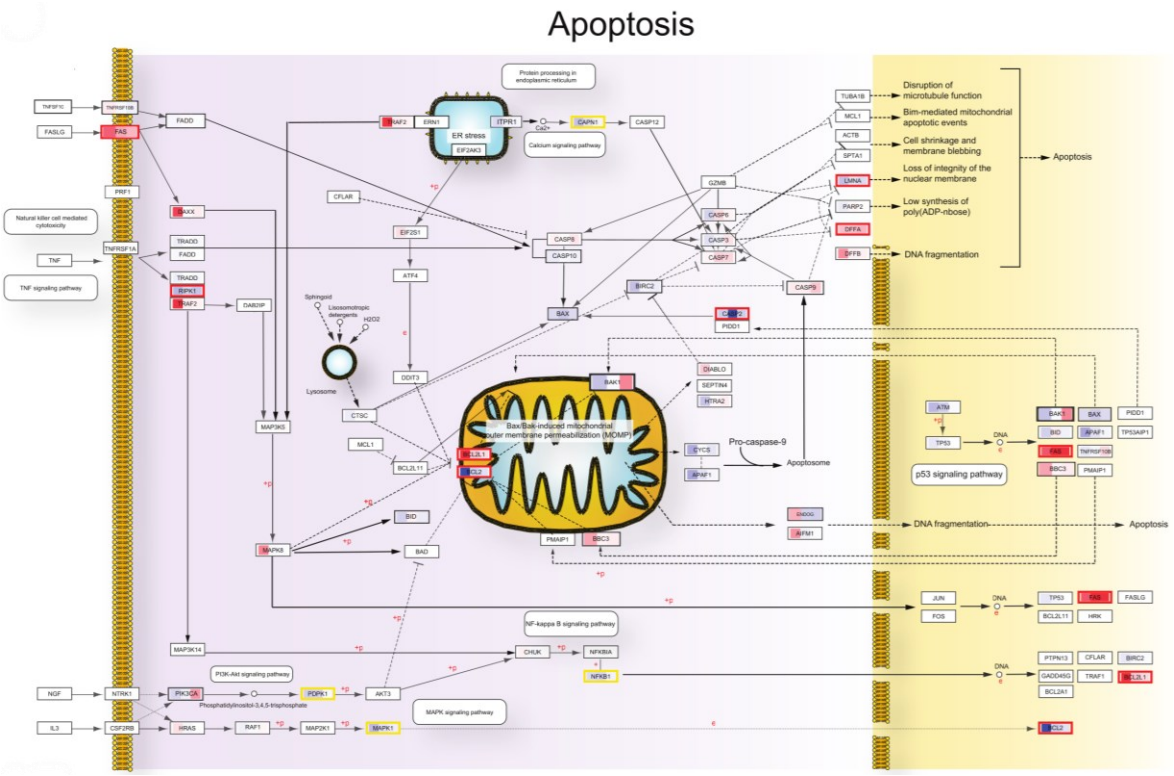

A

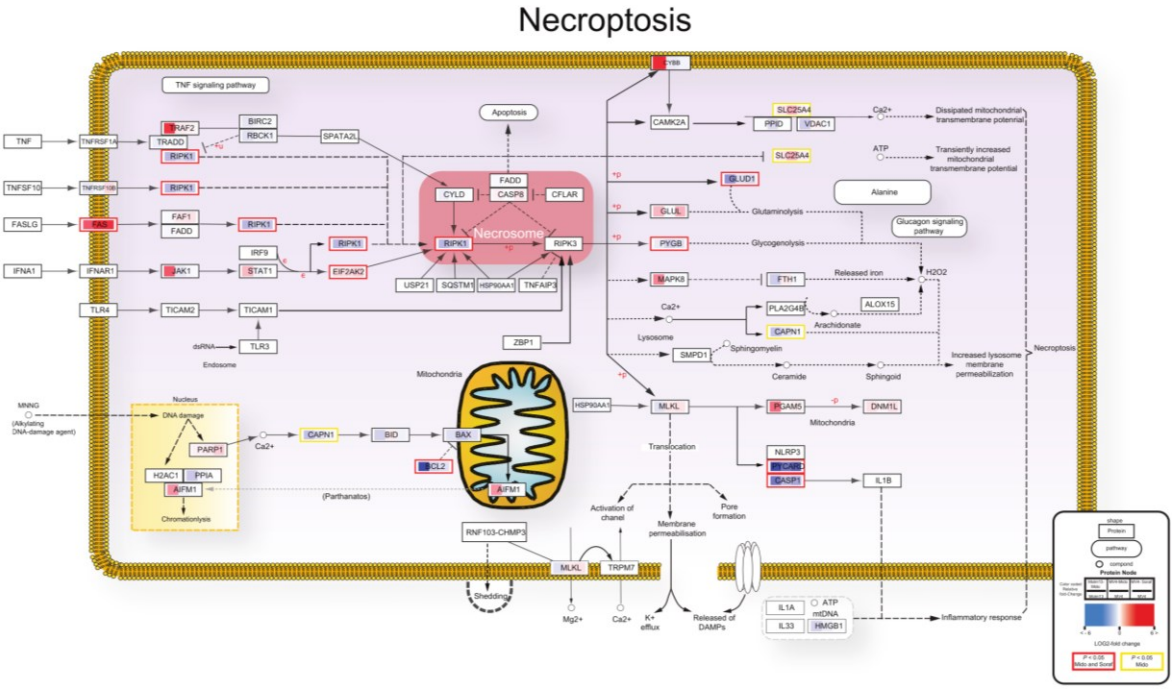

B

Figure 17 A and B: Apoptosis (A) and Necroptosis (B) networks with altered protein expressions in TKI resistant cells, compared to their drug- naïve counterparts. The colour code indicates the fold change of protein expression. It is divided into three areas on each protein, indicating the change in Molm-13 or MV4-11 cells and the resistant drug described in the legend. Significant changes ($p< 0.05$) are shown through coloured frames on each protein, visualizing whether changes in the respective protein expression were significant in only one condition (black), both Midostaurin-resistant cell pools (yellow), or all three conditions (red).

Another interesting finding was the upregulation of several components necessary for the activation of platelets in all investigated conditions, such as Thromboxane A synthase 1 (TBXA1) or Prostaglandin G/H Synthase 1 (PTGS1), probably leading to higher levels of Thromboxane A2 which has been shown to promote tumour cell survival, proliferation, and migration.

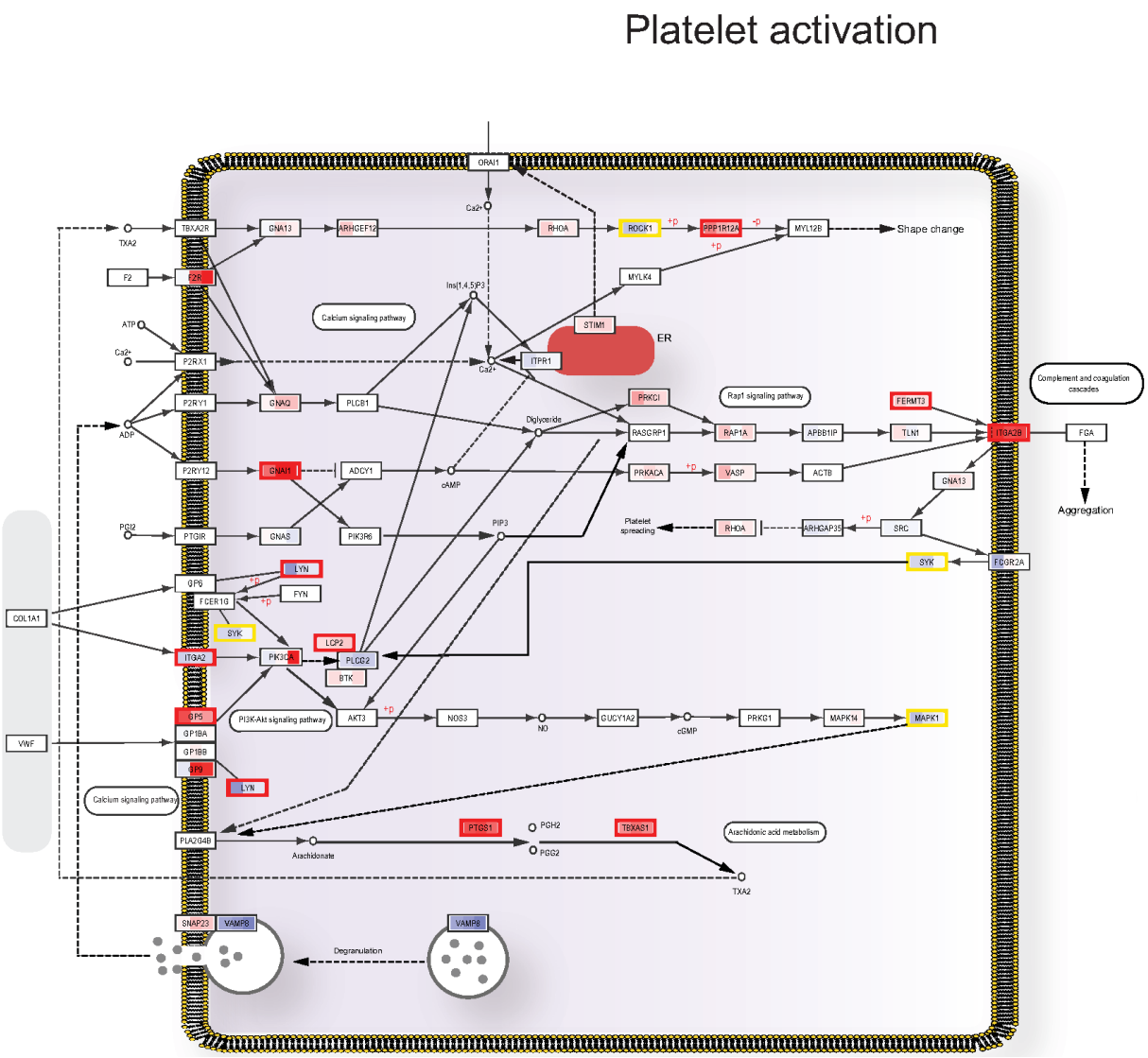

Figure 18: Platelet activation with altered protein expressions in TKI resistant cells, compared to their drug- naïve counterparts. The colour code indicates the fold change of protein expression. It is divided into three areas on each protein, indicating the change in Molm-13 or MV4-11 cells and the resistant drug described in the legend. The frame color of every protein node visualizes whether changes in the respective protein expression were significant in only one condition (black), both Midostaurin-resistant cell lines (yellow), or all three conditions (red).

Looking at cell cycle regulating proteins, we observed that Cyclin dependent kinase 2 (CDK2) was consistently upregulated in all experimental conditions. Furthermore, CHEK1 kinase implicated in DNA damage response pathways was overexpressed in all experimental conditions, possibly indicating a selective vulnerability of Midostaurin and Sorafenib resistant AML cells towards CHEK1 inhibitors.

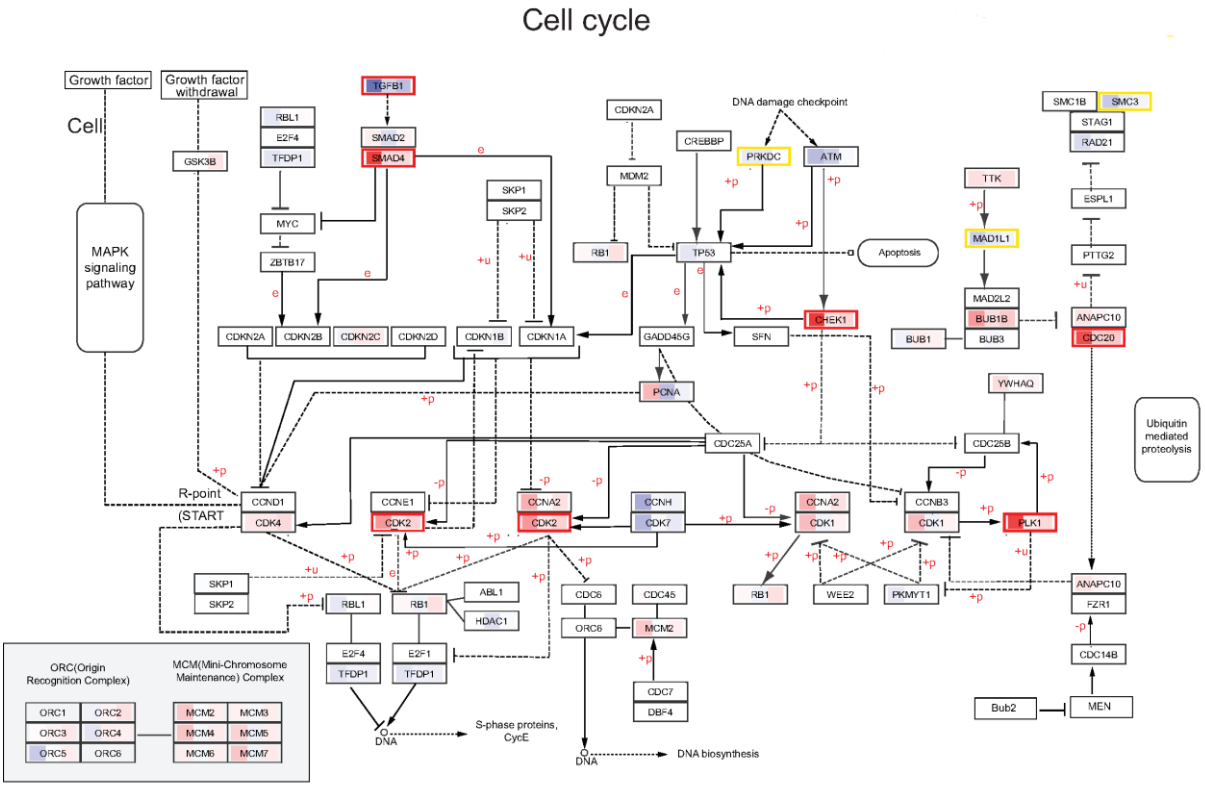

Figure 19: Cell cycle with altered protein expressions in TKI resistant cells, compared to their drug-naïve counterparts. The colour code indicates the fold change of protein expression. It is divided into three areas on each protein, indicating the change in Molm-13 or MV4-11 cells and the resistant drug described in the legend. The frame color of every protein node visualizes whether changes in the respective protein expression were significant in only one condition (black), both Midostaurin-resistant cell lines (yellow), or all three conditions (red).

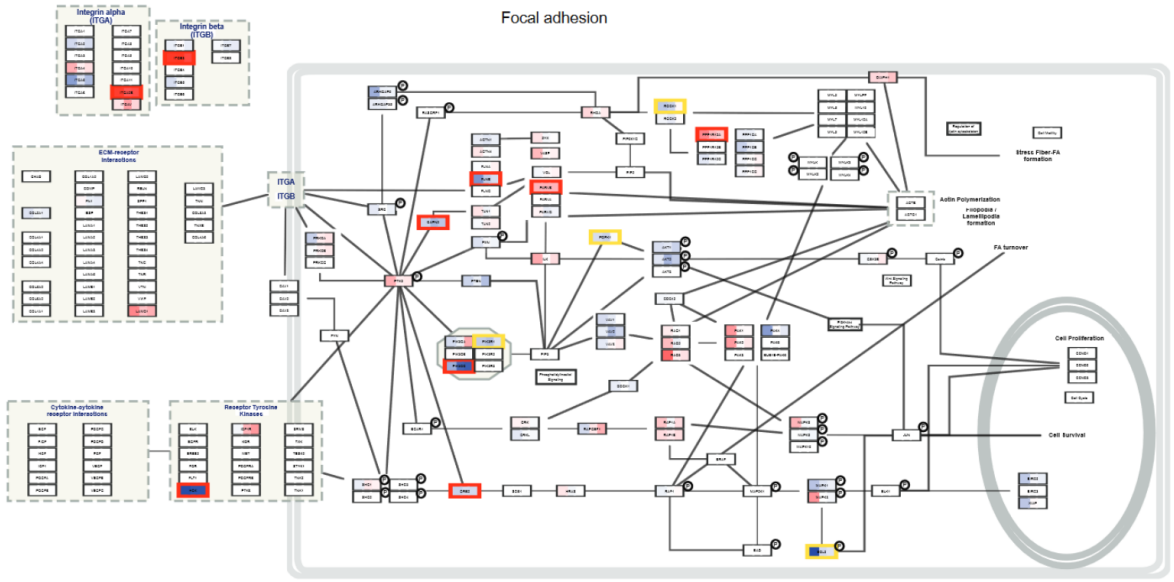

Figure 20: Pathway of focal adhesion with visualized changes in protein expression in TKI resistant cell pools. The colour code indicates the fold change of protein expression. It is divided into three areas on each protein, indicating the change in Molm-13 or MV4-11 cells and the resistant drug described in the legend. The frame color of every protein node visualizes whether changes in the respective protein

expression were significant in only one condition (black), both Midostaurin-resistant cell lines (yellow), or all three conditions (red).

Finally, we observed that all resistant cell lines showed an upregulation of pacemaker enzymes in the pathway of glycolysis, which correlated with the observation that our resistant cell lines metabolized the sugar in the cell culture medium much faster, as shown in Figure 21 below.

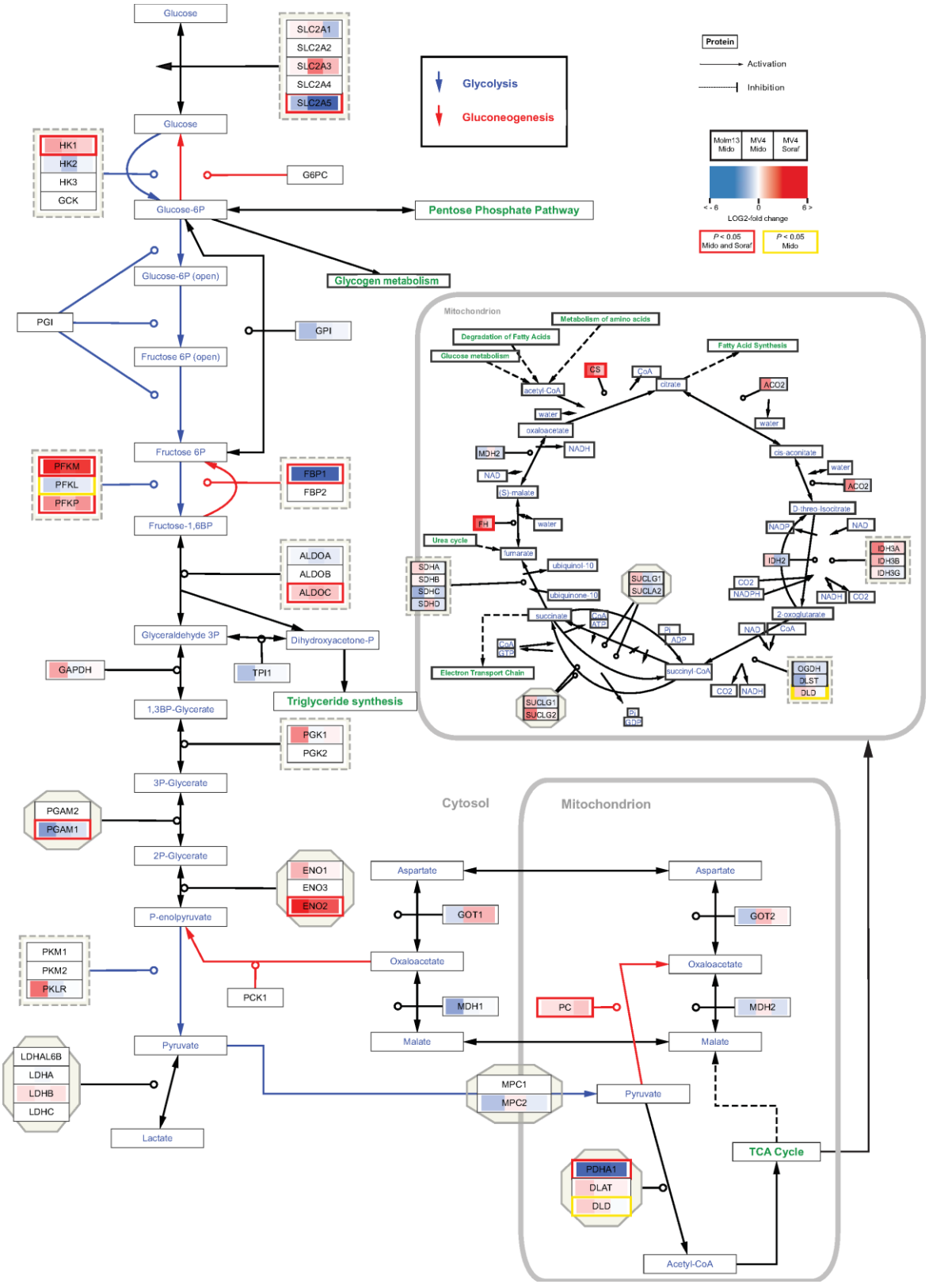

Figure 21: Glucose metabolism with altered protein expressions in TKI resistant cells, compared to their drug- naïve counterparts. The colour code indicates the fold change of protein expression. It is divided into three areas on each protein, indicating the change in Molm-13 or MV4-11 cells and the resistant drug described in the legend. Significant changes ($p < 0.05$) are shown through coloured frames on each protein.

These detailed insights into the modified pathways in the TKI resistant cells compared to their sensitive counterparts showed various mechanisms that might lead to the resistance. We were able to gain a better biochemical understanding of the processes going on in TKI resistant cells. At the same time, several clue proteins connecting essential signalling functions and representing potential targets were defined. JAK/STAT-family proteins and apoptosis mediating factors of the Bcl-2 family represent some of those and will be tested as potential treatment targets later.

3.2. Phospho-proteomic Data

The quantitative amount of protein expression in different cell types already reveals much information. Nevertheless, the quantitative data does not show the activation state of single proteins and, consequently, the activation of their respective signalling pathways. The most common and essential posttranslational regulation mechanism for proteins is phosphorylation. The modification of specific amino acids of a protein with a phosphate group is mediated through kinases and represents its activation. The removal of a phosphate group from a protein is called dephosphorylation and is mediated through phosphatases. The modification of proteins and transition between activated and inactivated states by phosphorylation is highly dynamic, thus enabling eukaryotic cells to adapt rapidly to changing environmental conditions. Hence, the additional protein phosphorylation information allowed us to analyse which pathways were activated in the TKI resistant cell lines.

To this aim, we performed an in depth-scale (phospho-)proteomic analysis via isobaric labelling using tandem mass tags (TMTs). We could detect 22875 phospho-peptides across all conditions (Figure 24). Among all identified phospho-peptides, the phosphorylated amino acid residues distribution was 84.0% of serine, 15.0% of threonine, and 1% of tyrosine. In comparison, 85.1% were single, 12.8% were double, and 2.2% were triple phosphorylated phosphorylation sites (Figure 24B). We normalized the detected phospho-peptides to their general protein expression to identify the alterations in the phosphorylation process.

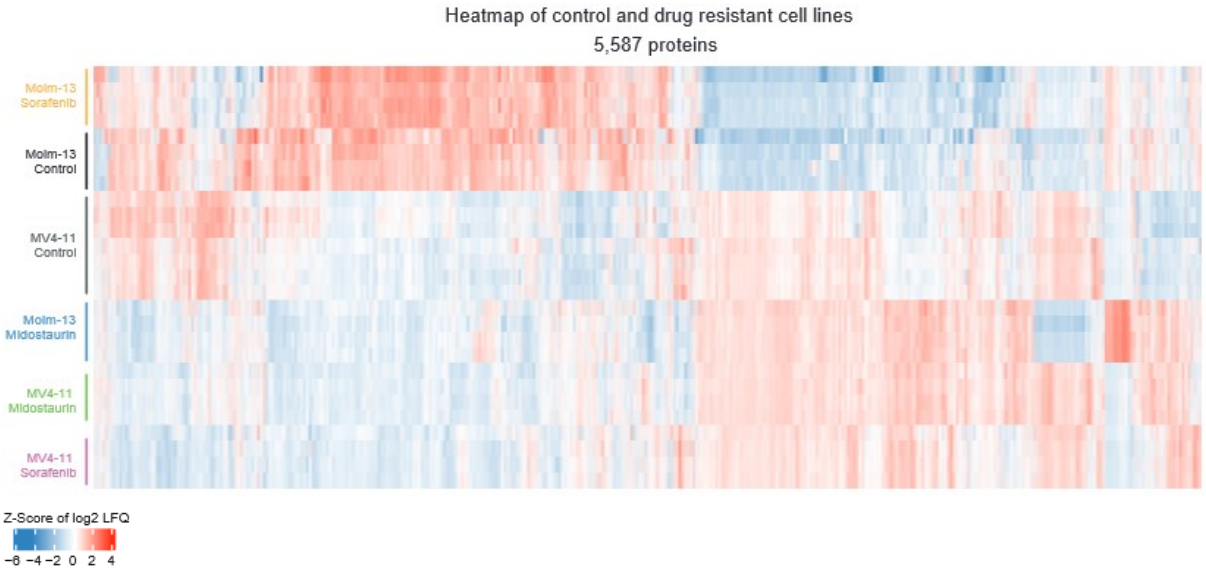

Figure 22: Heatmap of all identified proteins used as a reference for phospho- proteomic analysis. 5587 detected proteins remained after the quality filter for two cell lines tested under all six conditions. All detected proteins are represented as colour bars indicating their expression levels coded in a colour scale from blue (low expression) to red (high expression). The intensity of the colour indicates the strength of the change.

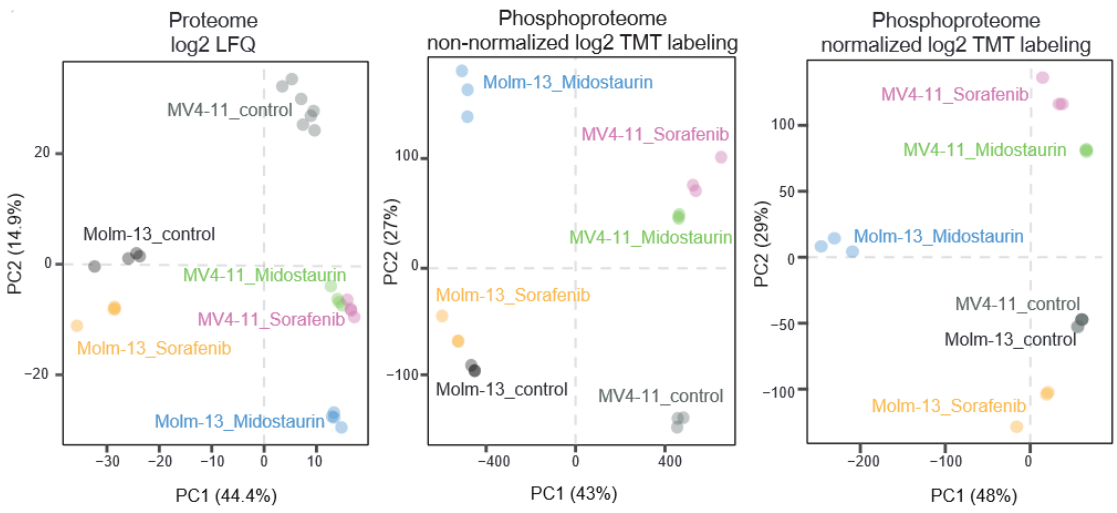

A

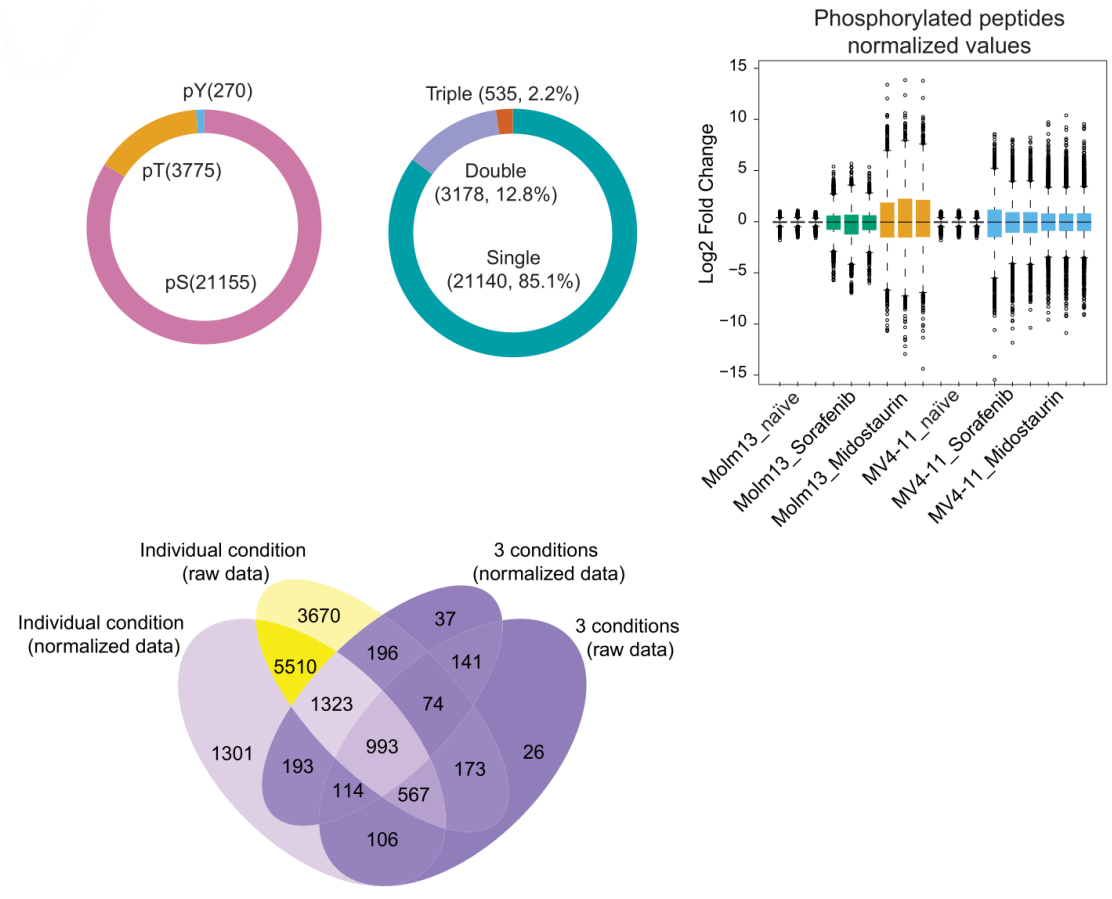

B

Figure 23 A and B: Summary of our phosphoproteomic Data. (A) Principal component analysis (PCA) on log_2 transformed label-free quantification (LFQ) for proteome data and log_2 transformed normalized and non-normalized FC for phosphorylated peptides data. (B) Pie chart of information of phosphorylate sites, boxplot of log_2 transformed normalized FC, and Venn diagram of identified significant phosphorylated peptides based on raw and normalized TMT labeling data, respectively.

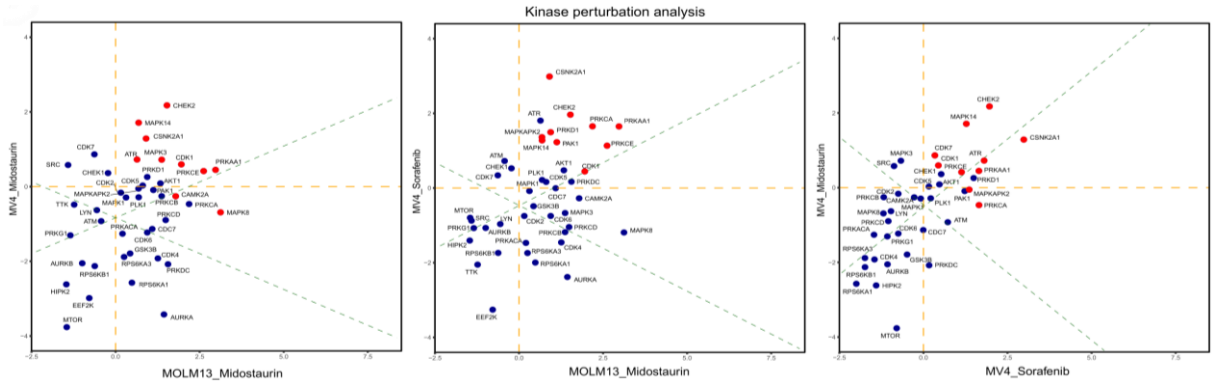

Figure 24: Kinase perturbation analysis. Site- and protein-centric analysis to visualize kinase activities between experimental treatments.

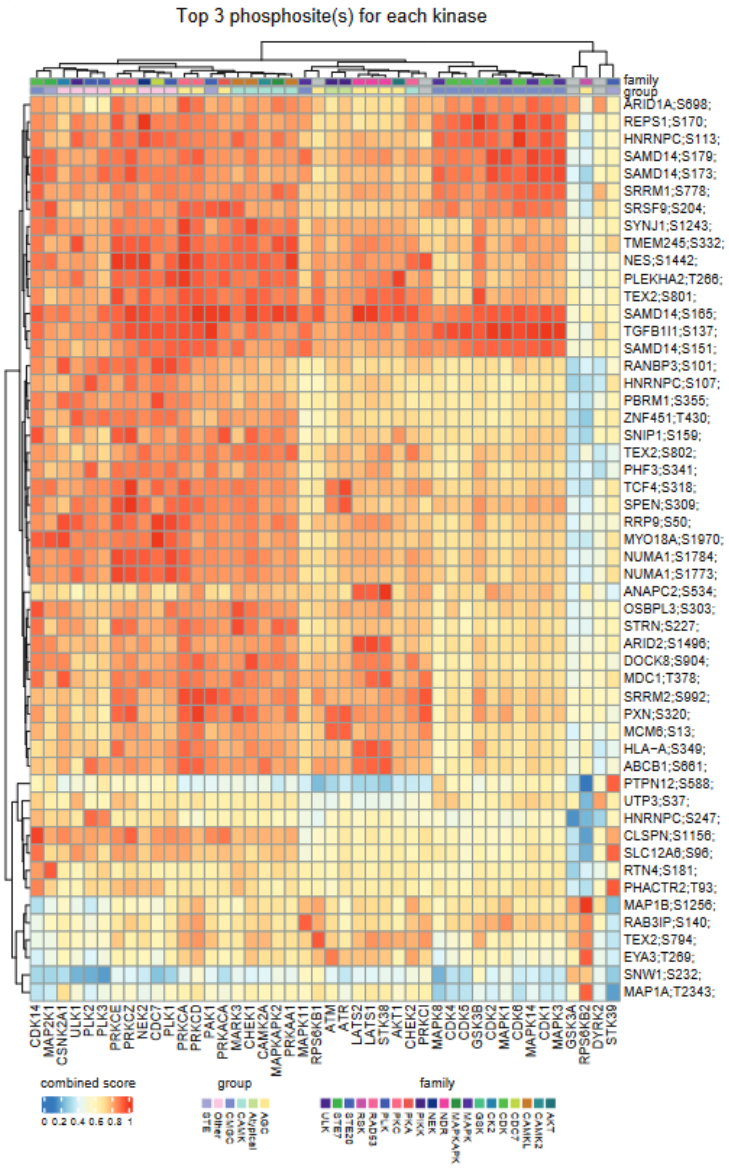

Figure 25: Heat map of a combined kinase-substrate function score from profile and motif score for the top three phosphosites of all kinases. The coloured scales on top represent the kinase family and group as described in the legend on the right. The specific kinases are described on the bottom, and their phosphosites are on the right-hand side. Expression intensity is represented by the colour scale from blue (0) to orange (1).

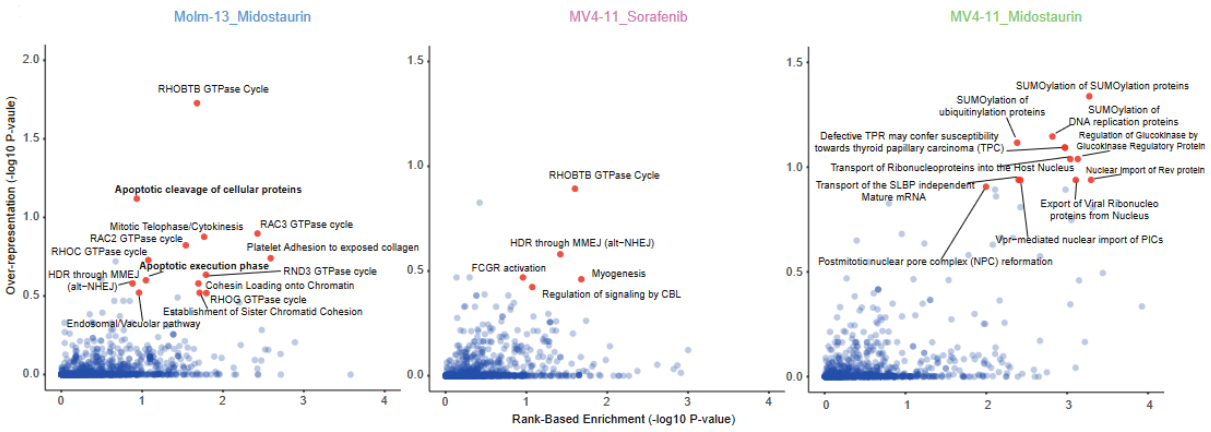

Figure 26: Detected signaling pathway of enrichment analysis, Network of 50 predicted most active kinases and a kinase-substrate score of CHEK1 substrates. KEGG enrichment analysis by plot over-representation and rank-based gene sets for each drug treatment condition. The most significantly enriched pathways were highlighted by red labeled dots identified by the threshold value of over-representation > 0.8 and rank-based enrichment > 0.5

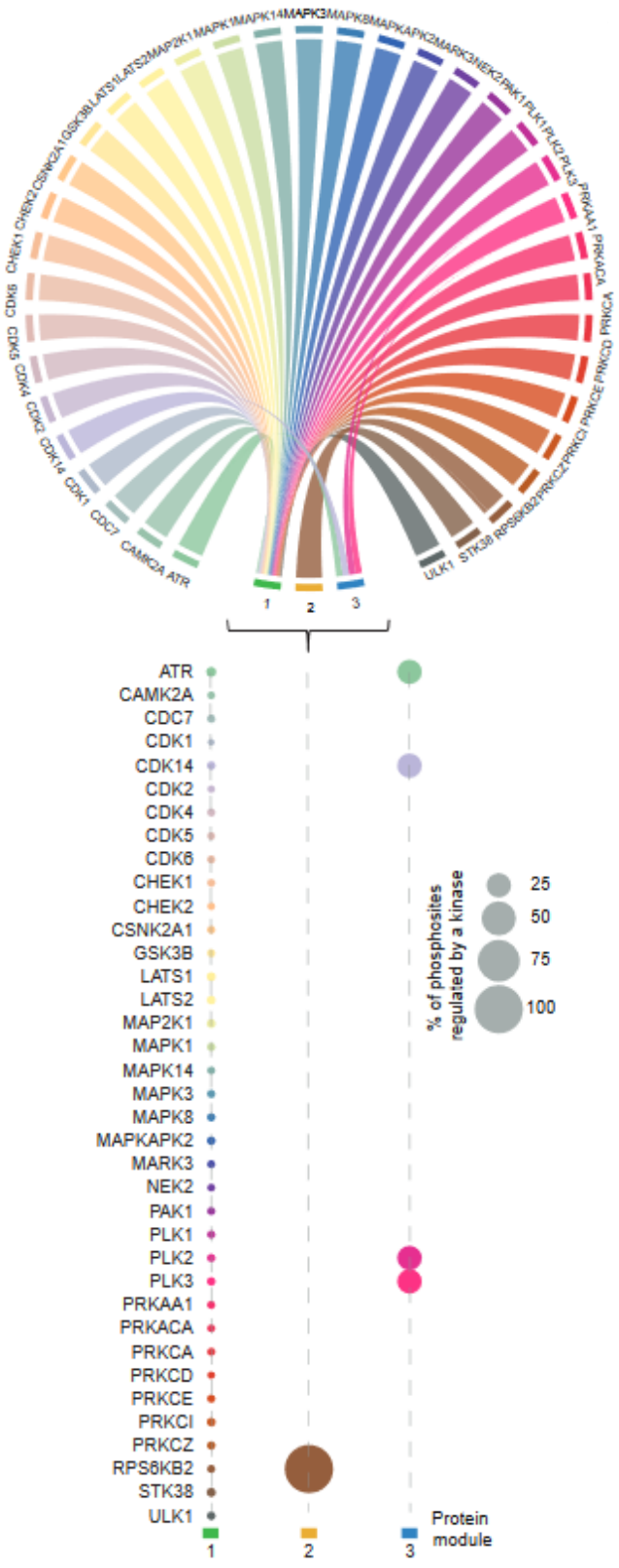

Figure 27: Protein modules detected and phosphosites regulated by kinases. A cluster diagram of the signalomes identified from the most active phosphoproteome. 50 predicted most active kinases were branched as 4 protein modules with distinct phosphorylation and regulatory profile. Underneath, the extended cluster map of signalomes of the figure above illustrates the percentage of phosphosites regulation by kinases indicated by the size of nodes within each protein module.

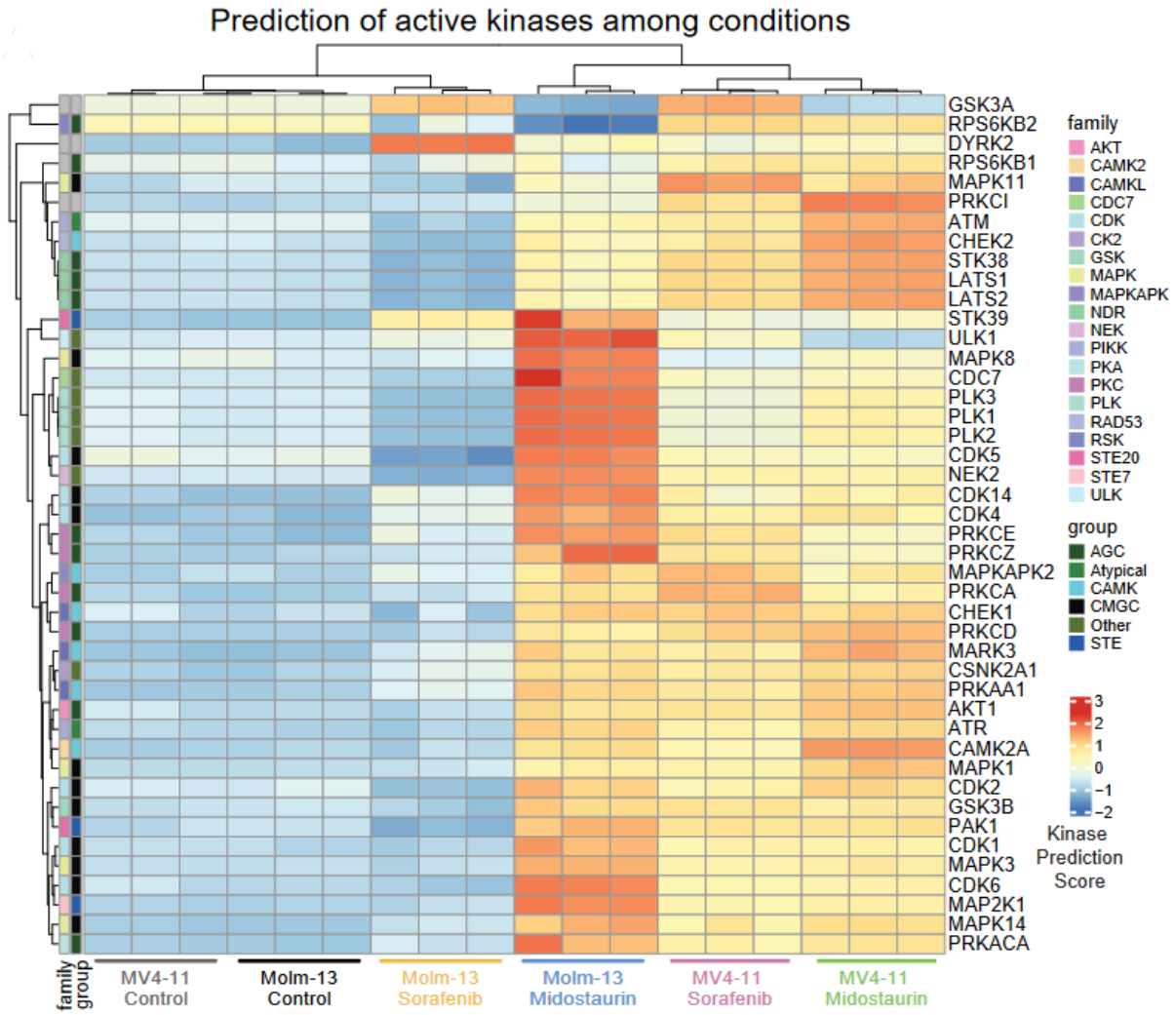

Figure 28: Alternated regulations of activated kinases between TKI resistant cells and their drug naïve counterparts. Heat map of a combined kinase-substrate function score from profile and Motif score for the top three phosphosites of every kinase. These kinases were clustered and assigned into distinct families and groups indicated by the color codes on the left side of the heat map. The changes of normalized intensity of phospho-proteomic data were z-score centralized, shown by red for upregulation and blue for downregulation. The specific kinases are described on the right-hand side.

To predict the activation of kinases related to protein phosphorylation, normalized phosphopeptides data were used for the kinases perturbation analysis by plotting the $\log_2$ transformed fold changes of drug resistant cells for all three experimental conditions (Figure 25). First of all, we observed that Cyclin-dependent kinase 1 (CDK1) and its CDK-activating kinase 7 (CDK7) were consistently predicted to be activated in all experimental conditions. Meanwhile, other CDKs, such as CDK2 and CDK6, were found to be activated in an experimental condition-dependent manner. CHEK1 and CHEK2 kinases implicated in DNA damage response pathways were overexpressed in all experimental conditions, indicating a vulnerability of Midostaurin and Sorafenib resistant AML cells towards selective CHEK1 and CHEK2 inhibitors. Similarly, CSNK2A1 kinase, involved in many apoptotic cellular processes, and ATR kinase, critical for regulating DNA damage response, showed highly significant activation in all resistant cells. The activation of PRKAA1 kinase, which is involved in cellular energy metabolism, might correlate with the observation that our resistant cell lines metabolized the sugar in the cell culture medium much faster. The PRKCA kinase, which can mediate anti-apoptotic pathways by phosphorylating Bcl-2 protein in leukemic cells, was activated in all resistant cells.

To further uncover potential kinase-substrate pairs and global relationships of kinases, we visualized the most activated kinases and their respective top 3 phosphosites evaluated by a multi-step kinase-substrate scoring method (PhosR citation) in a heat map (Figure 26). The kinase-substrate matrix revealed that the phosphoproteome kinases of our drug resistant cells were governed mainly by CDKs and their activating kinases (e.g. CDK1 and CDK7), cell cycle checkpoint kinase (e.g. CHEK1 and CHEK2) and CMGC kinases (e.g. MAPKs). CAMK kinases (PRKAA1 and PRKD1) and AGC kinases (PRKCA and PRKCE) were significant in phosphorylation.

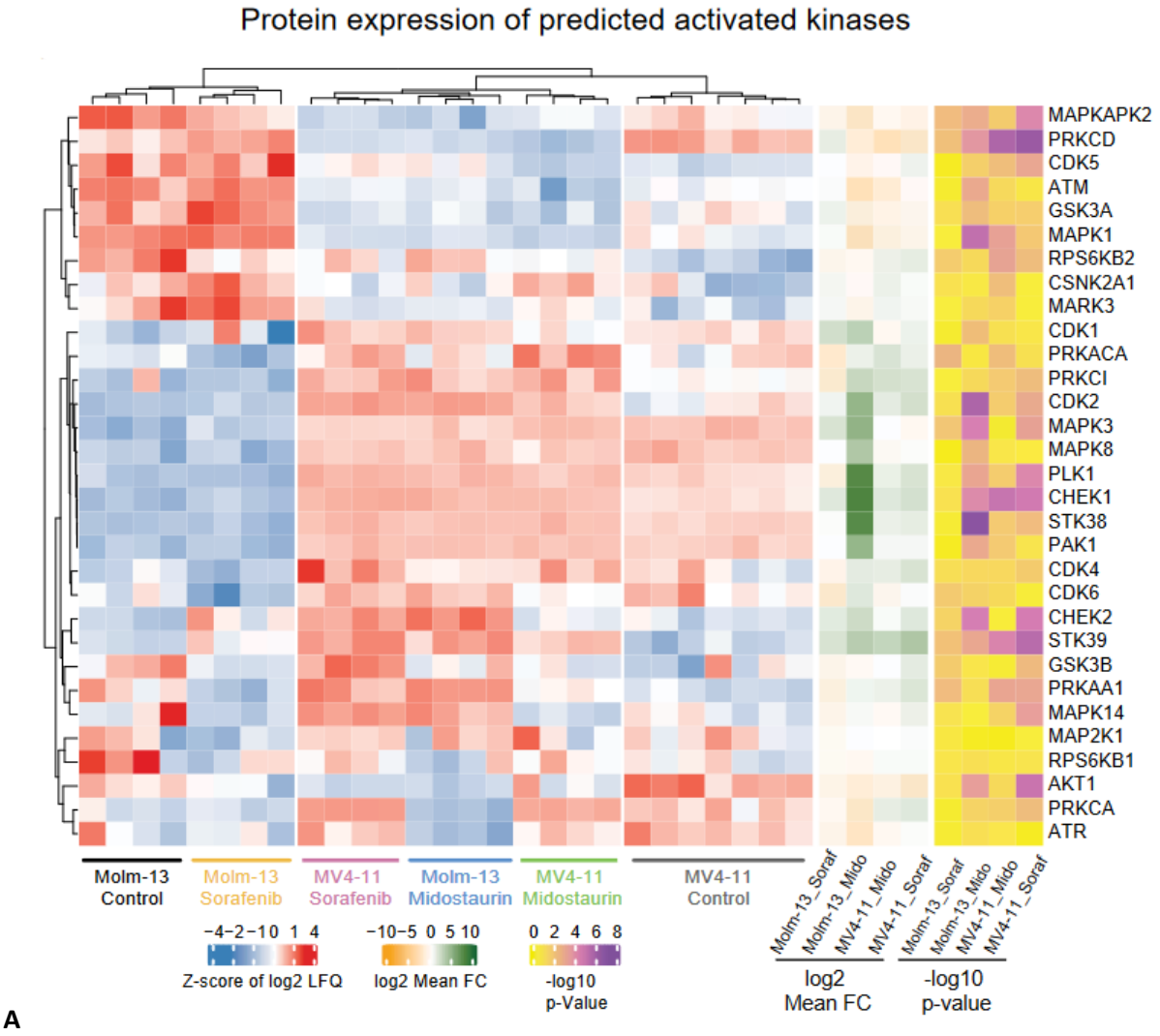

A

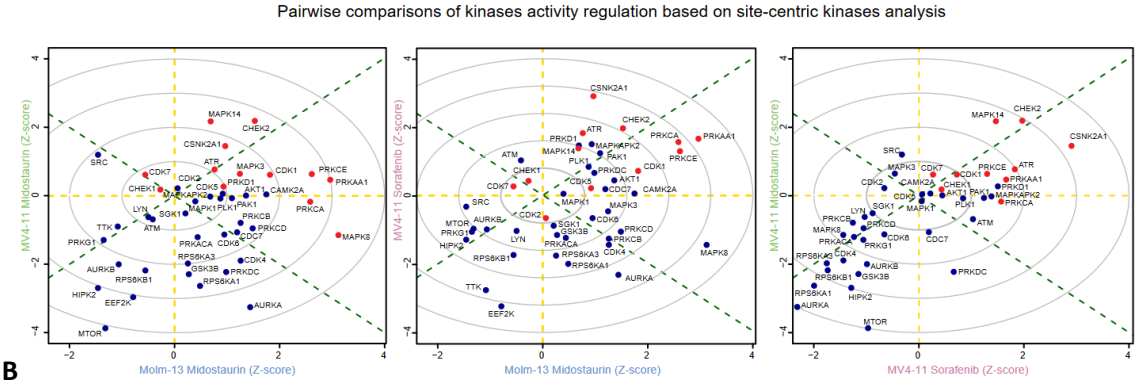

B

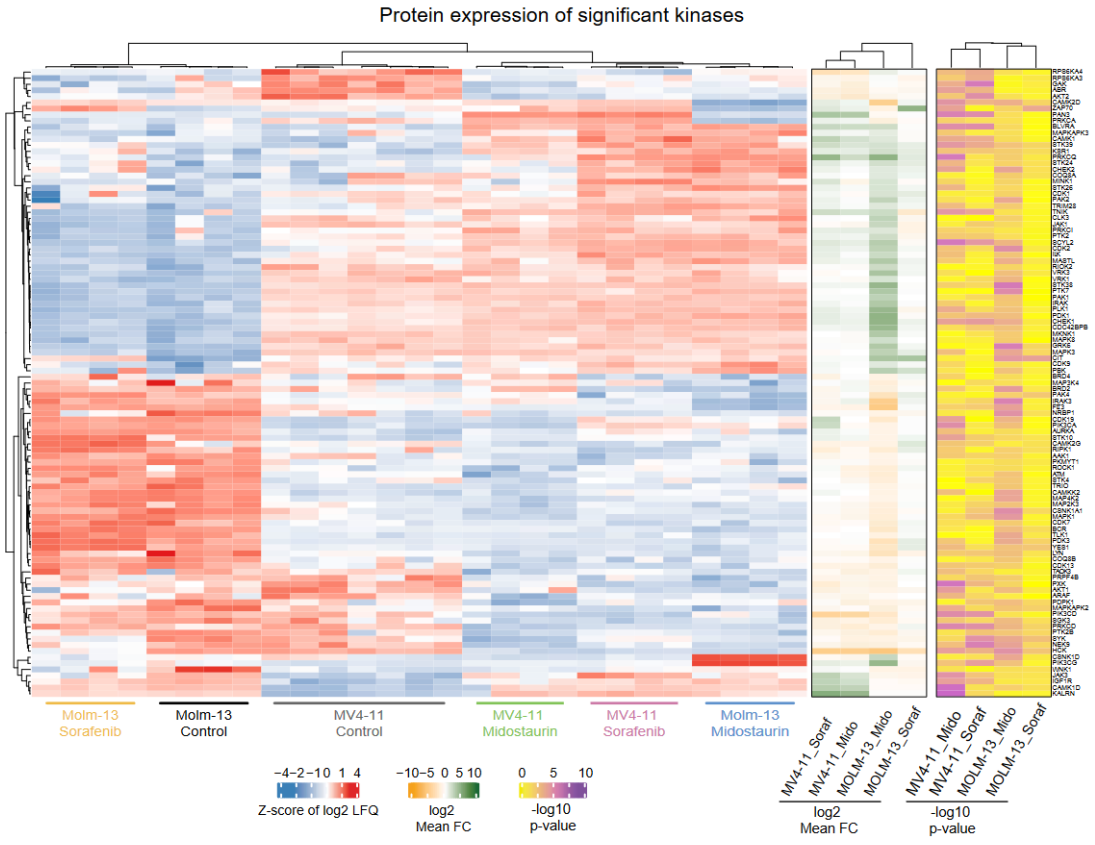

C

Figure 29 A, B, and C: (A) Heatmap of detectable predicted kinases and other significantly changed kinases on protein expression level, distinguished by the colour of protein names labeling. Protein names labelled in black represented detectable predicted active kinases, while blue indicated other significantly changed kinases. Detectable predicted active kinases, which were also found to have significant changes in protein expression, were shown in red labeling. The second column from the right indicates the logarithmic fold change of the expression in the different TKI-resistant cell lines compared to their control from -10 fold (strong downregulation) in dark blue to 10 fold (strong upregulation) in red. The column on the right represents the p-value of the observed fold changes in TKI resistant cells described before. Yellow indicates low, and purple high significance. (B) Kinase activity plots to compare activated kinases among two experimental resistance conditions. The x and y-axes are the Z-score of each kinase based on the overall changes of their substrates for the compared experimental conditions (phosphosites annotated to individual kinase based on PhosphoSitePlus, a built-in database of PhosR). (C) Heatmap of all kinases with a significant change in protein expression.

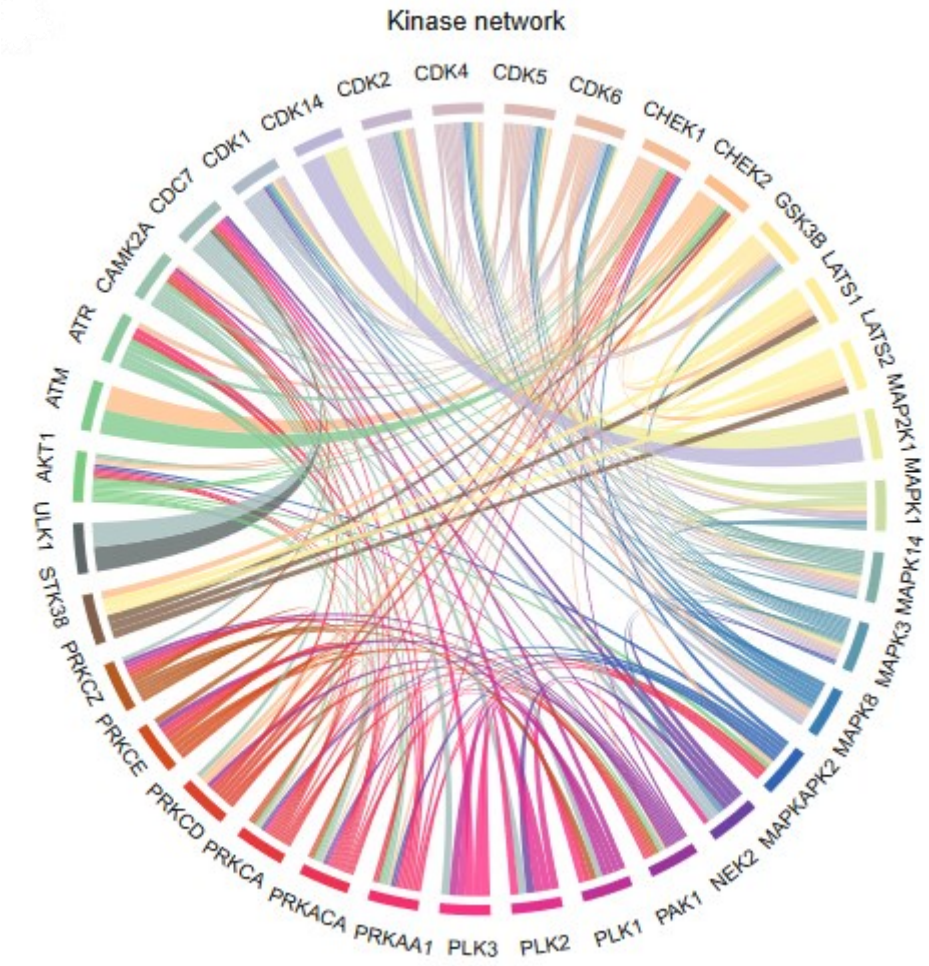

Figure 30: Detected signaling pathway of enrichment analysis, Network of 50 predicted most active kinases and the kinase-substrate score of CHEK1 substrates. Signalome network demonstrating the interaction of the predicted 50 most active kinases

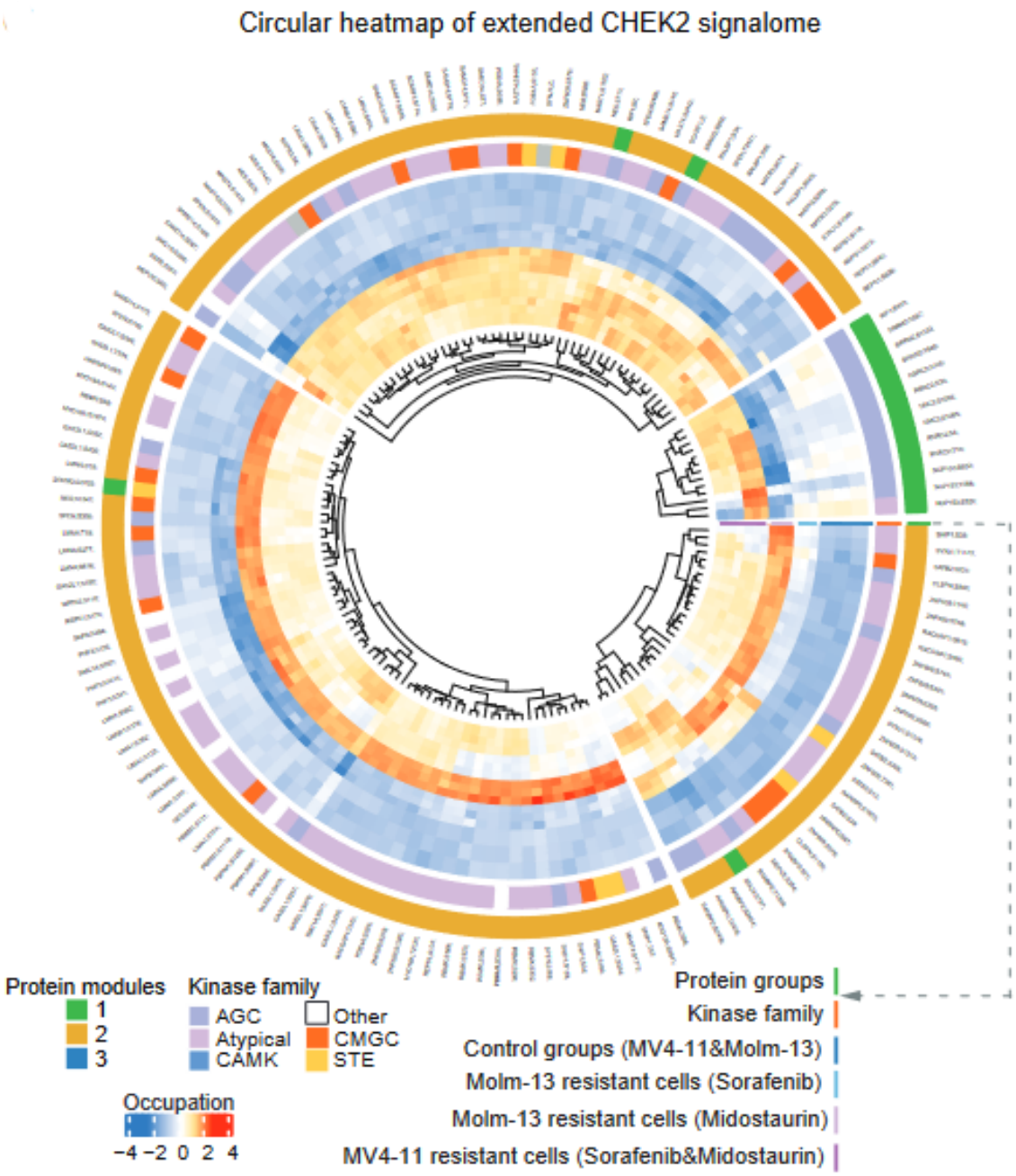

Figure 31: Bar plot showing profile, motif, combined, and prediction score of the top-ranked CHEK1 substrates. The phospho-sites are colour indicated by the predicted top active kinases annotated by the protein modules (outer circle), kinase groups (middle circle), and each phospho-site (inner circle) for all six experimental condition groups.

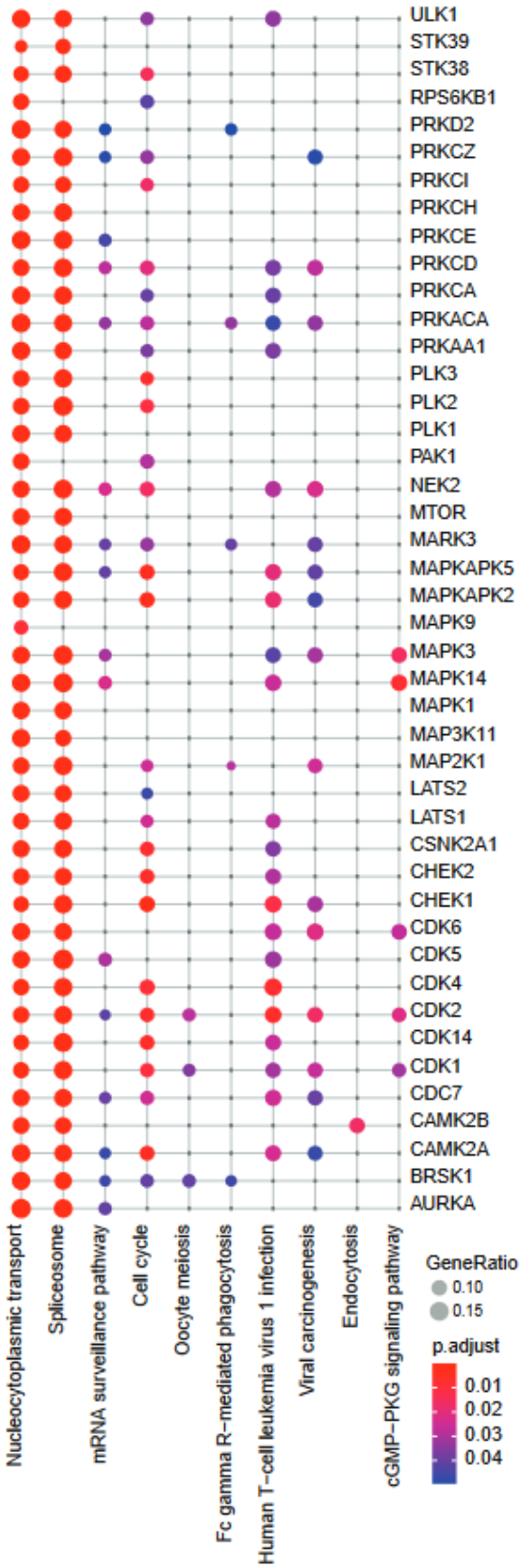

Figure 32: Pathway enrichment based on activated kinases and contribution of respective kinases to the pathway enrichment. KEGG pathway over-representation analysis of kinase-substrate with prediction score > 0.5. The nodes are colored by adjusted p-value and sized by the ratio of proteins in the KEGG set.

3.3. Western Blot analysis and validation

We aimed to analyse crucial and highly alternated proteins via Western Blot to validate our previously detected mass spectrometric findings. The following results show 4 biological replicates of each experimental group. Quantification with ImageJ and statistical analysis with Excel are presented beside the Western blot and in the Figure information.

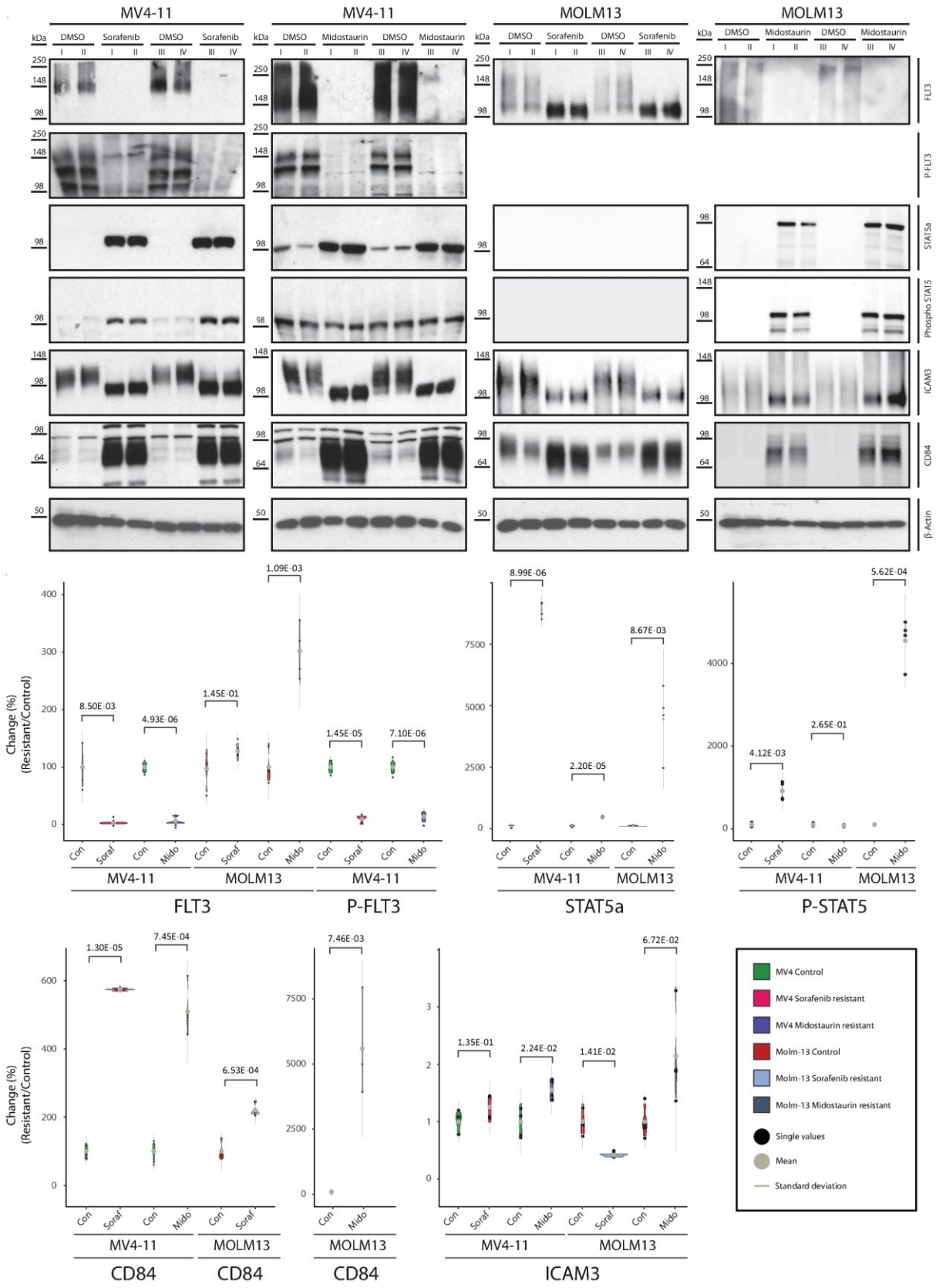

Figure 33: Summary of all experimental conditions for better comparison. The Western Blots of FLT3, P-FLT3, STAT5a, P- STAT5, CD84, and ICAM3, as well as ß- Actin as loading control are shown. The corresponding cell line and experiment are at the figure's top. Two lines of DMSO controls and two lines of TKI resistant cells are alternatingly shown, representing four biological replicates of each group

at the end. The detected protein is indicated on the right-hand side. The kD protein weight marker is displayed on each blot's left side. Underneath the Western blots, the relative expression change of each protein between treated samples and their controls is indicated in percentage. The p-value of each change is written over the percentage value to show significant changes in most cases.

We could show that FLT3 and its phosphorylated form P-FLT3 were concomitantly downregulated in Sorafenib and Midostaurin resistant MV4-11 and Midostaurin resistant Molm-13 cells. In Sorafenib-treated Molm-13 cells, we observed an altered running behaviour of FLT3 at a lower molecular weight suggesting an altered maturation of FLT3. However, in contrast to the other resistant cell lines, FLT3 expression was still present. Further, we could confirm that the STAT family member STAT5a was dramatically upregulated in Sorafenib and Midostaurin resistant MV4-11 cells and Midostaurin resistant Molm-13 cells by 86-, 5-, and 45-fold, respectively. Meanwhile, the regulation of phosphorylated STAT5 (P-STAT5) showed either an upregulation in Sorafenib-resistant MV4-11 and Midostaurin resistant Molm-13 cells or Midostaurin resistant MV4-11 cells with at least an expression level comparable to the respective MV4-11 control cells. During the proteomic analysis, we also observed significantly increased membrane proteins, of which two were the cell adhesion molecules ICAM3 and CD84, proposed to activate autophagy and promote the expression of antiapoptotic proteins such as MCL-1 or Bcl-2. We observed a consistent increase in CD84 and ICAM3 expression in all three investigated conditions. As we observed a consistent decrease in the expression of Bcl-2 and a concomitant rise in Bcl-XL expression in our mass spectrometry experiments, we additionally wanted to confirm these results by performing immunoblots.

3.3.1. Comparison of acute and chronic Sorafenib treated MV4- 11 cells

Next, we were interested in whether the observed proteome alterations were an acute event upon TKI inhibition with Midostaurin/Sorafenib or an effect of chronic treatment with TKIs in our experimental setup. To this aim, we treated Sorafenib and Midostaurin resistant and sensitive MV4-11 cells for two days with Midostaurin or Sorafenib or DMSO as solvent control.

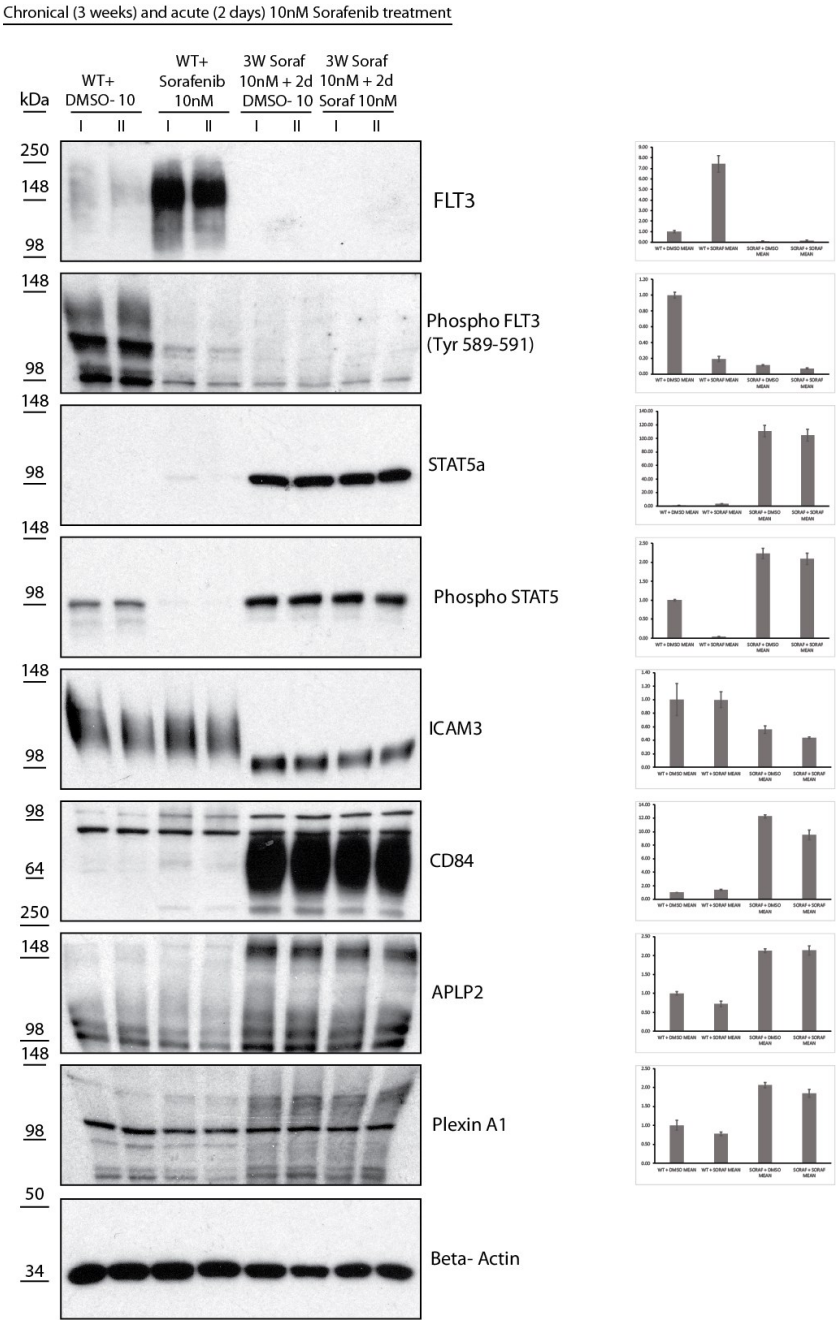

Figure 34: Acute (2 days) and chronically (3 weeks) with 10nM Sorafenib treated MV4-11 cells are compared to their untreated controls (2 biological replicates of each group). Quantifications with ImageJ are shown on the right side of the figure.

3.3.2. Comparison of acute and chronic Midostaurin treated MV4- 11 cells

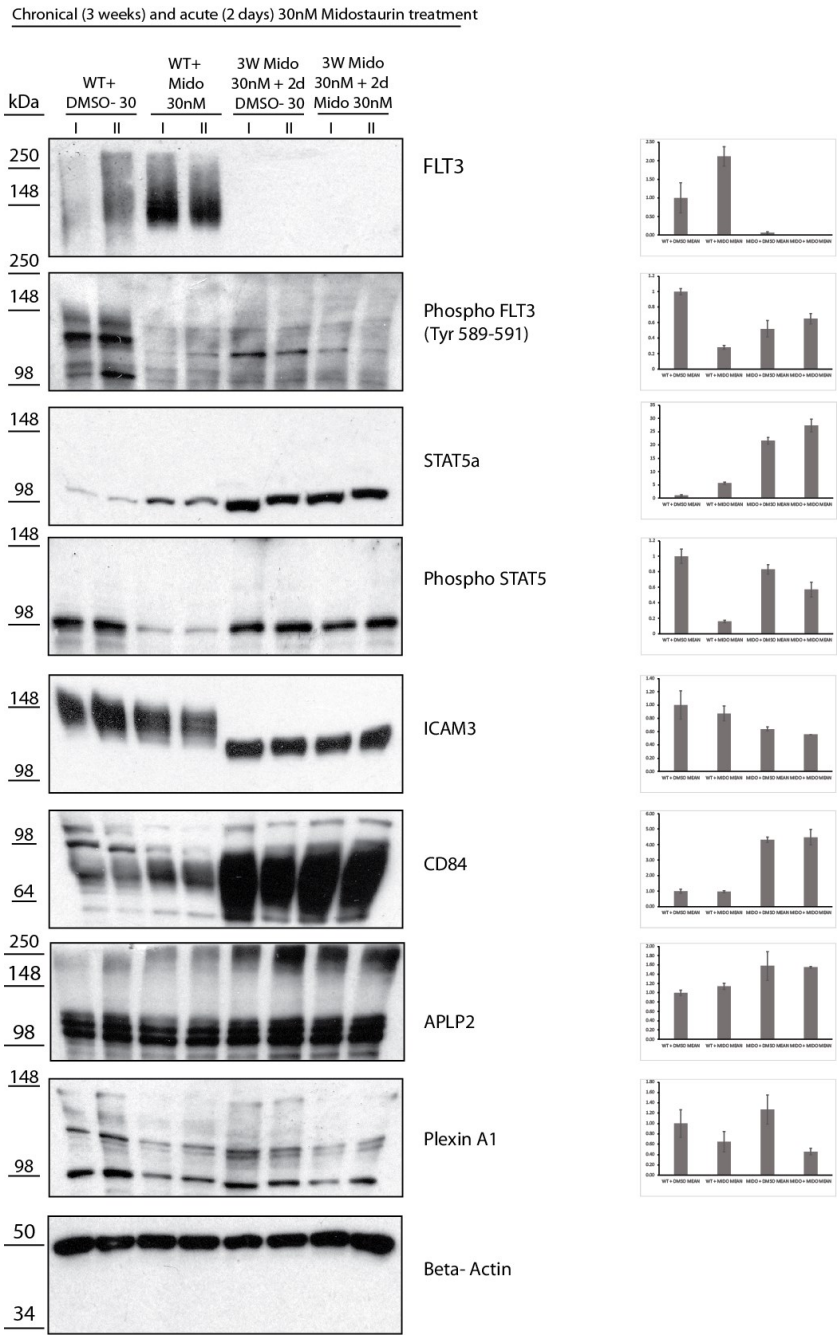

Figure 35: Acute (2 days) and chronically (3 weeks) with 30nM Midostaurin treated MV4-11 cells are compared to their untreated controls (2 biological replicates of each group). Quantifications with ImageJ are shown on the right side of the figure.

In Midostaurin and Sorafenib resistant cells, FLT3 expression was diminished and did not return under treatment with DMSO. In contrast, upon acute treatment with Midostaurin and Sorafenib, FLT3 expression was upregulated in treatment-naive MV4-11 cells. At the same time, P-FLT3 was strongly downregulated upon acute treatment. Furthermore, we observed a slight upregulation of STAT5 and P-STAT5 levels in acutely treated Midostaurin or Sorafenib-sensitive MV4-11 cells. In contrast, their levels remained unaltered upon DMSO or further TKI treatment with the respective drugs in

Midostaurin and Sorafenib resistant MV4-11 cells. In summary, the downregulation of FLT3 results from long-term TKI treatment with Sorafenib or Midostaurin, while acute TKI treatment even leads to an upregulation of FLT3.

3.3.3. Concentration experiment

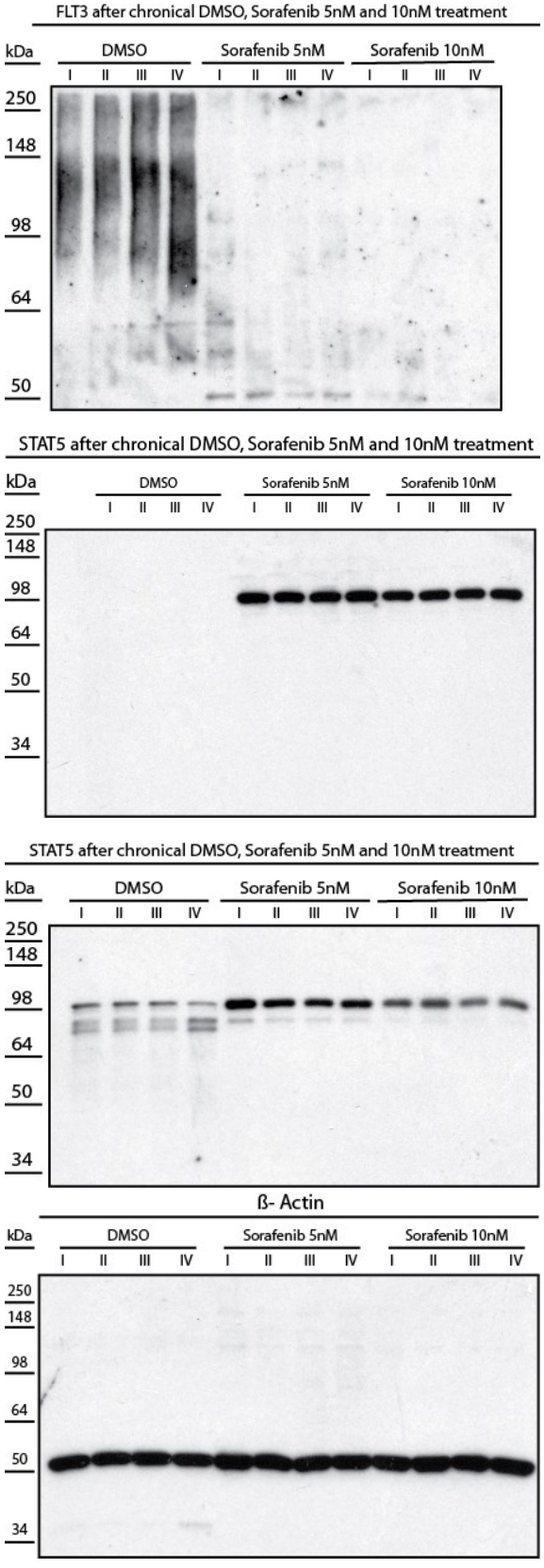

Figure 36: Concentration experiment Western blot. MV4-11 cells were chronically treated with either DMSO as control, 5nM Sorafenib, or 10nM Sorafenib before being lysated. The effects of different concentrations on FLT3, STAT5, P- STAT5, and loading control with ß- Actin are shown.

We observed similar effects on the detected proteins between both concentrations but even stronger pronounced under treatment with 10nM. FLT3 was strongly downregulated in 5nM treated cells and completely vanished in the 10nM treatment condition. STAT5 and P-STAT5 were strongly upregulated under both treatments, showing a stronger expression in the 5nM treatment group.

3.3.4. Patient samples

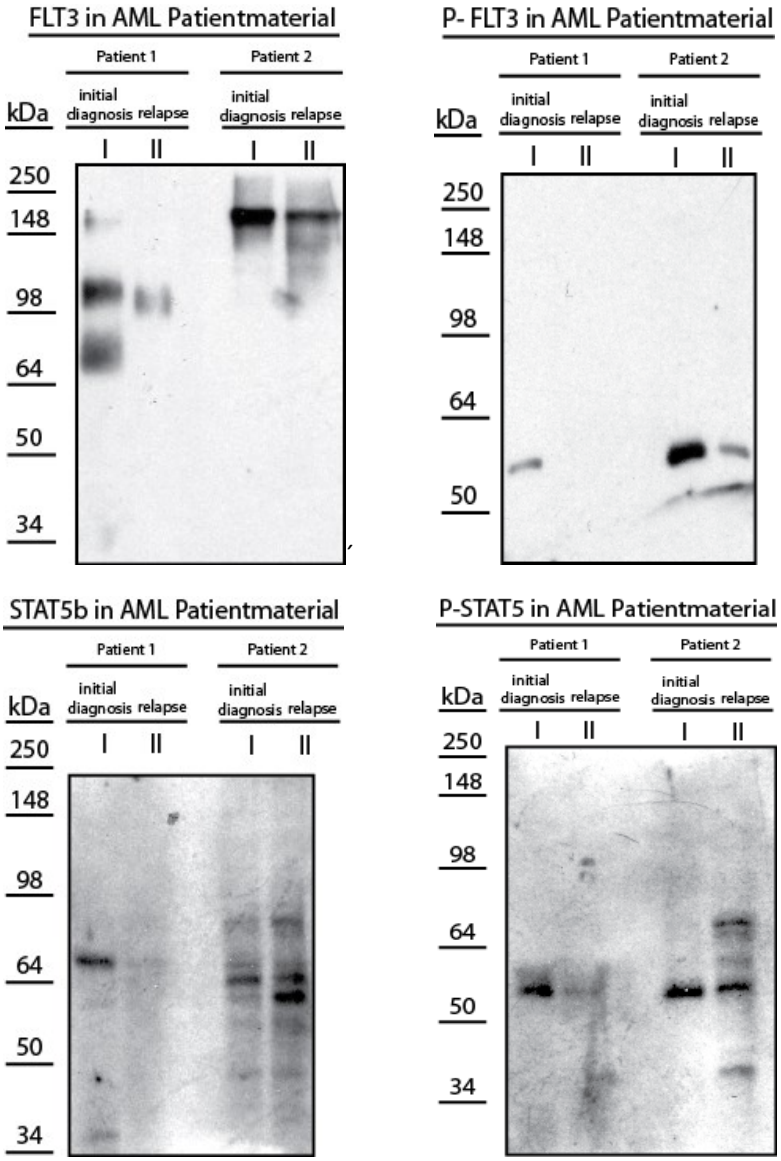

CD84 in AML Patientmaterial Bcl-XL in AML Patientmaterial

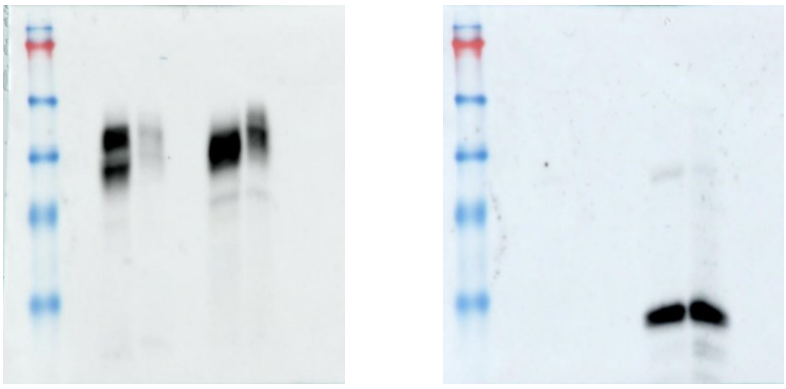

Figure 37: Bone marrow aspirates of two patients with FLT3- mutated AML, who underwent Tyrosine kinase inhibitor treatment in addition to chemotherapy, were analysed. The first sample was collected during the initial diagnosis of the disease, and the second was once the patient relapsed from chemotherapy and TKI treatment. The samples were loaded according to their protein concentrations and relative blast count in the sample.

FLT3 and P-FLT3 seemed stronger expressed in the samples taken at the initial diagnosis of the disease. STAT5 showed divergent expressions in the two patients, with a downregulation in the first and an upregulation in the second case. P-STAT5 and CD84 generally decreased in the samples gained after the disease relapse. Bcl-XL was not detected in the samples of the first patient and was nearly unchanged between the initial diagnosis and relapse in the second patient. Due to the rareness of FLT3 mutated AML patients who underwent polychemotherapy plus FLT3 inhibitor treatment and relapsed, we only had the opportunity to collect and proceed with two different patient samples. This small sample count did not allow general observations or conclusions.

3.4. Survival assays on FLT3 inhibitor resistant cells towards secondary inhibitors

After identifying deregulated pathways such as proliferation, apoptosis, and metabolism of cells, we wanted to know more about the functional impact of some of those regulations. In the case of the identified apoptosis regulating proteins BCL2 and BCL2L1 (Bcl-Xl), we used the Bcl-2-specific inhibitor Venetoclax (also called ABT-199) and the Bcl-XL- specific inhibitor WEHI- 539 (Fig. 38). As JAK-STAT signalling was upregulated and activated in resistant cells (Fig. 39 and 40) we compared the sensitivity of treatment naïve and resistant cells towards a JAK inhibitor. FLT3 inhibitor resistant cells and their control were cultured under standard conditions, and the different inhibitors were applied in geometrical concentration lines (see chapter 2.1.3. material and methods)

3.4.1. Overview proteomic changes

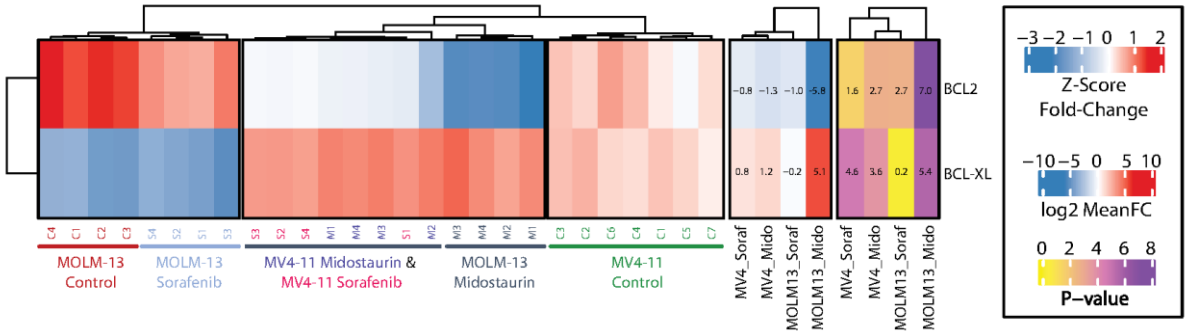

Figure 38: Heatmap showing the proteomic changes of Bcl-2 and Bcl-XL expression in TKI resistant cells compared to untreated controls. The fold change between the treated and untreated samples is shown on the left and represented by a colour scale from blue = -3 fold change, strong downregulation, to red = 2 fold change, strong upregulation. We can see a strong expression of Bcl2 in Molm-13 and MV4-11 control cells and a weak one in the TKI resistant cells. Bcl-XL shows the opposite expression, hardly expressed in drug- naïve cells with a strong upregulation in the TKI resistant. On the right, p-value of detected fold-changes is shown with yellow indicating a low significance and purple a high one.

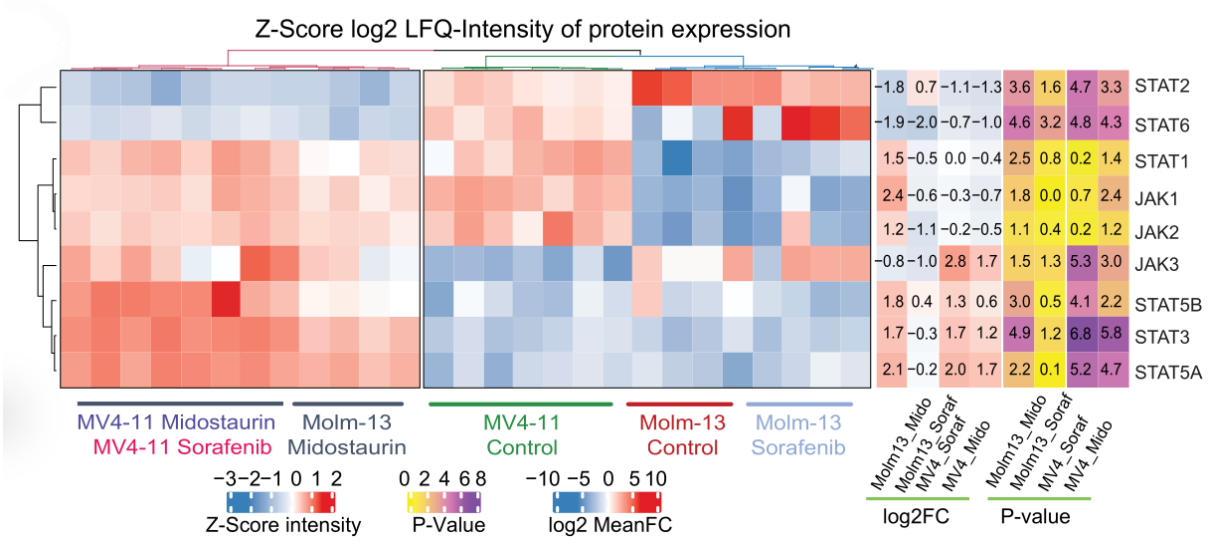

Figure 39: JAK/STAT Protein expression in TKI resistant cells compared to untreated controls. The z-normalized fold change is indicated with a colour scale from blue = -3, strong downregulation to red = 2 fold upregulation. The logarithmic mean fold change of all replicates is shown in the second column from the right with a similar colour scale. The last column shows the p-value of the observed changes indicating a low significance in yellow and purple a high one.

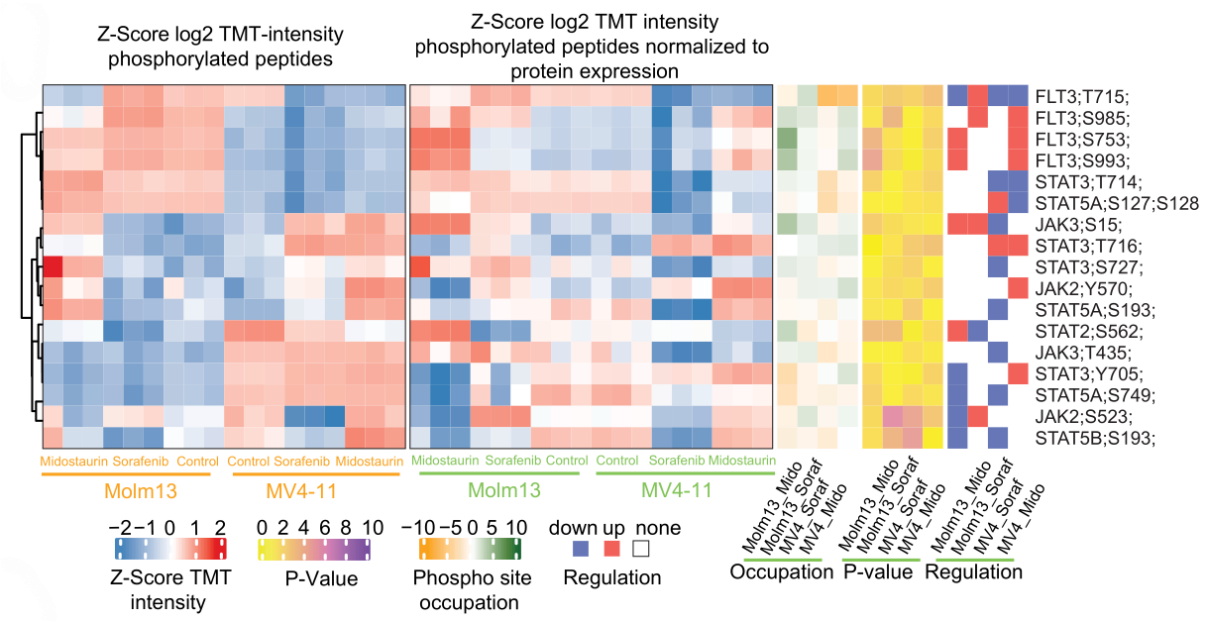

Figure 40: Heat map of phosphorylated JAK and STAT proteins based on non- and normalized data together with occupation, p-value, and indicators for regulation.

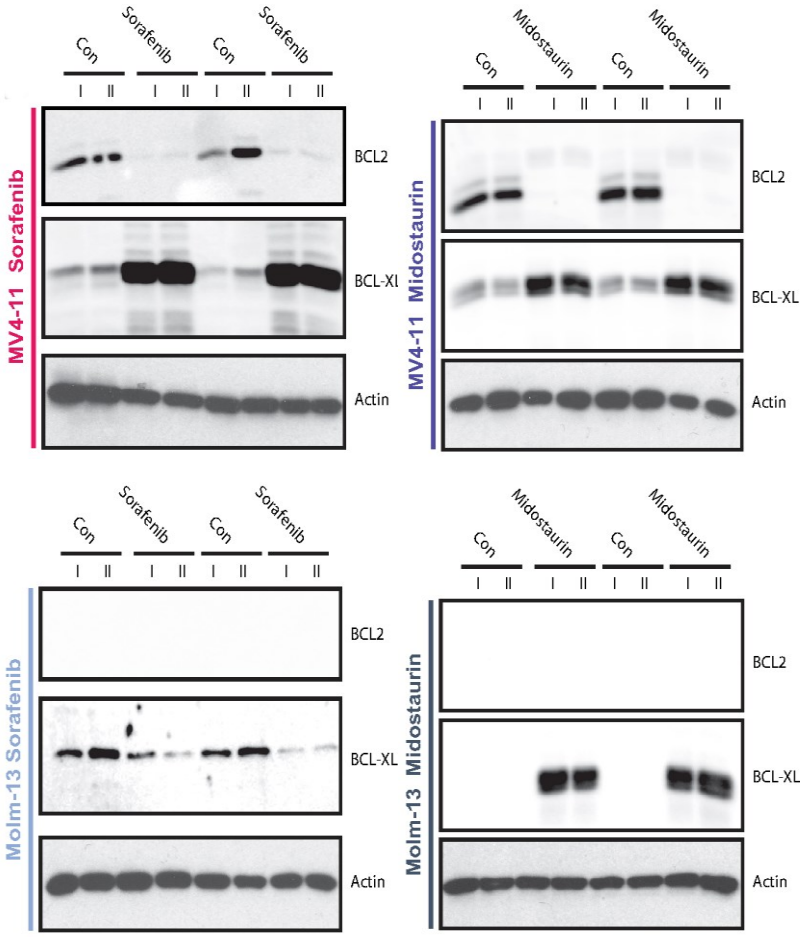

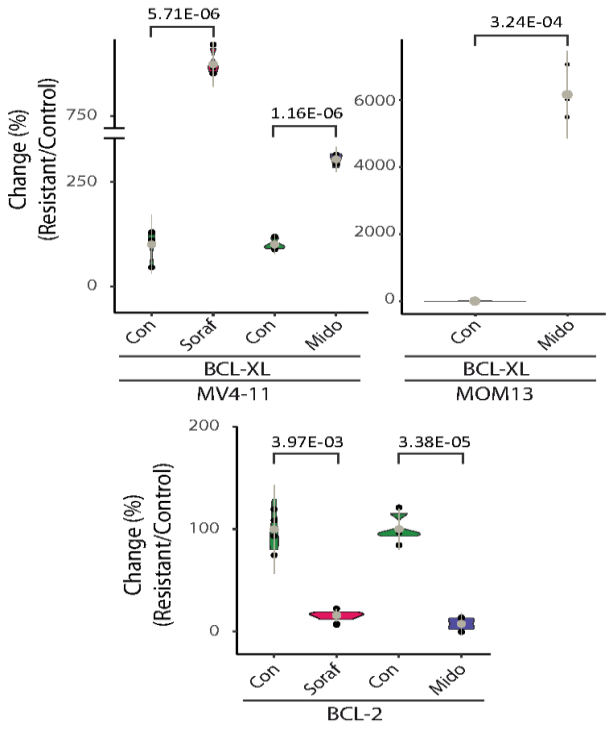

Figure 41: Bcl-2 and Bcl-XL expression analysis via Western blot. The shown cell line is indicated on the left border of the blot, with the experimental condition on top. As the mass spectrometric data shows, Bcl-2 showed strong downregulation in TKI treated MV4-11 cells. Molm-13 cells don't express Bcl-2 in a sufficient amount to be detected via Western blot. Conversely, Bcl-XL shows a strong upregulation in TKI resistant cells compared to their control. The figure on the bottom right shows the quantitative relative change between the experimental groups.

3.4.2. Bcl-2 inhibition with Venetoclax, ABT-199

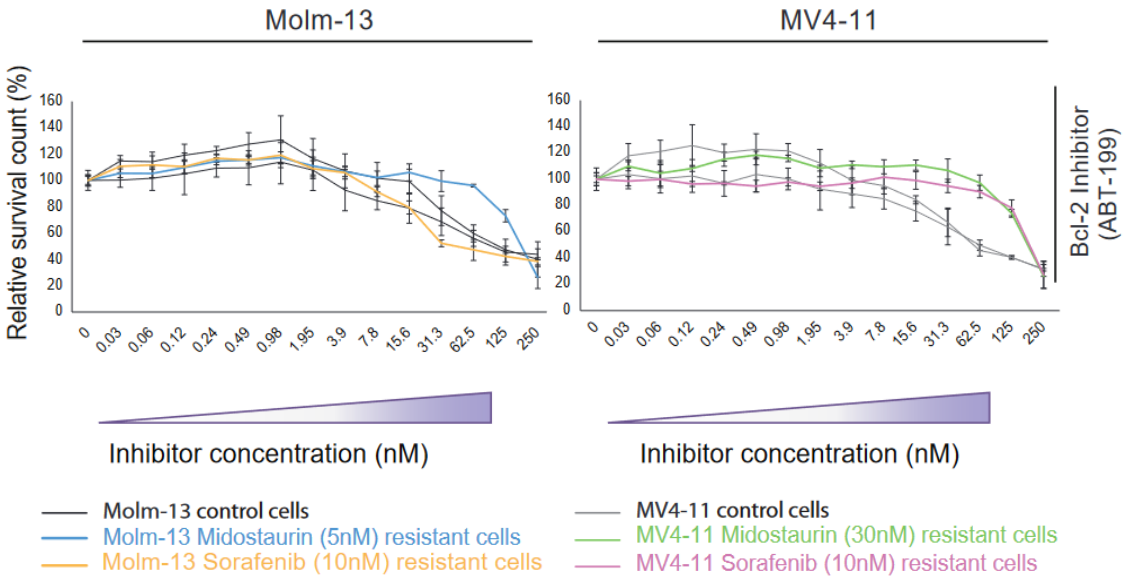

Figure 42: Molm-13 (left) and MV4-11 (right) Navitoclax treated cells. The horizontal axis represents the concentration of Navitoclax used, the Vertical axis represents the percentage of living cells compared to untreated controls.

We could show that Venetoclax in both TKI naïve MV4-11 and Molm-13 cells had a dose-dependent effect on cell viability with an IC50 of 3.75nM for MV4-11 cells and 7.5nM for Molm-13 cells. However, the Sorafenib and Midostaurin resistant cohorts of both cell lines showed nearly no effective reduction in cell count under the Venetoclax treatment. This reaction is in good accordance with our previously described strong downregulation of Bcl-2 in the TKI resistant cells. ABT-199 is a specific inhibitor of Bcl-2 thus, affecting the untreated cells with a higher amount of Bcl-2 more than the resistant ones.

3.4.3. Bcl-XL specific inhibitor WEHI- 539

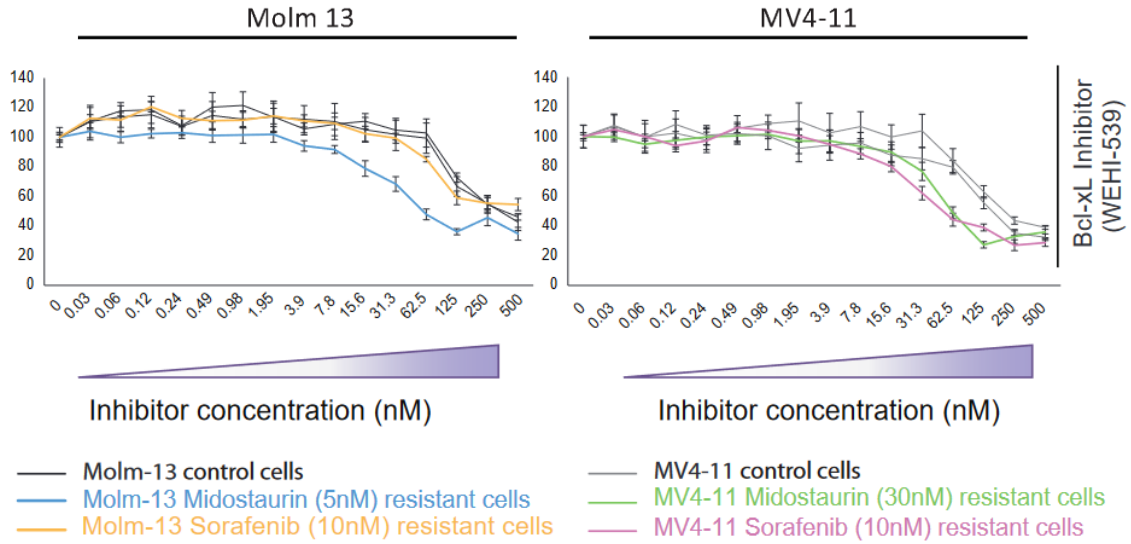

Figure 43: Molm-13 (left) and MV4-11 (right) Bcl-XL specific inhibitor treated cells. The horizontal axis represents the concentration of Bcl-XL inhibitor used, the vertical axis represents the percentage of living cells compared to untreated controls.

We observed strong suppression of cell viability in the resistant samples, while treatment naïve cells were unaffected. In the MV4-11 cell line, both Midostaurin and Sorafenib resistant samples only showed 20% of their initial cell count under the inhibition, with an IC50 lower than 16nM. In the Molm-13 line, Midostaurin treated cells showed a strong repression with an IC50 lower than 16nM again, while the Sorafenib-treated cells had a nearly average level. These results fit our prior observation that Bcl-XL protein is strongly upregulated in TKI resistant cells contributing to their survival. The Molm-13 Sorafenib treated cells did not show this upregulation, which explains their reduced vulnerability towards the Bcl-XL inhibition. In summary, Sorafenib and Midostaurin resistance came along with a sensitization towards Bcl-XL inhibition in our experiment. This might be an outlook on a second therapeutic strategy for relapsed patients after tyrosine kinase inhibitor treatment.

3.4.4. JAK- inhibitor

As we observed an apparent upregulation for several members of the STAT family, including STAT5A, STAT5B, and STAT3, for all investigated conditions (Figure 36), we were curious whether JAK-inhibition would help to suppress tumour cell growth in Midostaurin or Sorafenib-resistant cell lines.

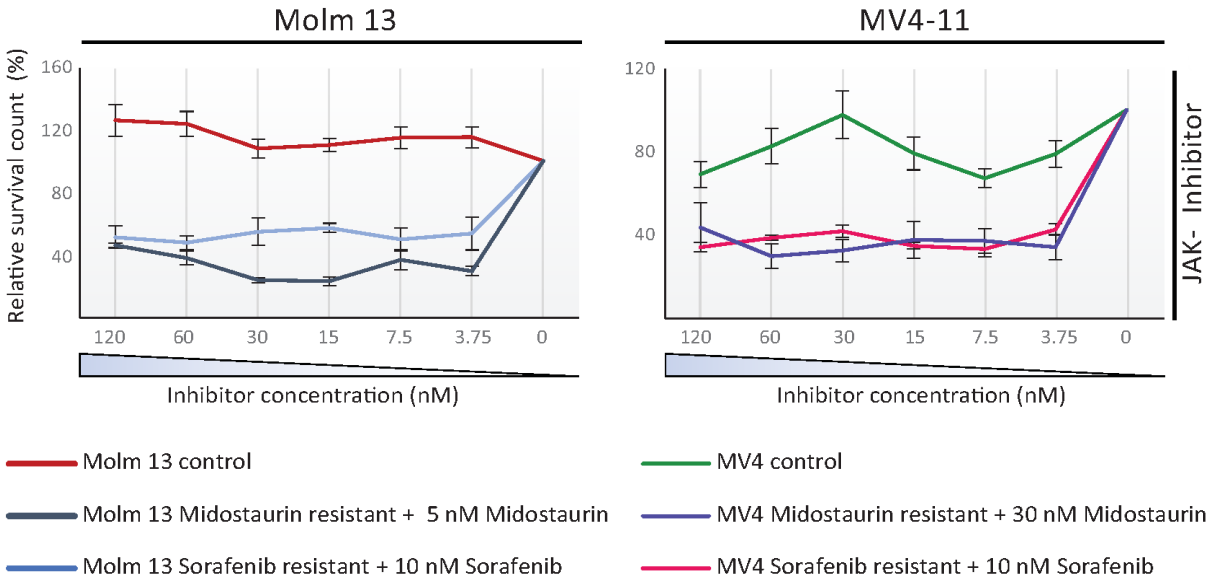

Figure 44: Molm-13 (left) and MV4-11 (right) JAK inhibitor treated cells. The horizontal axis represents the concentration of ABT 737 used, and the vertical axis represents the percentage of living cells compared to untreated controls.

As expected, we could observe a growth suppressive effect of JAK-inhibition in both resistant Molm-13 and MV4-11 cells, which, however, was not as pronounced as observed for the Bcl-XL inhibitor. These effects did not occur in naïve MV4-11 and Molm-13 cells, which stands again in good accordance with our proteomic data showing a strong upregulation of JAK/STAT proteins in the TKI treated cells. This might be an outlook on a potential second-line treatment in Sorafenib, or Midostaurin relapsed AML.

3.4.5. Hypomethylating agents and PARP Inhibitors

Hypomethylating agents and PARP- Inhibitors are important chemotherapeutic agents used to treat various cancer types. Decitabine, one of the hypomethylating agents, is commonly used in treating AML, even as Monotherapy in especially vulnerable patient groups. Olaparib is a PARP- inhibitor, which inhibits the DNA- repair capacity of the cells, especially established in the treatment of solid tumors. We monitored alterations of the pathways, addressed by either hypomethylating agents or PARP inhibitors, as shown in the Figures below (Figure 45, 46).

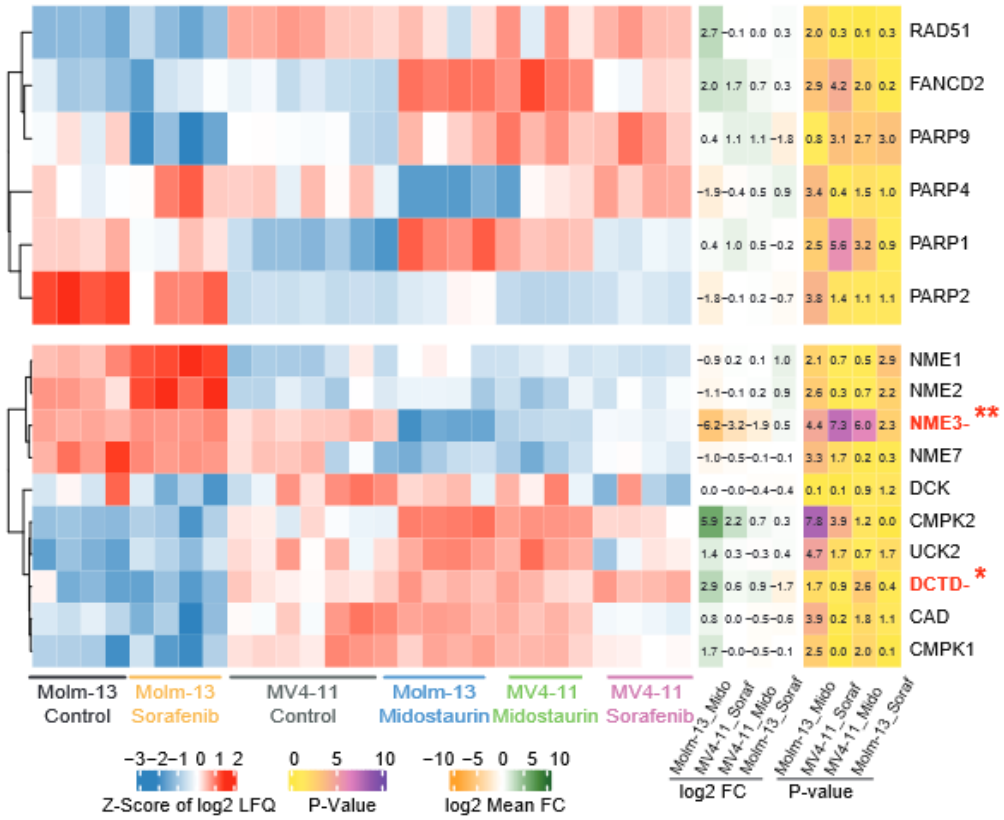

Figure 45: Heat map of z-scores of protein expression for critical enzymes involved in the pathway of hypomethylating agents (HMA) metabolism and PARP family proteins. Upregulations on protein-expression levels are coded in red and downregulations in blue. P- Value of the detected fold- change is indicated on the right-hand side.

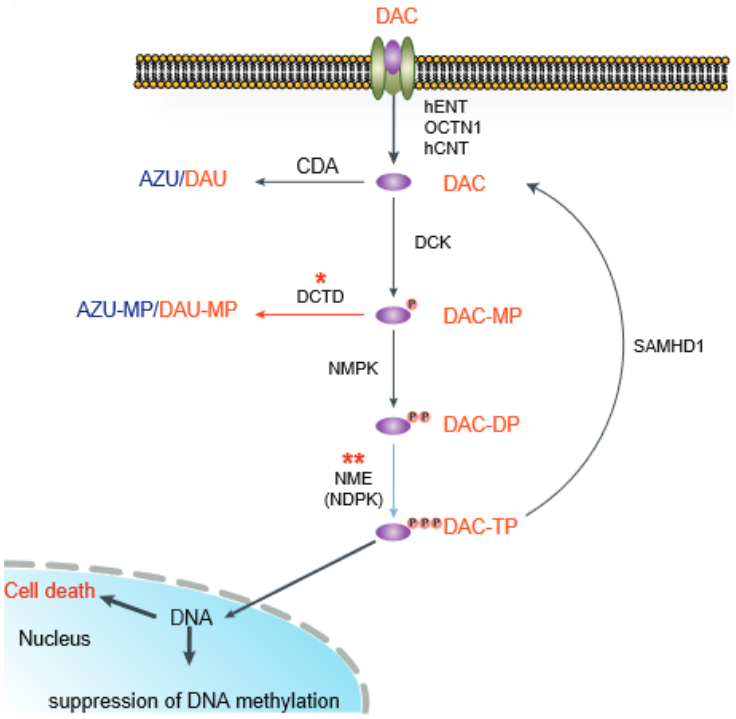

Figure 46: Hypomethylating agents (HMA) metabolic pathway with critical proteins involved.

We detected a significant downregulation of NME3, a protein involved in DNA repair and regulating haematopoiesis, influenced PARP- Inhibitors. This downregulation was seen in all resistant cell pools. Another protein of interest, due to its upregulation, was DCTD, which can be influenced by hypomethylating agents. We analysed the treatment response of our resistant cell pools compared to their naïve counterparts towards either Olaparib or Decitabine (Figure 47).

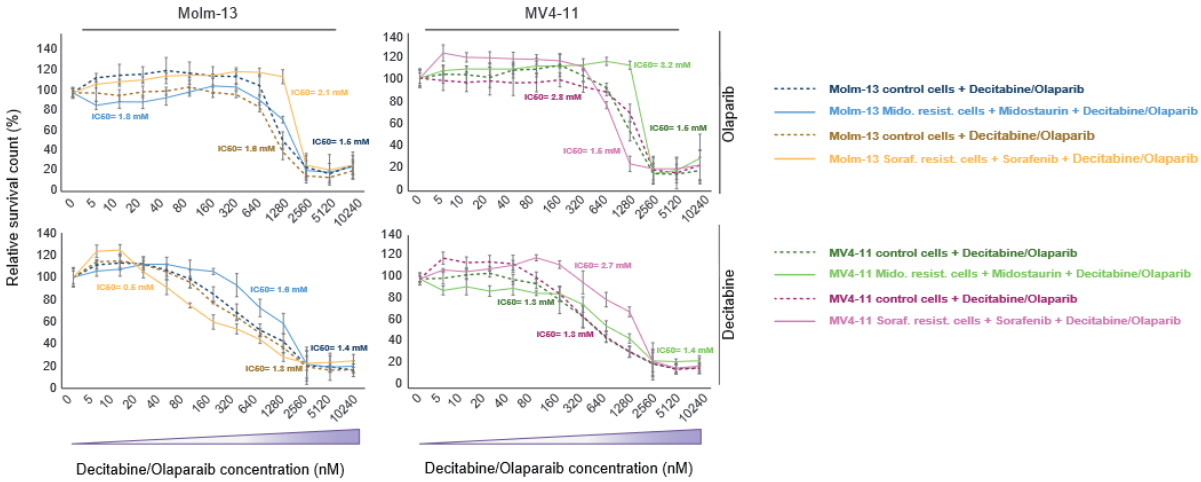

Figure 47: Survival assay of Midostaurin-/Sorafenib-resistant Molm-13 cells (left) and Midostaurin-/Sorafenib-resistant MV4-11 cells (right) compared to respective naïve cells concerning increasing concentrations of the PARP inhibitor Olaparib (upper panel) and Decitabine (lower panel).

The cell survival rates of our resistant cell pools differed from their treatment naïve counterparts when treated with Olaparib or Decitabine. In the Molm-13 cell groups, Sorafenib-resistant cells showed a slightly higher tolerance towards Olaparib up to a concentration of 1280nM. The cell survival curves under Decitabine treatment showed a higher tolerance of the Molm-13 Midostaurin resistant cell pool. For the MV4-11 cells, Midostaurin resistant cells showed higher survival counts, up to a concentration of 1280nM Olaparib, compared to the other pools. For Decitabine treatment, MV4-11 Sorafenib-resistant cells showed the highest tolerance.

4. Discussion

4.1. Biochemical changes in TKI resistant FLT3 mutated AML cells

The FLT3 mutation in acute myeloid leukaemia was one of the first and most important genetic alterations found in AML (Gilliland & Griffin, 2002; Rosnet et al., 1996). Soon a correlation between the FLT3 mutational status and the disease dynamic and overall survival could be demonstrated. Different mutations have been detected since, the most common representing an internal tandem duplication of the juxta-membrane region, found in up to 30% of all AML patients (Levis & Small, 2003; Metzeler et al., 2016). Besides the ITD mutation, the receptor site and kinase domain point mutations have been found. The impact on survival and aggressivity of the disease is divergent between the mutational types, dependent on its location and whether the mutation is heterogenous or monogenous. In non-mutated AML cells, the FLT3 receptor tyrosine kinase is activated by binding the FLT3-ligand, only promoting downstream signalling while in contact with it (McKenna et al., 2000). Mutations of this tyrosine kinase induce a ligand independent perpetual activation of the kinase followed by constitutive activation of downstream signalling pathways (Kiyoi et al., 1998; Tse et al., 2000). These activated pathways are some of the essential proliferation and cell survival promoting cascades, such as the PI3K/MAPK/AKT and JAK/STAT pathways. These biochemical changes explain the lower treatment response rates and higher dynamic of FLT3- ITD mutated AML types compared to the normal genotype (Papaemmanuil et al., 2016). Small molecular tyrosine kinase inhibitors showed promising response rates and effective inhibition of those effects. Midostaurin as a multi-tyrosine kinase inhibitor was approved as standard therapy in FLT3 mutated AML patients in addition to Chemotherapy after showing a significant improvement in median overall survival (Schlenk et al., 2019; Stone, Mandrekar et al., 2017). Sorafenib is another multityrosine kinase inhibitor that showed promising effects in FLT3-mutated AML but did not meet the criteria of improvement in overall survival for general approval in the SORAML study (Röllig et al., 2015). Nevertheless, this study did not stratify for FLT3-ITD mutational status, and Sorafenib was established as a potent agent for maintenance therapy after stem cell transplantation in FLT3-ITD AML (Brunner et al., 2016; Burchert et al., 2020; Chappell et al., 2019). In 2018, the FDA approved Gilteritinib as a specific FLT3 inhibitor as treatment in relapsed or refractory FLT3- mutated AML (Perl et al., 2019). Nevertheless, the development of resistance mechanisms under long-term therapy undermined those effective treatment options, reducing the effects on overall- and long-term survival (Piloto et al., 2007). Different studies aimed to identify those resistance mechanisms and were able to describe some potential mechanisms in this process. The FLT3 tyrosine kinase itself was analysed, and point mutations in its kinase domain, such as Asn-676, among others, have been proposed as resistance promoting mechanisms against these tyrosine kinase inhibitors (Daver et al., 2015; Heidel et al., 2006; Smith et al., 2015). Besides the receptor mutation, an upregulation of the FLT3-ligand has been described as another potential resistance mechanism to overcome FLT3 inhibition (Sato et al., 2011). Other studies found changes in the surrounding bone marrow of leukemic cells, providing microenvironment protection (Traer et al., 2016; Zeng et al., 2009). Finally, the activation of alternative proliferation pathways such as JAK/STAT and PI3K/mTOR were found as targets in resistant cells (Zhou et al., 2009a).

Our proteomic analysis of TKI resistant cell lines compared to their sensitive counterparts generated essential insights into the biology of these processes. Our mass spectrometric approach provided us with broader information than these previous studies. We confirmed some of the most important described resistance mechanisms on the protein level. Besides identifying potential key agents, we

mapped the cells' whole pathways and functional structures (Frejno et al., 2020). We observed links within the different resistance promoting alterations as the interaction from FLT3 signalling to the JAK/STAT pathway to the apoptosis regulation through Bcl-proteins. Due to the complexity of these resistance mechanisms, also reflected by the lack of breakthroughs in treating TKI relapsed patients despite a tremendous research effort in this field, this overview might provide new insights for a deeper understanding of TKI resistance. The dynamic adaptations of leukemic cells under treatment can only be decoded by knowing these networks. We chronically treated FLT-ITD mutated AML cells (MV4-11 and Molm-13) with either Sorafenib, Midostaurin, or DMSO as solvent control in therapeutic doses until the cells gained resistance towards the respective drugs. We then performed a comparative high resolution mass spectrometric analysis of their proteomes.

4.2. The FLT3- Kinase

The first interesting finding was the downregulation of the FLT3 receptor in TKI resistant cells. We could show that this effect only occurred under long-term treatment, whereas acute TKI treatment induced an upregulation of the FLT3 expression (Figures 37 and 38). This finding was similar to previous studies of another group using the FLT3- Inhibitor Quizartinib in MV4-11 cells (Reiter et al., 2018). We concluded that the TKI resistance mechanism in our experiments was not mediated through adaptations of the FLT3 receptor itself. Besides the significantly weaker expression of the receptor in the TKI-resistant cells, its activation through phosphorylation was still effectively inhibited by the treatment. Upregulation of the FLT3 receptor seems to be a short-term strategy to overcome its inhibition. Nevertheless, the TKI inhibition in our trial was strong enough to block FLT3 phosphorylation and the activation of its downstream pathways despite higher FLT3 expression levels. The missing success of this reaction towards the TKI treatment might explain the strong downregulation of FLT3 after long-term treatments and resistance development. However, its previously described downstream pathways as JAK/STAT and PI3k/Akt are reactivated in resistant cells, indicating an FLT3-independent activation mechanism.

Another striking finding was the divergent reaction of the cells toward the different tyrosine kinase inhibitors. The MV4-11 cell line, carrying a homozygous FLT3-ITD mutation and thus only expressing the mutated variant of the kinase, showed similar strong reactions towards Sorafenib (10nM concentration) and Midostaurin (30nM concentration). In contrast, the Molm-13 cell line, carrying a heterozygous FLT3- ITD mutation, meaning that the cells express the mutated and the wild-type version of the tyrosine kinase, showed a diverging behaviour concerning cell survival for both inhibitors. Whereas Midostaurin effectively induced apoptosis in Molm-13 cells, even requiring a dose reduction from 30nM to 10nM, to enable the survival of at least a few cells for resistance development, Sorafenib did not significantly alter cell survival. The Molm-13 cells did not undergo apoptosis under treatment with 10nM of Sorafenib, demonstrated by hardly any reduction in cell count. An increase in the applied drug concentration resulted in more apoptosis, but the concentration needed for an adequate induction of cell apoptosis to induce resistance development was not in a reasonable therapeutic window for modelling clinical conditions. This observation might follow the clinical effectiveness of both drugs: Midostaurin showed high treatment responses in nearly all patients with FLT3 mutated AML, and Sorafenib showed more divergent effects, finally leading to its rejection as a treatment agent. Both drugs are multi-tyrosine kinase inhibitors, showing a high affinity for the FLT3 kinase but not being specific to it. Therefore, a final understanding of those inhibitors' therapeutic effects still needs to be completed. Nevertheless, a link between the mutational status, the amount of wild-type FLT3 expressed by the leukemic cells, and the effectiveness of the used inhibitor seem probable (Chen et al., 2016).

4.3. The JAK/STAT Pathway

One of the closest and most crucial downstream pathways of the FLT3 kinase is the JAK/STAT signalling. It has been shown to promote cell proliferation and metabolism, regulating cell death and tumour development (Kiu & Nicholson, 2012). Cell receptors for various ligands, such as cytokines or interferons, activate the Janus kinases, activating the STAT proteins through their SH2 domains (Schindler, Levy, & Decker, 2007). The STAT molecules then move into the nucleus of the cells, mediated by importin proteins, where they act as transcription factors (Aaronson & Horvath, 2002). The activity of this pathway is already upregulated in FLT3-mutated AML cells. Nevertheless, we observed an even higher upregulation in Sorafenib and Midostaurin resistant MV4-11 and Molm-13 cells. These higher expression rates were observed in several STAT proteins, such as STAT5A, -B, and STAT3. Despite the still effective FLT3 inhibition described above, their activated phosphorylated form was upregulated or at least equal to the non-resistant cells (Steelman et al., 2008). Especially the observed upregulation of STAT5 was in good accordance with the findings of previous studies (Yoshimoto et al., 2009; Zhou et al., 2009b). The JAK proteins inducing the activation of STATs showed divergent regulation in the different treatment groups. Sorafenib-resistant MV4-11 cells showed an upregulation of JAK1 and JAK2, whereas Midostaurin resistant MV4-11 and Molm-13 cells showed a more robust upregulation of JAK3. Least is linked to Interleukin mediated signal transduction by binding their gamma-cites. Besides those upregulations, we found that PTPN6, an essential JAK/STAT signalling inhibitor, was strongly downregulated in all cell types, promoting the pathway's activity. In summary, the mechanisms seen in the TKI-resistant cells lead to increased activity of the JAK/STAT pathway, indicating its importance as a proliferation and survival mechanism. Like other tyrosine kinases, Janus-kinases might escape the inhibition through Sorafenib and Midostaurin and become an essential alternative as growing signal receptors and transducers in the resistant leukemic blasts.

These changes seem to play an important role in Sorafenib and Midostaurin resistance development, as they can be found in both cell lines and all resistance conditions. We assumed that higher expression of JAK proteins and activation of STAT signalling should render TKI-resistant cells more sensitive towards JAK-inhibition. Hence, we treated TKI resistant cell lines and their drug- naïve counterparts with a JAK-inhibitor. Indeed, TKI-resistant cells showed a higher sensitivity in the form of significantly lower cell counts toward the JAK-inhibitor. The induced cell death was twice as strong, regardless of the applied concentration in the Midostaurin and Sorafenib resistant cell lines. Hence, JAK-inhibition might be a therapeutic option in Midostaurin and Sorafenib resistance in AML patients.

Our findings regarding the FLT3 kinase showed us that activation of JAK/STAT signalling in Sorafenib and Midostaurin resistant AML cells must occur through an alternative mechanism. We used our proteomic data to monitor some of the most important known alternative activators of Janus kinases. We found an upregulation of Insulin-like Growth factor 1 receptor (IGF1R) in Sorafenib and Midostaurin resistant MV4-11 cells, known to activate the JAK/STAT signalling. In Midostaurin-resistant Molm-13 cells, cytokine receptor-like factor 3 (CRLF3) and the plasminogen receptor PLGRKT were found to be upregulated (Vago et al., 2019; Vainchenker & Constantinescu, 2013; Yang et al., 2009). Activation of cell survival and proliferation promoting signals from the JAK/STAT pathway might be enhanced by the overexpression of alternative membrane receptors for cytokines and hormones besides FLT3.

The transcription effects of STAT proteins have been shown to regulate various genes, such as the Bcl-2 family protein expression, which is crucially involved in the regulation of apoptosis (Green et al., 2015; Groot, Raaijmakers, Lammers, & Koenderman, 2000). Bcl-XL, one of its members, which shows strong anti-apoptotic effects, was strongly upregulated in our resistant cell lines.

4.4. Apoptotic signalling via Bcl- family proteins

Due to its functional importance in developing resistance, we took a closer look at apoptosis pathways in our proteomic dataset. We observed a strong downregulation of Bcl-2 in all cell types. Bcl-2, located in the outer mitochondrial membrane, promotes the resistance against apoptotic signalling and hereby cell survival. Bcl-2 is an oncogene in different cancer types, especially in interaction with additional proto-oncogenes. At the same time, Bcl-XL (also known as Bcl-2L1) was strongly upregulated in our TKI-resistant cells, supporting its antiapoptotic effects. Bc-2 family proteins form a balance in the highly regulated process of apoptosis, which is critical to the formation of healthy organisms. Resilience to apoptosis is necessary to enable cell survival and for cell maintenance under conditions of cellular stress. Nevertheless, self-renewal and the removal of emerging neoplastic and misfunctioning cells require apoptosis to maintain general homeostasis in multicellular organisms. Under certain circumstances, apoptosis is accelerated, such as in degeneration. Dysregulation of this balance is an important part of carcinogenesis, enabling cancer cells to proliferate and survive regardless of their microenvironment. The regulation of intrinsic apoptosis occurs at the mitochondria, where the proteins Bax and Bad induce the release of Cytochrome C, which leads to the building of the apoptosome and activation of caspases, degrading the proteins and destroying the cell. The signalling by Bax and Bad is counter regulated by inhibitors of apoptosis as the Bcl2- family proteins, cytokine response modifier A inhibiting caspases, and further proteins in this group. The tendency of our Sorafenib and Midostaurin resistant cells towards antiapoptotic signalling might enable their proliferation despite the presence of the inhibitors. We again wanted to evaluate the functional impact of the observed changes in the TKI resistant cells. Therefore, we analysed the response of the different cell lines toward specific inhibitors of the Bcl-2 protein family. The Bcl-XL specific inhibitor WEHI-539 suppressed the growth of Sorafenib and Midostaurin resistant cells at x-fold lower concentrations than in the respective wild-type cells. The effect of Bcl-XL upregulation inducing a higher resistance towards tyrosine kinase inhibitors or chemotherapy is in accordance with prior studies (Bagrintseva et al., 2005). On the other hand, Bcl-2 downregulation in TKI resistant cells made them less sensitive toward a treatment with ABT-199 known as Venetoclax. This treatment seemed effective only in the drug-naïve cells, whereas TKI resistance coincided with resistance to Bcl-2 inhibition. In accordance with our proteomic findings, the unspecific Bcl- Inhibitor ABT-737 inhibiting Bcl-2, Bcl-XL, and Bcl-W did not show a difference in effectiveness in the TKI-resistant and naïve cells. The divergent regulation of Bcl-2 and Bcl-XL might explain this observation.

Venetoclax was approved by the FDA in 2019 as a combination agent with Azacytidine, Decitabine, or Cytarabine in newly diagnosed AML patients aged 75 or older. Several clinical trials investigate its potential in younger or relapsed patients. Our data might confirm the approach of using Bcl2 inhibitors in first-line therapy for patients who are not eligible for the standard of care. This important apoptosis modulator played an essential role in our *in vitro* model. On the other hand, Venetoclax was no longer a suitable therapeutic agent upon the emergence of Midostaurin/Sorafenib resistance in our experimental model. In those cases, our data suggest that a broader inhibition of the Bcl-protein family, including Bcl-XL, is better suited to overcome this resistance. The promising results of ABT-737 and its successor ABT-263 (Navitoclax) in current clinical trials are limited by their side effects, such as thrombocytopenia (Kohl et al., 2007). Thrombocyte survival has been described to be highly dependent on the pro-survival function of Bcl-XL. The inhibition of Bcl-XL function led to strong thrombocytopenia coming along with severe bleeding complications, especially in the already leukaemia weakened organism (Kohl et al., 2007; Tse et al., 2008). Therefore, despite their potential for relapsed AML patients, Bcl-XL-specific inhibitors such as WEHI- 539 are not yet generally suited for

standard therapy (Lessene et al., 2013). Nevertheless, a further optimized patient treatment and management of thrombocytopenia via supplementation of thrombocyte concentrates or by performing a prior bone-marrow stimulation of thrombopoiesis through low-dose Bcl-XL inhibitor priming might overcome those side effects. These methods have been approved for the use of Navitoclax in B-cell chronic lymphatic leukaemia (Kipps et al., 2015). Hence, further investigations in this field are necessary and beneficial due to the commonness of thrombocytopenia in patients with leukemic disease.

4.5. Alterations of the inflammasome expression

The inflammasome is part of the innate immune system of cells and represents another central pathway in the regulation of the functions and survival of a cell. In cooperation with the aforementioned process of apoptosis, inflammation-induced inflammasome activation may lead to pyroptosis, a particular form of programmed cell death. A major difference to the process of apoptosis is the release of cytokines during pyroptosis that trigger a strong immune reaction. A wide range of receptors activates downstream proteins such as ASC/PYCARD and Caspase-1 (CASP1), which were strongly downregulated in all our TKI resistant cell lines. These proteins are important mediators of pyroptosis, activating Caspase 1 mediated cleavage of Gasdermin, whose cleavage products induce apoptosis via Bid, Caspase- 9 and 3 (Tsuchiya et al., 2019; Vainchenker & Constantinescu, 2013). Besides apoptosis, those proteins induce inflammatory pathways via pro-IL1β and pro-IL18 (Karki & Kanneganti, 2019). Those effects usually represent cells' vulnerability to the organism's immune reactions. Their significant downregulation in our Midostaurin and Sorafenib resistant cell lines might be another critical survival mechanism under treatment conditions. Indeed, previous studies proposed the activation of the inflammasome to induce pyroptotic cell death in AML as a therapeutic strategy (Johnson et al., 2018). Nevertheless, according to our data, this treatment strategy seems less effective in Midostaurin and Sorafenib resistant cells, making it more suited as first-line therapy.

4.6. Metabolic reprogramming

An interesting observed side effect was changes in cellular metabolism upon the development of resistance during our *in vitro* treatment experiments. Once the lowest cell counts were reached during treatment and cell proliferation started to rise again, we observed an over- proportional glucose consumption in the TKI-resistant cells. Despite the same medium preparation and culturing method, refreshing the cells every 3rd day, the pH indicator Phenolphthalein present in the RPMI Medium showed an earlier and stronger colour change to yellow (lower pH) in the resistant cells compared to their controls. Even a lower cell count, through stronger dilution, of resistant cells compared to control cells did not alleviate this effect. This high consumption of sugars and metabolites in the medium sometimes even restricted the highest possible cell count of resistant cells in our *in vitro* model due to the lack of supplements after a few hours. Therefore, we expected to see metabolic activations in the proteome of our Midostaurin and Sorafenib resistant cells. Indeed, we observed metabolic reprogramming with the upregulation of pacemaker enzymes of glycolysis. These included the upregulation of Hexokinase 1, Phosphofructokinase M, and B, some central catalysators of glycolysis and sugar metabolism. At the same time, the pyruvate dehydrogenase A1 was downregulated, which leads to a stronger activation of anaerobic glycolysis through lactate production and impairs the citric acid cycle. The observed alterations are in accordance with our previously described increased glucose

consumption and lactate production via anaerobic glycolysis in the drug resistant cells. This upregulation of glycolysis and shift towards anaerobic forms, allowing a faster gain of energy, has been described in various cancers (Tanner et al., 2018). The mechanism in our TKI-resistant cells might indicate a more substantial vulnerability toward chemotherapeutics and antimetabolites. At the same time, this unregulated form of hypermetabolism might explain the remarkable speed of proliferation in resistant cells.

4.7. SAMHD1

After we observed the changes in glucose metabolism, we wanted to investigate potential changes in the drug metabolism that might lead to treatment resistance. One of the most downregulated proteins in all our resistant cell lines was SAMHD1. This enzyme has been found to regulate the homeostasis of intracellular deoxynucleotide triphosphate (dNTP) that controls DNA replication and damage repair by homologous recombination. Downregulation of SAMHD1 has been found in various tumours and leads to increased dNTP concentration, thereby enhancing cell cycle and proliferation. The lack of a homologous recombination mechanism also increases sensitivity to DNA damage by ionic radiation or drugs. Therefore, SAMHD1 can be considered a tumour suppressor, and its downregulation simplifies tumour cell proliferation (Clifford et al., 2014; Rentoft et al., 2016). In SAMHD1 lacking cells, a shift towards the error-prone non-homologous end-joining pathway as the primary DNA reparation mechanism has been observed (Daddacha et al., 2017). Therefore, our Midostaurin and Sorafenib resistant cells should become more sensitive to inhibitors of the non-homologous end joining repair pathway as Olaparib. The higher vulnerability of the cells towards DNA damage might also increase their sensitivity towards DNA hypomethylating agents such as Decitabine. This effect has already been shown in SAMHD1 deficient AML cells, independent of an FLT3 mutation or TKI treatment (Oellerich et al., 2019).

4.8. Summary

Our mass spectrometric analysis of Midostaurin and Sorafenib resistant FLT3 mutated AML cells and their drug- naïve counterparts revealed a wide range of proteomic alterations upon resistance formation. We generated a pathway enrichment and network analysis, giving us a functional overview of changes upon resistance development. Highly altered pathways included glucose metabolism and glycolysis, the inflammasome, and platelet activation. The most crucial functions securing cancer cells' survival were also strongly modified. Apoptosis, Pyroptosis, DNA repair mechanisms, and the cell cycle showed strong up and down regulations in some of their essential proteins. Those included the Bcl-2 protein family, which elicits strong pro- and anti-apoptotic effects. Indeed, the anti-apoptotic agent Bcl-XL was strongly upregulated, whereas its functional counterpart Bcl-2, inducing apoptosis, was strongly downregulated. This disbalance in the apoptotic signalling towards cell survival could also be demonstrated in TKI-resistant cells in our treatment experiments. These showed a high vulnerability towards Bcl-XL inhibitors, whereas Bcl-2 inhibitors such as Venetoclax were ineffective. Another crucial mechanism was the downregulation of Caspase 1, which is involved in regulating inflammasome-mediated cell death, also known as pyroptosis. The downstream activity of the usually FLT3-mediated pathways was maintained through strong upregulation of the JAK/STAT signalling system. This indicated an increased vulnerability of the Sorafenib and Midostaurin-resistant cells towards JAK-inhibitors, which we could confirm *in vitro*. The strong downregulation of SAMHD1 induced changes in the DNA repair mechanisms in TKI-resistant cells, which might lead to sensitivity towards NHEJ

pathway inhibitors such as Olaparib. At the same time, the higher stress vulnerability of the DNA might be beneficial for the use of hypomethylating drugs, such as Decitabine, in TKI-resistant cells.
Another interesting finding was the different vulnerability of the MV4-11 and Molm-13 cell line towards Sorafenib and Midostaurin, depending on their FLT3- mutational status. The low sensitivity of the Molm-13 cell line towards Sorafenib might indicate that a closer match of the FLT3 mutational status to a specific inhibitor would be beneficial for successful tyrosine kinase inhibitor treatment. Besides these described potential resistance mechanisms and their implications for second-line treatment, our proteomic data still shows many alterations with an unknown impact. We published our data as open source to enable their analysis and the elaboration of further mechanisms to allow their most extensive use possible.
Our mass spectrometric findings, their validation through western blots, and their good functional consistency in our *in vitro* second-line treatment experiments make them interesting for further clinical validation. The identified key proteins described above could be screened in patient samples, relapsed from Sorafenib or Midostaurin treatment. The broader use of Midostaurin since its FDA approval in 2018 might allow a large-scale analysis in this field. The used second-line inhibitors might be investigated under *in vivo* conditions in mice. Specific inhibitors showing promising effects against leukemic cells, such as Bcl-XL inhibitors, might be used under improved therapy regimens to investigate their suitability as the standard of care. Those investigations might lead to better treatment options for patients that are unsuitable for or have relapsed under standard therapies. These might be crucial steps to improve the overall survival chances of patients with FLT3-mutated AML.

5. Abstract

Whereas the age adjusted incidence of leukaemia decreased since 1990, acute myeloid leukaemia showed an increase in incidence and represented the second most common type of leukaemia. The survival prognosis improved to a 5-year survival rate of 31% in 2020, remaining one of the deadliest types of blood cancer and malignant neoplasms in general. Evolving from the initial FAB classification, developed in the 1970th, whose subtype classification was solely based on the morphology of leukemic cells, the WHO classification of AML, defined in the early 2000th, additionally incorporated genetic features of AML. This new classification was required due to the high prevalence of genetic alterations in AML and their impact on survival and remission. In short, complex karyotypes showing multiple mutations were correlated with poorer prognoses. One of the most important mutations found was the constitutive activation of the Fms-like tyrosine kinase 3 through internal-tandem duplications of the juxtamembrane region or activating point mutations in the cytoplasmic tyrosine kinase domain. Those could be detected in nearly 1/3 of all AML patients, making it the most common genetic aberration. The permanent activation of FLT3 was shown to be a crucial factor for cell survival enabling uncontrolled cell proliferation. Those effects are mediated by the activation of downstream pathways of the kinase, finally resulting in the activation of transcription factors, promoting cell survival. Some of those pathways were already described and known mediators in carcinogenesis and cell cycle activation as the PI3K/Akt or JAK/STAT pathway. The high incidence of FLT3 mutations and their correlation with worse survival and treatment response rates made it an important therapeutic target. Small molecular tyrosine kinase inhibitors were developed to block the activation of FLT3 and its proliferative and antiapoptotic functions in leukemic cells. Sorafenib was one of the first small molecular inhibitors with broad application in AML due to its effectiveness against FLT3. However, not all patients benefited from the effects of Sorafenib, and the inhibitor failed to show a significant increase in overall survival rates in the SORAML trial. If not, this study did not stratify the participants for FLT3 mutations, which might have masked its therapeutic effectiveness. Good response rates in FLT3 mutated AML patients led to its application in additional clinical studies or off-label use. In 2017, the tyrosine kinase inhibitor Midostaurin obtained FDA approval as a therapeutic agent in FLT3 mutated AML after significantly improved overall survival in the RATIFY trial. However, Midostaurin mainly showed a delay in disease progression, and the survival rates became similar to the placebo group after three years. Resistance development against tyrosine kinase inhibitors and the subsequent relapse of AML represents a strong hurdle for the long-term survival of those patients. Research efforts based on a genomic approach enlightened the underlying resistance mechanism. Some important alternations were found, such as secondary mutations of the FLT3 receptor or higher expression rates of its ligand. Additionally, reactivation or overexpression of downstream pathways such as JAK/STAT described before were identified. Another wide research field was the adaptation of the surrounding cellular microenvironment of tumour cells, building a protective niche. These findings were important steps in the understanding of potential resistance mechanisms. Still, genomic alterations are difficult to validate on a functional level due to complex modifications between the genomic alteration and the final functional output. Furthermore, most of the findings above present only part of the underlying resistance mechanisms, lacking a broad overview of interactions and alternated signalling pathways in resistant leukemic cells. To overcome those difficulties, we performed a mass spectrometry-based whole proteome analysis to investigate changes in proteomic composition upon the development of Midostaurin or Sorafenib resistance in FLT3 mutated AML. We developed an *in vitro* model of Sorafenib and Midostaurin resistance in FLT3 mutated cells based on chronic treatment with both drugs in the FLT3 mutation carrying AML cell lines MV4-11 and Molm-13 until drug resistance occurred. The same cell lines were treated with DMSO for the same period to obtain respective control conditions. The

cells of the different treatment conditions were subsequently lysed and processed via the SP3 protocol to obtain tryptic peptides for the proteomic bottom-up analysis. Peptides were analysed by high-resolution mass spectrometry and specialised phospho-proteomic enrichment and detection strategy via mass spectrometry. Many significantly alternated proteins could be detected between TKI resistant cells and their drug-naïve controls. A principal component analysis showed a high consistency between the biological replicates of our experiments and a clear proteomic distinction between the treated and untreated groups. Molm-13 cells, nevertheless, did not respond well enough to therapeutic doses of Sorafenib to induce the necessary reduction in cell viability for adequate development of resistance. This experimental observation was confirmed by our proteomic data, which did not show many alternations compared to their solvent control. Hence, we excluded Molm-13 Sorafenib-treated cells from the comparative analysis. To better understand the functional implications of the variant protein expression, we superimposed our data to known cell functions and pathways. Hereby we found strong dysregulation in the pathways regulating apoptosis, necroptosis, cell cycle, platelet activation, and metabolism (glycolysis, platinum drug resistance). Within significantly up- and downregulated proteins, a large number was shared among all TKI-resistant cell lines, pointing towards a general adaptation driving Sorafenib and Midostaurin resistance. Some of those critical mediators were FLT3, STAT5, Bcl-2, Bcl-XL, and SAMHD1. Despite some previous studies showing FLT3 upregulation upon resistance towards TKI, we found a strong downregulation in all our resistant cell lines. We therefore concluded that FLT3 itself might not play an important role in resistance development. Despite the weak expression and still effective inhibition of FLT3, its downstream pathways, such as JAK/STAT and PI3K/Akt, were still highly active, showing strong upregulations of some of their proteins. The apoptosis regulators of the Bcl-protein family also showed strong and highly significant alterations in all of our experiments, resulting in an upregulation of anti-apoptotic signalling in TKI resistant cells. SAMHD1, a key protein for the regulation of nucleoside triphosphates in the cell and the resistance of cells against DNA damages, was significantly downregulated in TKI-resistant cells enabling further uncontrolled cellular proliferation but also indicating a higher vulnerability towards DNA hypomethylating agents such as Azacytidine. Validation of our findings for selected proteins such as FLT3, P-FLT3, STAT5b, P-STAT5, ICAM3, CD84, Bcl-2, and Bcl-XL confirmed findings in the mass spectrometry data. To investigate the functional implications of those proteomic alterations of the cells and to detect potential second-line treatment agents for TKI-resistant AML, we tested the sensitivity of our different treatment cohorts towards targeted inhibitors. We showed a strong increase in sensitivity of the TKI-resistant cells towards the Bcl-XL specific inhibitor WEHI-539 compared to untreated control cells. This observation is in good accordance with the strong upregulation of Bcl-XL expression in resistant cells. The rather unspecific Bcl- protein inhibitor Venetoclax (ABT-199), mainly targeting Bcl-2, did not show a higher effectiveness in the TKI-resistant cells, as expected due to a strong downregulation of Bcl-2 in this cohort. An unspecific JAK-inhibitor showed slightly higher efficacy against TKI-resistant cells, pointing towards a functional implication of the JAK/STAT signalling in resistance development, albeit not to the same extent as for Bcl-XL. These *in vitro* data lack clinical approval and require further investigation in patients but might provide interesting hints towards potential resistance mechanisms and new treatment options in a resistance scenario. We picked out the most interesting proteins and pathways for our analysis but did not reach the bottom of possible information gained by the whole proteome data. Therefore, we published our data on an open-source platform to enable further evaluation of it. Nevertheless, our mass spectrometric analysis might indicate potential second-line treatments in TKI relapsed patients as Hypomethylating agents or Bcl-XL specific inhibitors, and a deeper understanding of the underlying biochemical alterations driving resistance might enable more focussed strategies to avoid these.

References

Aaronson, D. S., & Horvath, C. M. (2002). A road map for those who don't know JAK-STAT. *Science (New York, N.Y.)*, *296*(5573), 1653–1655. https://doi.org/10.1126/science.1071545

Abelson, S., Collord, G., Ng, S. W. K., Weissbrod, O., Mendelson Cohen, N., Niemeyer, E., . . . Shlush, L. I. (2018). Prediction of acute myeloid leukaemia risk in healthy individuals. *Nature*, *559*(7714), 400–404. https://doi.org/10.1038/s41586-018-0317-6

Adhikari, S., Nice, E. C., Deutsch, E. W., Lane, L., Omenn, G. S., Pennington, S. R., . . . Baker, M. S. (2020). A high-stringency blueprint of the human proteome. *Nature Communications*, *11*(1), 5301. https://doi.org/10.1038/s41467-020-19045-9

Aebersold, R., & Mann, M. (2016). Mass-spectrometric exploration of proteome structure and function. *Nature*, *537*(7620), 347–355. https://doi.org/10.1038/nature19949

The American Cancer Society medical and editorial content team (9,2014). Early Detection, Diagnosis and types: How is Acute Myeloid Leukaemia classified? Retrieved from https://www.cancer.org/cancer/acute-myeloid-leukemia/detection-diagnosis-staging/how-classified.html#written_by

Arber, D. A., Orazi, A., Hasserjian, R., Thiele, J., Borowitz, M. J., Le Beau, M. M., . . . Vardiman, J. W. (2016). The 2016 revision to the World Health Organization classification of myeloid neoplasms and acute leukaemia. *Blood*, *127*(20), 2391–2405. https://doi.org/10.1182/blood-2016-03-643544

Audi, G. (2006). The history of nuclidic masses and of their evaluation. *International Journal of Mass Spectrometry*, *251*(2-3), 85–94. https://doi.org/10.1016/j.ijms.2006.01.048

Bagrintseva, K., Geisenhof, S., Kern, R., Eichenlaub, S., Reindl, C., Ellwart, J. W., . . . Spiekermann, K. (2005). Flt3-ITD-TKD dual mutants associated with AML confer resistance to FLT3 PTK inhibitors and cytotoxic agents by overexpression of Bcl-x(L). *Blood*, *105*(9), 3679–3685. https://doi.org/10.1182/blood-2004-06-2459

Bagrintseva, K., Schwab, R., Kohl, T. M., Schnittger, S., Eichenlaub, S., Ellwart, J. W., . . . Spiekermann, K. (2004). Mutations in the tyrosine kinase domain of FLT3 define a new molecular mechanism of acquired drug resistance to PTK inhibitors in FLT3-ITD-transformed hematopoietic cells. *Blood*, *103*(6), 2266–2275. https://doi.org/10.1182/blood-2003-05-1653

Baryawno, N., Przybylski, D., Kowalczyk, M. S., Kfoury, Y., Severe, N., Gustafsson, K., . . . Scadden, D. T. (2019). A Cellular Taxonomy of the Bone Marrow Stroma in Homeostasis and Leukaemia. *Cell*, *177*(7), 1915-1932.e16. https://doi.org/10.1016/j.cell.2019.04.040

Bennett, J. M., Catovsky, D., Daniel, M., Flandrin, G., Galton, D. A. G., Gralnick, H. R., & Sultan, C. (1976). Proposals for the Classification of the Acute Leukaemias French American British (FAB) Cooperative Group. *British Journal of Haematology*, *33*(4), 451–458. https://doi.org/10.1111/j.1365-2141.1976.tb03563.x

Biemann, K., Gapp, G., & Seibl, J. (1959). APPLICATION OF MASS SPECTROMETRY TO STRUCTURE PROBLEMS. I. AMINO ACID SEQUENCE IN PEPTIDES. *Journal of the American Chemical Society*, *81*(9), 2274–2275. https://doi.org/10.1021/ja01518a069

Blakley, C. R., McAdams, M. J., & Vestal, M. L. (1978). Crossed-beam liquid chromatoraph—mass spectrometer combination. *Journal of Chromatography a*, *158*, 261–276. https://doi.org/10.1016/S0021-9673(00)89972-0

Brinda, B., Khan, I., Parkin, B., & Konig, H. (2018). The rocky road to personalized medicine in acute myeloid leukaemia. *Journal of Cellular and Molecular Medicine*, *22*(3), 1411–1427. https://doi.org/10.1111/jcmm.13478

Brunner, A. M., Li, S., Fathi, A. T., Wadleigh, M., Ho, V. T., Collier, K., . . . Chen, Y.-B. (2016). Haematopoietic cell transplantation with and without sorafenib maintenance for patients with FLT3 -ITD acute myeloid leukaemia in first complete remission. *British Journal of Haematology*, *175*(3), 496–504. https://doi.org/10.1111/bjh.14260

Burchert, A., Bug, G., Fritz, L. V., Finke, J., Stelljes, M., Röllig, C., . . . Metzelder, S. K. (2020). Sorafenib Maintenance After Allogeneic Hematopoietic Stem Cell Transplantation for Acute Myeloid Leukaemia With FLT3-Internal Tandem Duplication Mutation (SORMAIN). *Journal of Clinical Oncology : Official Journal of the American Society of Clinical Oncology*, *38*(26), 2993–3002. https://doi.org/10.1200/JCO.19.03345

Burnett, A., & Stone, R. (2020). Aml: New Drugs but New Challenges. *Clinical Lymphoma, Myeloma & Leukaemia.* Advance online publication. https://doi.org/10.1016/j.clml.2020.02.005

Burnett, A. K., Hills, R. K., Milligan, D., Kjeldsen, L., Kell, J., Russell, N. H., . . . Wheatley, K. (2011). Identification of patients with acute myeloblastic leukaemia who benefit from the addition of gemtuzumab ozogamicin: Results of the MRC AML15 trial. *Journal of Clinical Oncology : Official Journal of the American Society of Clinical Oncology*, *29*(4), 369–377. https://doi.org/10.1200/JCO.2010.31.4310

Cancer Treatment Centers of America (2015, September 10). Leukaemia symptoms. Retrieved from https://www.cancercenter.com/leukemia/symptoms/

Chappell, G., Geer, M., Gatza, E., Braun, T., Churay, T., Brisson, J., . . . Choi, S. W. (2019). Maintenance sorafenib in FLT3-ITD AML following allogeneic HCT favorably impacts relapse and overall survival. *Bone Marrow Transplantation*, *54*(9), 1518–1520. https://doi.org/10.1038/s41409-019-0493-5

Chen, F., Ishikawa, Y., Akashi, A., Naoe, T., & Kiyoi, H. (2016). Co-expression of wild-type FLT3 attenuates the inhibitory effect of FLT3 inhibitor on FLT3 mutated leukaemia cells. *Oncotarget*, *7*(30), 47018–47032. https://doi.org/10.18632/oncotarget.10147

Clifford, R., Louis, T., Robbe, P., Ackroyd, S., Burns, A., Timbs, A. T., . . . Schuh, A. (2014). Samhd1 is mutated recurrently in chronic lymphocytic leukaemia and is involved in response to DNA damage. *Blood*, *123*(7), 1021–1031. https://doi.org/10.1182/blood-2013-04-490847

Comisarow, M. B., & Marshall, A. G. (1974). Fourier transform ion cyclotron resonance spectroscopy. *Chemical Physics Letters*, *25*(2), 282–283. https://doi.org/10.1016/0009-2614(74)89137-2

Daddacha, W., Koyen, A. E., Bastien, A. J., Head, P. E., Dhere, V. R., Nabeta, G. N., . . . Yu, D. S. (2017). Samhd1 Promotes DNA End Resection to Facilitate DNA Repair by Homologous Recombination. *Cell Reports*, *20*(8), 1921–1935. https://doi.org/10.1016/j.celrep.2017.08.008

Daver, N., Cortes, J., Ravandi, F., Patel, K. P., Burger, J. A., Konopleva, M., & Kantarjian, H. (2015). Secondary mutations as mediators of resistance to targeted therapy in leukaemia. *Blood*, *125*(21), 3236–3245. https://doi.org/10.1182/blood-2014-10-605808

DiNardo, C. D., Jonas, B. A., Pullarkat, V., Thirman, M. J., Garcia, J. S., Wei, A. H., . . . Pratz, K. W. (2020). Azacitidine and Venetoclax in Previously Untreated Acute Myeloid Leukaemia. *The New England Journal of Medicine*, *383*(7), 617–629. https://doi.org/10.1056/NEJMoa2012971

DiNardo, C. D., Stein, E. M., Botton, S. de, Roboz, G. J., Altman, J. K., Mims, A. S., . . . Kantarjian, H. M. (2018). Durable Remissions with Ivosidenib in IDH1-Mutated Relapsed or Refractory AML. *The New England Journal of Medicine*, *378*(25), 2386–2398. https://doi.org/10.1056/NEJMoa1716984

Döhner, H., Estey, E. H., Amadori, S., Appelbaum, F. R., Büchner, T., Burnett, A. K., . . . Bloomfield, C. D. (2010). Diagnosis and management of acute myeloid leukaemia in adults: Recommendations from an international expert panel, on behalf of the European LeukemiaNet. *Blood*, *115*(3), 453–474. https://doi.org/10.1182/blood-2009-07-235358

Döhner, H., Estey, E., Grimwade, D., Amadori, S., Appelbaum, F. R., Büchner, T., . . . Bloomfield, C. D. (2017). Diagnosis and management of AML in adults: 2017 ELN recommendations from an international expert panel. *Blood*, *129*(4), 424–447. https://doi.org/10.1182/blood-2016-08-733196

Doll, S., Gnad, F., & Mann, M. (2019). The Case for Proteomics and Phospho-Proteomics in Personalized Cancer Medicine. *Proteomics. Clinical Applications*, *13*(2), e1800113. https://doi.org/10.1002/prca.201800113

Dupree, E. J., Jayathirtha, M., Yorkey, H., Mihasan, M., Petre, B. A., & Darie, C. C. (2020). A Critical Review of Bottom-Up Proteomics: The Good, the Bad, and the Future of this Field. *Proteomes*, *8*(3). https://doi.org/10.3390/proteomes8030014

El Fakih, R., Rasheed, W., Hawsawi, Y., Alsermani, M., & Hassanein, M. (2018). Targeting FLT3 Mutations in Acute Myeloid Leukaemia. *Cells*, *7*(1). https://doi.org/10.3390/cells7010004

Ferries, S., Perkins, S., Brownridge, P. J., Campbell, A., Eyers, P. A., Jones, A. R., & Eyers, C. E. (2017). Evaluation of Parameters for Confident Phosphorylation Site Localization Using an Orbitrap Fusion Tribrid Mass Spectrometer. *Journal of Proteome Research*, *16*(9), 3448–3459. https://doi.org/10.1021/acs.jproteome.7b00337

Fiegl, M. (2016). Epidemiology, pathogenesis, and etiology of acute leukaemia. In W. Hiddemann (Ed.), *Handbook of Acute Leukaemia* (pp. 3–13). Cham: Springer International Publishing. https://doi.org/10.1007/978-3-319-26772-2_2

Frejno, M., Meng, C., Ruprecht, B., Oellerich, T., Scheich, S., Kleigrewe, K., . . . Kuster, B. (2020). Proteome activity landscapes of tumour cell lines determine drug responses. *Nature Communications*, *11*(1), 3639. https://doi.org/10.1038/s41467-020-17336-9

Genomic Classification in Acute Myeloid Leukaemia (2016). *The New England Journal of Medicine*, *375*(9), 900–901. https://doi.org/10.1056/NEJMc1608739

Gilliland, D. G., & Griffin, J. D. (2002). The roles of FLT3 in haematopoiesis and leukaemia. *Blood*, *100*(5), 1532–1542. https://doi.org/10.1182/blood-2002-02-0492

Gohlke, R. S. (1959). Time-of-Flight Mass Spectrometry and Gas-Liquid Partition Chromatography. *Analytical Chemistry*, *31*(4), 535–541. https://doi.org/10.1021/ac50164a024

Green, A. S., Maciel, T. T., Hospital, M.-A., Yin, C., Mazed, F., Townsend, E. C., . . . Tamburini, J. (2015). Pim kinases modulate resistance to FLT3 tyrosine kinase inhibitors in FLT3-ITD acute myeloid leukaemia. *Science Advances*, *1*(8), e1500221. https://doi.org/10.1126/sciadv.1500221

Gregorich, Z. R., & Ge, Y. (2014). Top-down proteomics in health and disease: Challenges and opportunities. *Proteomics*, *14*(10), 1195–1210. https://doi.org/10.1002/pmic.201300432

Groot, R. P. de, Raaijmakers, J. A., Lammers, J. W., & Koenderman, L. (2000). Stat5-Dependent CyclinD1 and Bcl-xL expression in Bcr-Abl-transformed cells. *Molecular Cell Biology Research Communications : MCBRC*, *3*(5), 299–305. https://doi.org/10.1006/mcbr.2000.0231

Grunwald, M. R., & Levis, M. J. (2013). Flt3 inhibitors for acute myeloid leukaemia: A review of their efficacy and mechanisms of resistance. *International Journal of Hematology*, *97*(6), 683–694. https://doi.org/10.1007/s12185-013-1334-8

Han, X., Aslanian, A., & Yates, J. R. (2008). Mass spectrometry for proteomics. *Current Opinion in Chemical Biology*, *12*(5), 483–490. https://doi.org/10.1016/j.cbpa.2008.07.024

Heidel, F., Solem, F. K., Breitenbuecher, F., Lipka, D. B., Kasper, S., Thiede, M. H., . . . Fischer, T. (2006). Clinical resistance to the kinase inhibitor PKC412 in acute myeloid leukaemia by mutation of Asn-676 in the FLT3 tyrosine kinase domain. *Blood*, *107*(1), 293–300. https://doi.org/10.1182/blood-2005-06-2469

Hernandez-Valladares, M., Bruserud, Ø., & Selheim, F. (2020). The Implementation of Mass Spectrometry-Based Proteomics Workflows in Clinical Routines of Acute Myeloid Leukaemia: Applicability and Perspectives. *International Journal of Molecular Sciences*, *21*(18). https://doi.org/10.3390/ijms21186830

Hills, R. K., Castaigne, S., Appelbaum, F. R., Delaunay, J., Petersdorf, S., Othus, M., . . . Burnett, A. K. (2014). Addition of gemtuzumab ozogamicin to induction chemotherapy in adult patients with acute myeloid leukaemia: a meta-analysis of individual patient data from randomised controlled trials. *The Lancet Oncology*, *15*(9), 986–996. https://doi.org/10.1016/S1470-2045(14)70281-5

Hoy, S. M. (2019). Glasdegib: First Global Approval. *Drugs*, *79*(2), 207–213. https://doi.org/10.1007/s40265-018-1047-7

Ivanov, A. R., Colangelo, C. M., Dufresne, C. P., Friedman, D. B., Lilley, K. S., Mechtler, K., . . . Weintraub, S. T. (2013). Interlaboratory studies and initiatives developing standards for proteomics. *Proteomics*, *13*(6), 904–909. https://doi.org/10.1002/pmic.201200532

Javidi-Sharifi, N., Martinez, J., English, I., Joshi, S. K., Scopim-Ribeiro, R., Viola, S. K., . . . Traer, E. (2019). Fgf2-FGFR1 signalling regulates release of Leukaemia-Protective exosomes from bone marrow stromal cells. *ELife*, *8.* https://doi.org/10.7554/eLife.40033

Johnson, D. C., Taabazuing, C. Y., Okondo, M. C., Chui, A. J., Rao, S. D., Brown, F. C., . . . Bachovchin, D. A. (2018). Dpp8/dpp9 inhibitor-induced pyroptosis for treatment of acute myeloid leukaemia. *Nature Medicine*, *24*(8), 1151–1156. https://doi.org/10.1038/s41591-018-0082-y

Jones, L. M., Melgar, K., Bolanos, L., Hueneman, K., Walker, M. M., Jiang, J.-K., . . . Thomas, C. J. (2020). Targeting AML-associated FLT3 mutations with a type I kinase inhibitor. *The Journal of Clinical Investigation.* Advance online publication. https://doi.org/10.1172/JCI127907

Kampen, K. R. (2012). The discovery and early understanding of leukaemia. *Leukaemia Research*, *36*(1), 6–13. https://doi.org/10.1016/j.leukres.2011.09.028

Kantarjian, H. M., Kadia, T. M., DiNardo, C. D., Welch, M. A., & Ravandi, F. (2021). Acute myeloid leukaemia: Treatment and research outlook for 2021 and the MD Anderson approach. *Cancer*, *127*(8), 1186–1207. https://doi.org/10.1002/cncr.33477

Karki, R., & Kanneganti, T.-D. (2019). Diverging inflammasome signals in tumorigenesis and potential targeting. *Nature Reviews Cancer*, *19*(4), 197–214. https://doi.org/10.1038/s41568-019-0123-y

Kim, E. S. (2017). Enasidenib: First Global Approval. *Drugs*, *77*(15), 1705–1711. https://doi.org/10.1007/s40265-017-0813-2

Kindler, T., Lipka, D. B., & Fischer, T. (2010). Flt3 as a therapeutic target in AML: Still challenging after all these years. *Blood*, *116*(24), 5089–5102. https://doi.org/10.1182/blood-2010-04-261867

Kipps, T. J., Eradat, H., Grosicki, S., Catalano, J., Cosolo, W., Dyagil, I. S., . . . Pylypenko, H. (2015). A phase 2 study of the BH3 mimetic BCL2 inhibitor navitoclax (ABT-263) with or without rituximab, in previously untreated B-cell chronic lymphocytic leukaemia. *Leukemia & Lymphoma*, *56*(10), 2826–2833. https://doi.org/10.3109/10428194.2015.1030638

Kiu, H., & Nicholson, S. E. (2012). Biology and significance of the JAK/STAT signalling pathways. *Growth Factors (Chur, Switzerland)*, *30*(2), 88–106. https://doi.org/10.3109/08977194.2012.660936

Kiyoi, H., Towatari, M., Yokota, S., Hamaguchi, M., Ohno, R., Saito, H., & Naoe, T. (1998). Internal tandem duplication of the FLT3 gene is a novel modality of elongation mutation which causes constitutive activation of the product. *Leukaemia*, *12*(9), 1333–1337. https://doi.org/10.1038/sj.leu.2401130

Kohl, T. M., Hellinger, C., Ahmed, F., Buske, C., Hiddemann, W., Bohlander, S. K., & Spiekermann, K. (2007). Bh3 mimetic ABT-737 neutralizes resistance to FLT3 inhibitor treatment mediated by FLT3-independent expression of BCL2 in primary AML blasts. *Leukaemia*, *21*(8), 1763–1772. https://doi.org/10.1038/sj.leu.2404776

Kojima, K., McQueen, T., Chen, Y., Jacamo, R., Konopleva, M., Shinojima, N., . . . Andreeff, M. (2011). P53 activation of mesenchymal stromal cells partially abrogates microenvironment-mediated resistance to FLT3 inhibition in AML through HIF-1α-mediated down-regulation of CXCL12. *Blood*, *118*(16), 4431–4439. https://doi.org/10.1182/blood-2011-02-334136

Kouchkovsky, I. de, & Abdul-Hay, M. (2016). 'acute myeloid leukaemia: A comprehensive review and 2016 update'. *Blood Cancer Journal*, *6*(7), e441. https://doi.org/10.1038/bcj.2016.50

Lam, S. S. Y., & Leung, A. Y. H. (2020). Overcoming Resistance to FLT3 Inhibitors in the Treatment of FLT3-Mutated AML. *International Journal of Molecular Sciences*, *21*(4). https://doi.org/10.3390/ijms21041537

Lancet, J. E., Uy, G. L., Cortes, J. E., Newell, L. F., Lin, T. L., Ritchie, E. K., . . . Medeiros, B. C. (2018). Cpx-351 (cytarabine and daunorubicin) Liposome for Injection Versus Conventional Cytarabine Plus Daunorubicin in Older Patients With Newly Diagnosed Secondary Acute Myeloid Leukaemia. *Journal of Clinical Oncology : Official Journal of the American Society of Clinical Oncology*, *36*(26), 2684–2692. https://doi.org/10.1200/JCO.2017.77.6112

Lessene, G., Czabotar, P. E., Sleebs, B. E., Zobel, K., Lowes, K. N., Adams, J. M., . . . Watson, K. G. (2013). Structure-guided design of a selective BCL-X(L) inhibitor. *Nature Chemical Biology*, *9*(6), 390–397. https://doi.org/10.1038/nchembio.1246

Levis, M., & Small, D. (2003). Flt3: Itdoes matter in leukaemia. *Leukaemia*, *17*(9), 1738–1752. https://doi.org/10.1038/sj.leu.2403099

Lindblad, O., Cordero, E., Puissant, A., Macaulay, L., Ramos, A., Kabir, N. N., . . . Kazi, J. U. (2016). Aberrant activation of the PI3K/mTOR pathway promotes resistance to sorafenib in AML. *Oncogene*, *35*(39), 5119–5131. https://doi.org/10.1038/onc.2016.41

Makarov (2000). Electrostatic axially harmonic orbital trapping: A high-performance technique of mass analysis. *Analytical Chemistry*, *72*(6), 1156–1162. https://doi.org/10.1021/ac991131p

McKenna, H. J., Stocking, K. L., Miller, R. E., Brasel, K., Smedt, T. de, Maraskovsky, E., . . . Peschon, J. J. (2000). Mice lacking flt3 ligand have deficient haematopoiesis affecting hematopoietic progenitor cells, dendritic cells, and natural killer cells. *Blood*, *95*(11), 3489–3497.

Megías-Vericat, J. E., Ballesta-López, O., Barragán, E., Martínez-Cuadrón, D., & Montesinos, P. (2020). Tyrosine kinase inhibitors for acute myeloid leukaemia: A step toward disease control? *Blood Reviews*, 100675. https://doi.org/10.1016/j.blre.2020.100675

Method of the Year 2012 (2013). *Nature Methods*, *10*(1), 1. https://doi.org/10.1038/nmeth.2329

Metzeler, K. H., Herold, T., Rothenberg-Thurley, M., Amler, S., Sauerland, M. C., Görlich, D., . . . Spiekermann, K. (2016). Spectrum and prognostic relevance of driver gene mutations in acute myeloid leukaemia. *Blood*, *128*(5), 686–698. https://doi.org/10.1182/blood-2016-01-693879

Michalski, A., Damoc, E., Hauschild, J.-P., Lange, O., Wieghaus, A., Makarov, A., . . . Horning, S. (2011). Mass spectrometry-based proteomics using Q Exactive, a high-performance benchtop quadrupole Orbitrap mass spectrometer. *Molecular & Cellular Proteomics : MCP*, *10*(9), M111.011015. https://doi.org/10.1074/mcp.M111.011015

Miller, K. D., Fidler-Benaoudia, M., Keegan, T. H., Hipp, H. S., Jemal, A., & Siegel, R. L. (2020). Cancer statistics for adolescents and young adults, 2020. *CA: A Cancer Journal for Clinicians.* Advance online publication. https://doi.org/10.3322/caac.21637

Muller, R. A. (1977). Radioisotope dating with a cyclotron. *Science (New York, N.Y.)*, *196*(4289), 489–494. https://doi.org/10.1126/science.196.4289.489

Nagaraj, N., Wisniewski, J. R., Geiger, T., Cox, J., Kircher, M., Kelso, J., . . . Mann, M. (2011). Deep proteome and transcriptome mapping of a human cancer cell line. *Molecular Systems Biology*, *7*, 548. https://doi.org/10.1038/msb.2011.81

National Cancer Institute's Surveillance, Epidemiology and End Results Program. Cancer Statistics Review 1975-2013. Retrieved from [Web] http://www.lls.org/http%3A/llsorg.prod.acquia-sites.com/facts-and-statistics/facts-and-statistics-overview/facts-and-statistics

Oellerich, T., Schneider, C., Thomas, D., Knecht, K. M., Buzovetsky, O., Kaderali, L., . . . Cinatl, J. (2019). Selective inactivation of hypomethylating agents by SAMHD1 provides a rationale for therapeutic stratification in AML. *Nature Communications*, *10*(1), 3475. https://doi.org/10.1038/s41467-019-11413-4

Ossenkoppele, G., & Löwenberg, B. (2015). How I treat the older patient with acute myeloid leukaemia. *Blood*, *125*(5), 767–774. https://doi.org/10.1182/blood-2014-08-551499

Papaemmanuil, E., Gerstung, M., Bullinger, L., Gaidzik, V. I., Paschka, P., Roberts, N. D., . . . Campbell, P. J. (2016). Genomic Classification and Prognosis in Acute Myeloid Leukaemia. *The New England Journal of Medicine*, *374*(23), 2209–2221. https://doi.org/10.1056/NEJMoa1516192

Park, I.-K., Mundy-Bosse, B., Whitman, S. P., Zhang, X., Warner, S. L., Bearss, D. J., . . . Caligiuri, M. A. (2015). Receptor tyrosine kinase Axl is required for resistance of leukemic cells to FLT3-targeted therapy in acute myeloid leukaemia. *Leukemia*, *29*(12), 2382–2389. https://doi.org/10.1038/leu.2015.147

Perl, A. E., Martinelli, G., Cortes, J. E., Neubauer, A., Berman, E., Paolini, S., . . . Levis, M. J. (2019). Gilteritinib or Chemotherapy for Relapsed or Refractory FLT3-Mutated AML. *The New England Journal of Medicine*, *381*(18), 1728–1740. https://doi.org/10.1056/NEJMoa1902688

Piloto, O., Wright, M., Brown, P., Kim, K.-T., Levis, M., & Small, D. (2007). Prolonged exposure to FLT3 inhibitors leads to resistance via activation of parallel signalling pathways. *Blood*, *109*(4), 1643–1652. https://doi.org/10.1182/blood-2006-05-023804

Pratz, K. W., & Levis, M. (2017). How I treat FLT3-mutated AML. *Blood*, *129*(5), 565–571. https://doi.org/10.1182/blood-2016-09-693648

Rchardt, E. (1936). Zur Entdeckung der Kanalstrahlen vor fnfzig Jahren. *Die Naturwissenschaften*, *24*(30), 465–467. https://doi.org/10.1007/BF01473963

Reiter, K., Polzer, H., Krupka, C., Maiser, A., Vick, B., Rothenberg-Thurley, M., . . . Greif, P. A. (2018). Tyrosine kinase inhibition increases the cell surface localization of FLT3-ITD and enhances FLT3-directed immunotherapy of acute myeloid leukaemia. *Leukemia*, *32*(2), 313–322. https://doi.org/10.1038/leu.2017.257

Rentoft, M., Lindell, K., Tran, P., Chabes, A. L., Buckland, R. J., Watt, D. L., . . . Chabes, A. (2016). Heterozygous colon cancer-associated mutations of SAMHD1 have functional significance. *Proceedings of the National Academy of Sciences of the United States of America*, *113*(17), 4723–4728. https://doi.org/10.1073/pnas.1519128113

Röllig, C., Kramer, M., Schliemann, C., Mikesch, J.-H., Steffen, B., Krämer, A., . . . Bornhäuser, M. (2020). Does time from diagnosis to treatment affect the prognosis of patients with newly diagnosed acute myeloid leukaemia? *Blood*, *136*(7), 823–830. https://doi.org/10.1182/blood.2019004583

Röllig, C., Serve, H., Hüttmann, A., Noppeney, R., Müller-Tidow, C., Krug, U., . . . Ehninger, G. (2015). Addition of sorafenib versus placebo to standard therapy in patients aged 60 years or younger with newly diagnosed acute myeloid leukaemia (SORAML): a multicentre, phase 2, randomised

controlled trial. *The Lancet Oncology*, *16*(16), 1691–1699. https://doi.org/10.1016/S1470-2045(15)00362-9

Rosnet, O., Bühring, H. J., deLapeyrière, O., Beslu, N., Lavagna, C., Marchetto, S., . . . Birnbaum, D. (1996). Expression and signal transduction of the FLT3 tyrosine kinase receptor. *Acta Haematologica*, *95*(3-4), 218–223. https://doi.org/10.1159/000203881

Sato, T., Yang, X., Knapper, S., White, P., Smith, B. D., Galkin, S., . . . Levis, M. (2011). Flt3 ligand impedes the efficacy of FLT3 inhibitors in vitro and in vivo. *Blood*, *117*(12), 3286–3293. https://doi.org/10.1182/blood-2010-01-266742

Schindler, C., Levy, D. E., & Decker, T. (2007). Jak-STAT signalling: From interferons to cytokines. *The Journal of Biological Chemistry*, *282*(28), 20059–20063. https://doi.org/10.1074/jbc.R700016200

Schlenk, R. F., Weber, D., Fiedler, W., Salih, H. R., Wulf, G., Salwender, H., . . . Döhner, H. (2019). Midostaurin added to chemotherapy and continued single-agent maintenance therapy in acute myeloid leukaemia with FLT3-ITD. *Blood*, *133*(8), 840–851. https://doi.org/10.1182/blood-2018-08-869453

Smith, C. C., Lin, K., Stecula, A., Sali, A., & Shah, N. P. (2015). Flt3 D835 mutations confer differential resistance to type II FLT3 inhibitors. *Leukaemia*, *29*(12), 2390–2392. https://doi.org/10.1038/leu.2015.165.

Steelman, L. S., Abrams, S. L., Whelan, J., Bertrand, F. E., Ludwig, D. E., Bäsecke, J., . . . McCubrey, J. A. (2008). Contributions of the Raf/MEK/ERK, PI3K/PTEN/Akt/mTOR and Jak/STAT pathways to leukaemia. *Leukemia*, *22*(4), 686–707. https://doi.org/10.1038/leu.2008.26

Stölzel, F., Steudel, C., Oelschlägel, U., Mohr, B., Koch, S., Ehninger, G., & Thiede, C. (2010). Mechanisms of resistance against PKC412 in resistant FLT3-ITD positive human acute myeloid leukaemia cells. *Annals of Hematology*, *89*(7), 653–662. https://doi.org/10.1007/s00277-009-0889-1

Stone, R. M. (2017). 3 + 7 + FLT3 inhibitors: 1 + 1 ≠ 2. *Blood*, *129*(9), 1061–1062. https://doi.org/10.1182/blood-2016-12-754473

Stone, R. M., Mandrekar, S. J., Sanford, B. L., Laumann, K., Geyer, S., Bloomfield, C. D., . . . Döhner, H. (2017). Midostaurin plus Chemotherapy for Acute Myeloid Leukaemia with a FLT3 Mutation. *The New England Journal of Medicine*, *377*(5), 454–464. https://doi.org/10.1056/NEJMoa1614359

Stone, R. M., Manley, P. W., Larson, R. A., & Capdeville, R. (2018). Midostaurin: Its odyssey from discovery to approval for treating acute myeloid leukaemia and advanced systemic mastocytosis. *Blood Advances*, *2*(4), 444–453. https://doi.org/10.1182/bloodadvances.2017011080

Swerdlow, S. H. (Ed.). *World Health Organization classification of tumours: 2 (der 4. ed.)*. *Who classification of tumours of haematopoietic and lymphoid tissues: [… Reflects the views of a working group that convened for an Editorial and Consensus Conference at the International Agency for Research on Cancer (IARC), Lyon, October 25 - 27, 2007]* (4. ed.).

Tanner, L. B., Goglia, A. G., Wei, M. H., Sehgal, T., Parsons, L. R., Park, J. O., . . . Rabinowitz, J. D. (2018). Four Key Steps Control Glycolytic Flux in Mammalian Cells. *Cell Systems*, *7*(1), 49-62.e8. https://doi.org/10.1016/j.cels.2018.06.003

Thomas, X., & Heiblig, M. (2020). An evaluation of glasdegib for the treatment of acute myelogenous leukaemia. *Expert Opinion on Pharmacotherapy*, *21*(5), 523–530. https://doi.org/10.1080/14656566.2020.1713094

Traer, E., Martinez, J., Javidi-Sharifi, N., Agarwal, A., Dunlap, J., English, I., . . . Druker, B. J. (2016). Fgf2 from Marrow Microenvironment Promotes Resistance to FLT3 Inhibitors in Acute Myeloid Leukaemia. *Cancer Research*, *76*(22), 6471–6482. https://doi.org/10.1158/0008-5472.CAN-15-3569

Tse, C., Shoemaker, A. R., Adickes, J., Anderson, M. G., Chen, J., Jin, S., . . . Elmore, S. W. (2008). Abt-263: A potent and orally bioavailable Bcl-2 family inhibitor. *Cancer Research*, *68*(9), 3421–3428. https://doi.org/10.1158/0008-5472.CAN-07-5836

Tse, K. F., Mukherjee, G., & Small, D. (2000). Constitutive activation of FLT3 stimulates multiple intracellular signal transducers and results in transformation. *Leukaemia*, *14*(10), 1766–1776. https://doi.org/10.1038/sj.leu.2401905

Tsuchiya, K., Nakajima, S., Hosojima, S., Thi Nguyen, D., Hattori, T., Manh Le, T., . . . Suda, T. (2019). Caspase-1 initiates apoptosis in the absence of gasdermin D. *Nature Communications*, *10*(1), 2091. https://doi.org/10.1038/s41467-019-09753-2

Uy, G. L., Mandrekar, S. J., Laumann, K., Marcucci, G., Zhao, W., Levis, M. J., . . . Larson, R. A. (2017). A phase 2 study incorporating sorafenib into the chemotherapy for older adults with FLT3-mutated acute myeloid leukaemia: Calgb 11001. *Blood Advances*, *1*(5), 331–340. https://doi.org/10.1182/bloodadvances.2016003053

Vago, J. P., Sugimoto, M. A., Lima, K. M., Negreiros-Lima, G. L., Baik, N., Teixeira, M. M., . . . Sousa, L. P. (2019). Plasminogen and the Plasminogen Receptor, Plg-RKT, Regulate Macrophage Phenotypic, and Functional Changes. *Frontiers in Immunology*, *10*, 1458. https://doi.org/10.3389/fimmu.2019.01458

Vainchenker, W., & Constantinescu, S. N. (2013). Jak/stat signalling in hematological malignancies. *Oncogene*, *32*(21), 2601–2613. https://doi.org/10.1038/onc.2012.347

Virchow, R. (1856). *Virchow R. Gesammelte Abhandlungen zur Wissenschaftlichen Medizin: "Die Leukämie"*. p.190. Frankfurt: Meidinger.

Wei, A. H., Montesinos, P., Ivanov, V., DiNardo, C. D., Novak, J., Laribi, K., . . . Panayiotidis, P. (2020). Venetoclax plus LDAC for newly diagnosed AML ineligible for intensive chemotherapy: A phase 3 randomized placebo-controlled trial. *Blood*, *135*(24), 2137–2145. https://doi.org/10.1182/blood.2020004856

Wei, R., Wang, J., Jia, E., Chen, T., Ni, Y., & Jia, W. (2018). Gsimp: A Gibbs sampler based left-censored missing value imputation approach for metabolomics studies. *PLoS Computational Biology*, *14*(1), e1005973. https://doi.org/10.1371/journal.pcbi.1005973

Weisberg, E., Boulton, C., Kelly, L. M., Manley, P., Fabbro, D., Meyer, T., . . . Griffin, J. D. (2002). Inhibition of mutant FLT3 receptors in leukaemia cells by the small molecule tyrosine kinase inhibitor PKC412. *Cancer Cell*, *1*(5), 433–443. https://doi.org/10.1016/S1535-6108(02)00069-7

Weisberg, E., Sattler, M., Manley, P. W., & Griffin, J. D. (2018). Spotlight on midostaurin in the treatment of FLT3-mutated acute myeloid leukaemia and systemic mastocytosis: Design, development, and potential place in therapy. *OncoTargets and Therapy*, *11*, 175–182. https://doi.org/10.2147/OTT.S127679

Xuan, L., Wang, Y., Huang, F., Fan, Z., Xu, Y., Sun, J., . . . Liu, Q. (2020). Sorafenib maintenance in patients with FLT3-ITD acute myeloid leukaemia undergoing allogeneic haematopoietic stem-cell transplantation: an open-label, multicentre, randomised phase 3 trial. *The Lancet Oncology*, *21*(9), 1201–1212. https://doi.org/10.1016/S1470-2045(20)30455-1

Yamamoto, Y., Kiyoi, H., Nakano, Y., Suzuki, R., Kodera, Y., Miyawaki, S., . . . Naoe, T. (2001). Activating mutation of D835 within the activation loop of FLT3 in human hematologic malignancies. *Blood*, *97*(8), 2434–2439. https://doi.org/10.1182/blood.V97.8.2434

Yamashita, M., & Fenn, J. B. (1984). Electrospray ion source. Another variation on the free-jet theme. *The Journal of Physical Chemistry*, *88*(20), 4451–4459. https://doi.org/10.1021/j150664a002

Yang, F., Xu, Y.-P., Li, J., Duan, S.-S., Fu, Y.-J., Zhang, Y., . . . Liu, L. (2009). Cloning and characterization of a novel intracellular protein p48.2 that negatively regulates cell cycle progression. *The*

International Journal of Biochemistry & Cell Biology, *41*(11), 2240–2250. https://doi.org/10.1016/j.biocel.2009.04.022

Yoshimoto, G., Miyamoto, T., Jabbarzadeh-Tabrizi, S., Iino, T., Rocnik, J. L., Kikushige, Y., . . . Akashi, K. (2009). Flt3-ITD up-regulates MCL-1 to promote survival of stem cells in acute myeloid leukaemia via FLT3-ITD-specific STAT5 activation. *Blood*, *114*(24), 5034–5043. https://doi.org/10.1182/blood-2008-12-196055

Zeng, Z., Shi, Y. X., Samudio, I. J., Wang, R.-Y., Ling, X., Frolova, O., . . . Konopleva, M. (2009). Targeting the leukaemia microenvironment by CXCR4 inhibition overcomes resistance to kinase inhibitors and chemotherapy in AML. *Blood*, *113*(24), 6215–6224. https://doi.org/10.1182/blood-2008-05-158311

Zhou, J., Bi, C., Janakakumara, J. V., Liu, S.-C., Chng, W.-J., Tay, K.-G., . . . Chen, C.-S. (2009a). Enhanced activation of STAT pathways and overexpression of survivin confer resistance to FLT3 inhibitors and could be therapeutic targets in AML. *Blood*, *113*(17), 4052–4062. https://doi.org/10.1182/blood-2008-05-156422

Zhou, J., Bi, C., Janakakumara, J. V., Liu, S.-C., Chng, W.-J., Tay, K.-G., . . . Chen, C.-S. (2009b). Enhanced activation of STAT pathways and overexpression of survivin confer resistance to FLT3 inhibitors and could be therapeutic targets in AML. *Blood*, *113*(17), 4052–4062. https://doi.org/10.1182/blood-2008-05-156422